University of Alberta

Shear Modulus of Solid ^{4}He Confined in Aerogel

by

Arif Rabbani

A thesis submitted to the Faculty of Graduate Studies and Research
in partial fulfillment of the requirements for the degree of

Master of Science

Department of Physics

Spring 2011
Edmonton, Alberta

`

Examining Committee

John Beamish, Department of Physics

Mark Freeman, Department of Physics

Doug Schmitt, Department of Physics

Samer Adeeb, Department of Civil and Environmental Engineering

`

For my parents,

Abdur Rahman** and **Monira Begum

Abstract

Torsional oscillator experiments on solid ^{4}He show supersolid behavior which appears to be associated with disorder. However, confining helium in the pores of an aerogel does not enhance the supersolid decoupling, even though x-ray measurements confirm that the crystals are highly disordered. Solid helium's shear modulus also shows anomalous behavior below 150 mK, stiffening as mobile dislocations are pinned by ^{3}He impurities at low temperatures. A highly porous material should also provide effective pinning sites for dislocations. We have made shear modulus measurements on solid ^{4}He grown in a 95% porosity aerogel. We see large modulus decreases as the samples are warmed but at much higher temperatures and over a broader range than in bulk ^{4}He. The frequency dependence of the modulus and dissipation are consistent with a thermally activated process. The activation energies are roughly 10 to 15 K and may be associated with vacancy motion.

`

Acknowledgements

I am eternally grateful to Prof. John Beamish, my supervisor and mentor throughout the entire graduate program. Without his continuous efforts, guidance and patience, I cannot even think to have completed my thesis within a short period of time.

I would like to thank my friend Md. Abdul Halim Suhel for offering various kinds of support during my research; life could have been difficult without him around. I am also thankful to my committee (Prof. Mark Freeman, Prof. Doug Schmitt) and Dr. John Davis for their supports and valuable suggestions during my dissertation. My special appreciation goes to Sarah Derr for her friendly cooperation throughout my studies and to Don Mullin and Tony Walford for their technical supports.

Finally, heartfelt thanks to my family, who I miss a lot all the time, and all my friends here for distracting me at times and thus keeping me sane during the intense research activities.

`

Table of Contents

`

`

List of Figures:

`

`

`

`

`

List of symbols

X_3	Helium-3 concentrations
d_{15}	Piezoelectric constant
μ	Shear modulus
Q	Dissipation
σ	Stress
ε	Strain
C	Capacitance
K	Dielectric constants

`

Chapter 1

Introduction

Liquefaction of helium opened up a new field of research; properties like superfluidity were discovered with many unusual characteristics. The quantum nature of helium motivated theorists to search for the existence of a similar superfluid state in solid helium. Andreev and Lifshitz [1] proposed superfluid-like behaviour in solid helium in the presence of zero point vacancies and eventually the term supersolidity was introduced. Following many years of experimental searches for a superfluid signature in solid helium, Kim and Chan [2, 3] in 2004 found evidence of such a supersolid state. In their torsional oscillator (TO) experiment, they observed non classical rotational inertia (NCRI) in solid helium, which implies that some of the solid flows like a superfluid inside the oscillator, as expected in a supersolid. This TO experiment stimulated the study of other characteristics of the material, along with further TO experiments. Later, a shear modulus experiment [4] showed unusual stiffening in solid helium with similar dependence on temperature and ^{3}He concentration as was observed in the TO experiment. After many experimental studies and theoretical works [5-8], it has been shown that any superfluid like behavior in solid ^{4}He depends on the presence of defects on the sample. Therefore, the effects of crystal defects like vacancies, dislocations and grain boundaries are worth studying in solid ^{4}He.

In this thesis, we will mainly study the shear modulus behavior of solid ^{4}He confined in a porous material, to see the effects of disorder in solid ^{4}He. We grow solid ^{4}He in aerogel (95% of porosity), which should provide effective pinning sites for dislocations. This thesis includes five chapters, including this first Introduction chapter.

In Chapter 2, we briefly describe the TO experiments and the relevant shear modulus experiments. We also describe our motivation for using aerogel and some recent experimental studies involving solid helium in aerogel. Chapter 3 provides experimental details such as the measurement techniques, the instruments used, and details about the properties of aerogel.

In Chapter 4, the experimental results are shown, along with possible interpretations of the observations. In this chapter, we present the results of three experiments. The first is a shear modulus experiment of ^{4}He using vycor in the cell, which we expected would purify the ^{4}He crystal. This is followed by a shear modulus measurement using a new PZT stack design intended to minimize the electronic crosstalk. The last and most important experiment is a measurement of the shear modulus of solid ^{4}He in aerogel. Finally, we summarize the results of thesis in Chapter 5.

Chapter 2

Background

Helium, the most abundant element in the universe after hydrogen, has the highest ionization energy 24.6 eV of any element [9], zero permanent electric dipole moment, and weak diamagnetic susceptibility. It has the lowest boiling point among all elements and does not freeze unless pressure of at least 25 bar is applied. At low temperature it has many unique properties.

2.1 Liquid helium-Superfluidity

Just below its boiling point ^{4}He behaves as an ordinary liquid with small viscosity but a sudden change in its properties at 2.17 K makes it unique. At this temperature, ^{4}He undergoes an unusual transition- a second order phase transition accompanied by a specific heat anomaly. The anomaly is called the λ transition after the λ like shape of the specific heat. The point T_λ is a transition between two different forms of liquid as shown in the phase diagram, Fig. 2.1. One of the phases, normal liquid ^{4}He, known as HeI, occurs above T_λ. The other striking phase, superfluid, referred to as HeII, occurs below T_λ. Superfluidity, the great property of ^{4}He, was discovered 30 years after it was first liquefied by Kamerlingh Onnes. It is now known that ^{3}He and some cold atomic gases also exhibit this phenomenon [10]. Bose-Einstein condensation, a quantum mechanical transition, is responsible for this superfluid phase, which is characterized by

properties such as zero viscosity, a zero entropy component, the fountain effect, and nonclassical rotational inertia.

A theory, based on the ideal Bose-Einstein gas, was developed by Fritz London [11] to explain the phenomenon of superfluidity using Bose-Einstein condensation (BEC). Tisza [12] and Landau [13] used London's approach in liquid helium and proposed a two fluid model for explaining the distinct superfluid behaviour in liquid helium. The two fluid model treats liquid helium as a mixture of two interpenetrating fluid: normal fluid and superfluid. The fractional density of the two fluids varies with temperature, with all becoming superfluid at absolute zero temperature. The Andronikashvili experiment [14] validates the two fluid model by demonstrating the existence of such superfluid and normal fluid components.

The Andronikashvili experiment used a torsional oscillator in which a torsion rod has a pile of closely and equally spaced thin discs suspended on it. The period of this pendulum has the form $P = 2\pi(I/\kappa)^{1/2}$, where I and κ are moment of inertia of the system and the torsion constant of the rod, respectively. The oscillator was immersed in liquid helium and as the temperature dropped below T_λ the period of oscillation decreased sharply. Since temperature doesn't affect the torsion constant, the drop in oscillation period reflects a decrease in moment of inertia, which can only happen if some of the fluid ceases to oscillate with the rest, the behaviour known as nonclassical rotational inertia (NCRI). This NCRI observation validates the two fluid model as a description of superfluidity in liquid helium. Observation of superfluidity in liquid helium motivated theorists to

search for a similar superfluid like state in solid helium and hence the term supersolid was introduced.

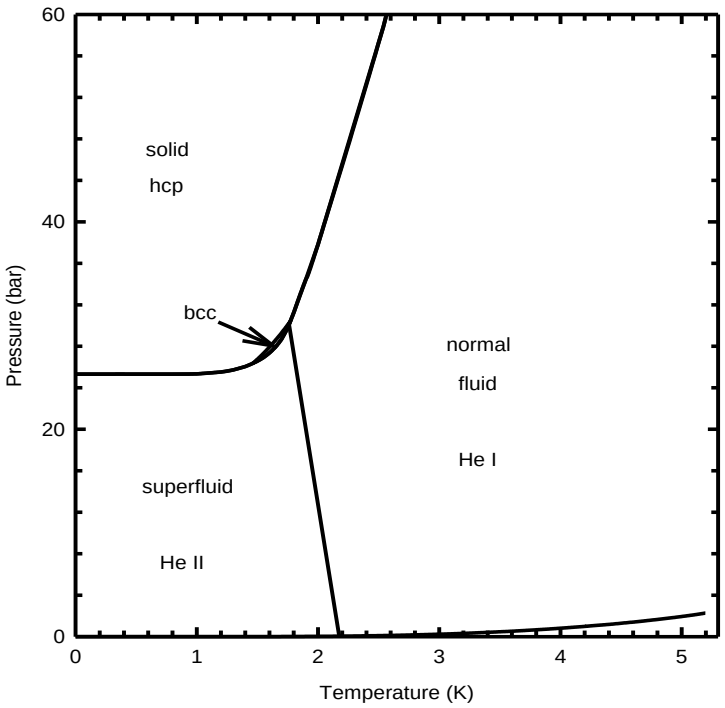

Figure 2.1: Phase diagram of ^{4}He.

2.2 Solid helium- Supersolidity

Superfluid phenomena in liquid helium inspired scientists to search for such phases in solid helium. First, Penrose & Onsager [15] used a mathematical derivation of Bose Einstein Condensation (BEC) and showed that it can occur in liquid helium but not in solid helium. Conversely, Andreev & Lifshitz [1] generalized the mathematical description of BEC and stated that under certain conditions BEC can exist in solid helium, producing superfluidity. Such superfluid like behavior of solid helium was also supported by Chester [16] and

by Leggett [17], who also suggested a superfluid like NCRI behavior in Bose-Einstein condensed solid ^{4}He and proposed a torsional oscillator experiment to detect the NCRI.

Several experiments were designed to study the superfluid behavior in solid ^{4}He. One of these initial attempts was to look for any type of mass flow in solid. Greywall [18] failed to detect any mass flow between two mass reservoirs at different pressures. A high Q mechanical oscillator [19] used to measure the rotational inertia of solid ^{4}He failed to identify any NCRI effect in the solid down to 25 mK temperature. This experiment put an upper limit on the supersolid fraction of less than 5×10^{-6}. Following this, several other experiments were done to see any supersolid behavior, but without any success. An ultrasonic experiment [20] in 1990 argued for possible vacancy induced supersolidity; however, the interpretation of the experiment was unclear.

Following many other attempts, finally in 2004 Kim and Chan detected an NCRI value for solid ^{4}He in their torsional oscillator (TO) experiment [2, 3]. This experiment renewed new interest in supersolidity. Kim and Chan used commercially available ^{4}He (300 ppb of ^{3}He) for growing their polycrystalline sample [2]. They found an increase in frequency below 200 mK, i.e. a drop in rotation period of their oscillator. They suggested it was due to decoupling of a small fraction of the solid helium from the oscillator, the 'nonclassical rotational inertia' (NCRI), which is expected in a supersolid. The onset of decoupling was accompanied by a dissipation peak. The onset temperature increased with frequency and was highly dependent on ^{3}He concentration (X_3). For example, at

X_3~300 ppb, the onset was around 200 mK but dropped to 75 mK at X_3~1 ppb. Although the magnitude of the decoupling was independent of oscillation frequency, its dependence on the amplitude of oscillation suggested a critical velocity of $v_c \approx 10$ μm/s for a possible superflow in the solid.

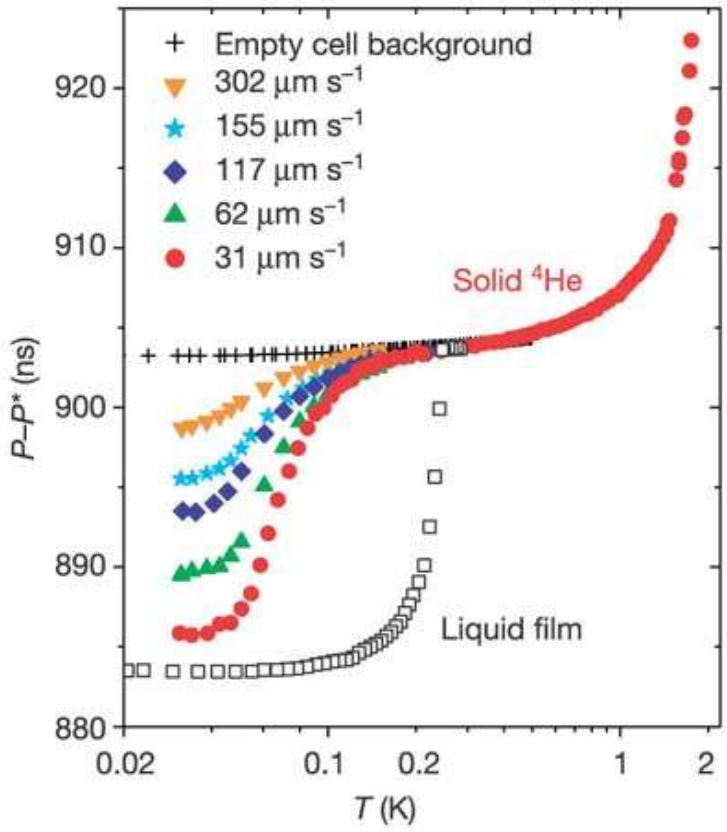

Figure 2.2: Torsional oscillator resonant period as a function of temperature for solid ^{4}He in vycor glass. The onset temperature of the supersolid state is around 175 K where the period ΔP drops. The strong dependence of the magnitude of ΔP on the oscillation velocity is also shown in the plot [2].

Following Kim and Chan's observation, various other experimental and theoretical studies of supersolid behavior in solid ^{4}He suggest that different types of defects such as dislocations [5], grain boundaries [6], and glassy regions [7] are

responsible for the NCRI behavior. Annealing of solid ^{4}He crystal, which reduces defect densities, often reduces the NCRIf [21].

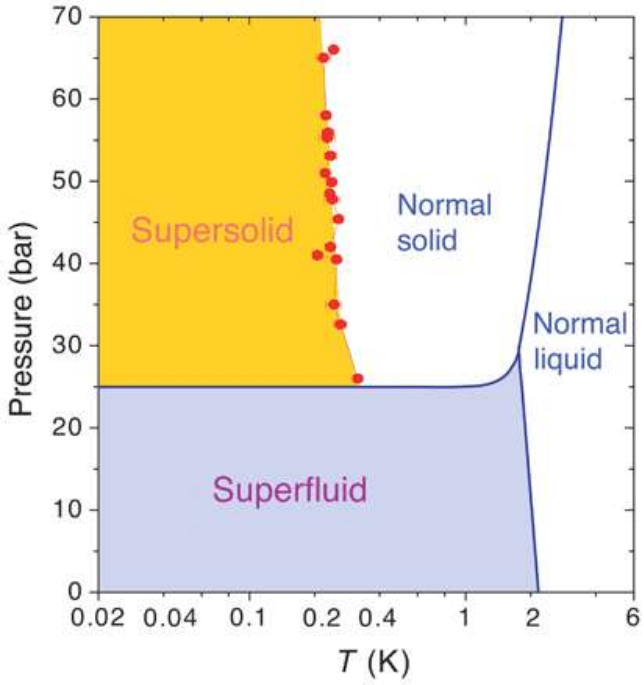

Figure 2.3: Proposed phase diagram of liquid and solid ^{4}He [3].

2.3 Shear Stiffening- mechanical effect

The observation of NCRI in solid ^{4}He began a new era in the field of supersolidity and initiated many other experiments to study other characteristics of this material. Among those, one significant experiment was the study of mechanical behavior of solid ^{4}He. The University of Alberta group developed an experiment to study the shear modulus of solid ^{4}He [4]. An increase in shear modulus was observed, i.e. solid ^{4}He became stiffer by almost by 20 % in the temperature range where the NCRI was detected. The shear stiffness and NCRI must be connected,

based on their similar dependences on temperature, amplitude, frequency, ^{3}He concentration and annealing [4].

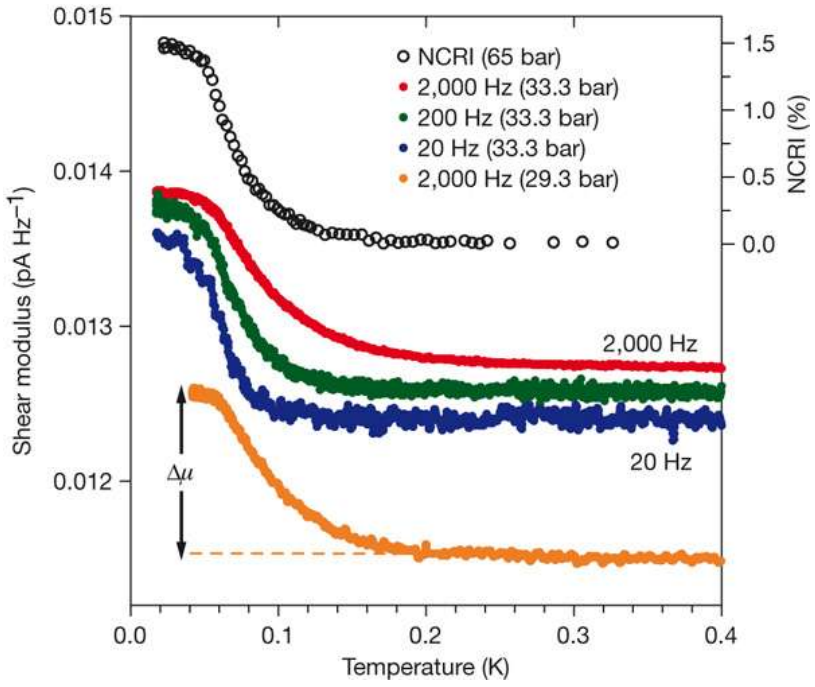

Figure 2.4: Shear modulus of solid ^{4}He as a function of temperature at strain of 2.2×10^{-8}. Shear modulus is measured as I/f; data have been offset for clarity [4].

Figure 2.4 shows the increase in shear modulus. The stiffening in shear modulus is explained in terms of a dislocation network. Dislocations are one dimensional crystallographic defects or irregularities in a crystal and are created during crystal growth or deformation. At low temperature, dislocations are pinned by ^{3}He impurities which results in an increase in shear modulus. As the temperature rises, thermal excitation unbinds the ^{3}He atoms and unpins the dislocations, and the mobile dislocations reduce the shear modulus [4]. Similar stiffening of solid ^{4}He was observed in the low frequency acoustic measurements of Yu Mukharsky et al. [22].

The KAIST group developed a new experiment to measure the shear modulus and NCRI simultaneously [23]. They designed a TO cell with an annular channel and a centre channel in the inner structure. The shear modulus measurement was done with a pair of shear piezoelectric transducers, placed in the centre channel of the TO cell. The geometry of their cell avoids interference between the shear modulus and NCRI measurements. As the temperature was lowered, they saw a 0.5% change in acoustic resonance frequency and more than 20% change in shear modulus, with similar temperature dependences [23].

In a recent experiment, X. Rojas et al. [24] measured the elastic properties (from the acoustic resonance frequency) of high quality single crystals. The crystals were grown from ultrapure ^{4}He gas at 25 mK in contact with a liquid in order to trap all ^{3}He impurities during growth. They found stiffening of the crystal at low temperatures after the sample was warmed up to 300 mK and cooled again, but no stiffening when the crystal was first grown.

2.4 Calculations of ^{3}He concentrations (X_3) in solid ^{4}He using vycor

If the solid helium is grown at low pressure, e.g. less than 35 bar, in contact with vycor, the liquid in vycor pores won't be frozen [25]. On the other hand, previous experiments [26] showed that if there is any liquid left in equilibrium with the hcp solid ^{4}He, the ^{3}He atoms will move to the liquid, making the solid ^{4}He more pure. This happens because the binding energy for ^{3}He atoms in liquid ^{4}He is larger than in bulk solid ^{4}He by 1.359 K [26].

C. Pantalei et al. [26] have derived an equation relating ^{3}He concentrations in solid and in liquid ^{4}He at temperature T.

$$\frac{X_3^h}{X_3^L} = 4.43T^{-3/2}\exp\left(\frac{-1.359}{T}\right) \qquad 2.1$$

Using the total volumes of our cell (10 cm^3) and of the vycor (0.68835 cm^3) in the cell (which gives a total volume for solid and liquid ^{4}He of 9.3116 cm^3 and 0.12743 cm^3, respectively), the equation above can be used to find the ^{3}He concentration X_3 in the solid at equilibrium. The results are shown in Fig. 2.5 for two different gas purities (300 ppb and 1 ppb ^{3}He).

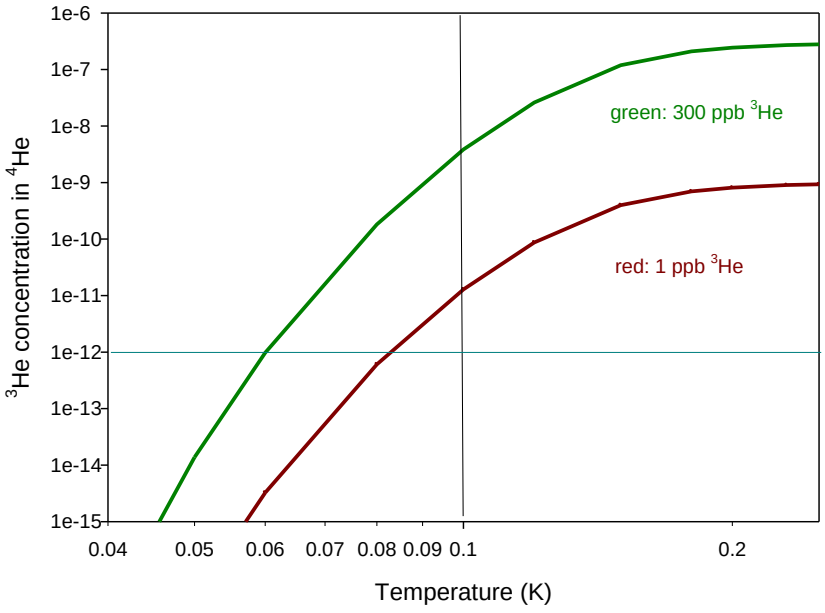

Figure 2.5: ^{3}He concentration (X_3) in solid ^{4}He with Temperature (a) for 1 ppb ^{4}He gas (b) for 300 ppb after using the vycor.

Figure 2.5 shows that the ^{3}He concentration in solid ^{4}He at 100 mK should reach 1.3×10^{-11} with 1 ppb ^{3}He and 6×10^{-9} with 300 ppb ^{3}He with vycor in the cell.

The plot also shows that to reach a ^{3}He concentration in solid ^{4}He of 1×10^{-12} with commercially available ^{4}He (300 ppb of ^{3}He) and with ultrapure ^{4}He (1 ppb of ^{3}He) requires temperatures of 60 mK and 82 mK, respectively.

2.5 Aerogel

Aerogel is a material which has the lowest bulk density of any known porous solid. It plays an important role in the investigations of phase transitions in quantum fluids, where its pseudo-random arrangement of pores and unparalleled openness in structure provide a source of static and quenched disorder.

Generally, aerogel is made by two major steps- forming a wet gel and then drying the wet gel to form an aerogel. The wet gel is made by aqueous condensation of a silica source like tetramethyl orthosilicate (TMOS, $Si(OCH_3)_4$), tetraethyl orthosilicate (TEOS, $Si(OCH_2CH_3)_4$) or sodium silicate (water glass). To speed up the gelation, a small amount of acid or base and water are used as catalyst (an acid catalyst causes shrinkage during supercritical drying and produces a less transparent aerogel than a base catalyst) (for more details see [27]).

The wet gel, called an alcogel, has a solid and a liquid part; after the supercritical drying the liquid part is removed and the remaining porous solid is referred as an aerogel. By diluting the reactant mixture the density and porosity of aerogel (up to 99.9% porosity) can be controlled.

The aerogel (with density 110 kg/m^3 and 95% porosity) used in my studies was synthesized from TMOS using a one step, base catalyzed process with 0.015M ammonium hydroxide used as catalyst to speed up the gelation [28].

Table 2.1: Details of the aerogel used in my studies [28].

Porosity	Density Kg/m3	Gelation time	TMOS		NH4OH aq		Methanol	
			mL	moles	mL	moles H2O	mL	moles
95%	110	a few hours	3 mL	0.019	0.73	0.040	7.3	0.18

2.6 Mechanical Properties of aerogel

In an aerogel, a network of strands of nanometer sized silica particles forms an open structure. The tenuous silica structure of aerogel results in very low elastic moduli, orders of magnitude smaller than the elastic moduli of corresponding bulk solids [29].

A relationship between the structure and properties of high-porosity materials such as aerogel has been developed by Ma et al. [29]. According to them [30], the total elastic Young's modulus (a combination of shear modulus and

bulk modulus) (E) of aerogels has a power law dependence on density (ρ) such that

$$E \propto \rho^m$$

where m is the the scaling exponent and has a value of 3–4 [30].

Most porous media are dense so that they have large elastic constants but aerogel's low elastic constants are a consequence of its low density.

In the aerogel (used in my experiment) with density 110 kg/m^3 and 95 % porosity, the bulk modulus measured is $K_b \approx 0.43 MPa$ [31]. Therefore, with a typical ratio of transverse and longitudinal sound speed in aerogel of $v_t / v_l \approx 1/1.6$, , and using the relations $v_l = \mu + \frac{4}{3} k_b$ and $\mu = v_t^2$, the estimated shear modulus of aerogel is $\mu_{aerogel} \approx 3 \times 10^5 Pa$, which is 100 times smaller than with the shear modulus of solid ^{4}He, $\mu_{He} \approx 2 \times 10^7 Pa$.

In an acoustic measurement, Daughton et al. [29] showed that the low temperature shear modulus of aerogel is roughly same as that at room temperature.

2.7 Freezing and Melting of solid ^{4}He in aerogel

Since we plan to study solid helium in aerogel and to use liquid helium in the pores of vycor, it is vital to know how helium freezes and melts in these media.

There is a narrow range of pressure where helium is partially frozen in aerogel or in vycor too but that range is much smaller in aerogel than in vycor. From the phase diagram of aerogel, Fig. 2.6, we found that at pressure above 30 bar there should be no liquid remaining in aerogel at low temperatures [25].

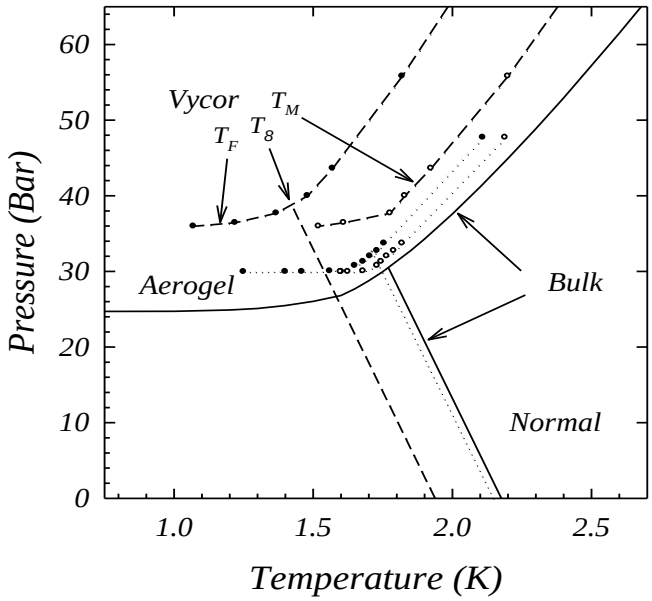

Figure 2.6: Phase diagram of ^{4}He in aerogel and vycor [25].

2.8 Motivation of the thesis

In 2008, torsional oscillator and X ray diffraction experiments on solid ^{4}He in aerogel carried out by N. Mulders et al. [32] showed that solid ^{4}He grown in aerogel, which is highly disordered, behaved like a high quality crystal (e.g. grown by constant pressure method) rather than a poor quality crystal (e.g. grown by blocked capillary method).

They found that the solid ^{4}He in aerogel (with porosity of 95%) had a crystallite size of 100 nm and a grain boundary size of 0.3 nm. Therefore, at least 1% of solid ^{4}He is in grain boundaries and hence the NCRIf was expected to be large. But they observed 0.04% NCRIf which is similar to that in high quality crystals [32]. High quality crystals have very few grain boundary or sometimes may not have any, but in the TO experiment with aerogel they concluded that the solid ^{4}He in aerogel behaves like high quality crystal even though it's not and has grain boundaries [32].

Inelastic neutron scattering studies by Kalinin et al. [33, 34] showed a roton-like dispersion curve at temperatures below 0.6 K, suggesting the existence of superfluid state in solid ^{4}He grown in silica aerogel at higher pressure (51 bar).

It's believed that dislocations are the most likely form of disorder associated with NCRIf in TO experiments and stiffness in shear modulus experiments [4, 32]. In bulk solid ^{4}He, dislocation line densities may be around 6×10^9 per cm^2, whereas the silica strand density in aerogel is 10^{11} per cm^2, which is much higher than the dislocation density [32]. This high strand density should give more pinning sites for dislocation lines which should increase the stiffness and NCRIf even more effectively than by pinning by ^{3}He impurities.

Kim and Chan's torsional oscillator experiment on solid ^{4}He and their discovery of a possible supersolid state [2, 3] have attracted the attention of both experimentalists and theorists during the last few years. Many experiments have been done and are ongoing to understand this state, including heat capacity

measurements [35], DC mass flow [36, 37], and different TO experiments. These magnificent works motivated my research on solid ^{4}He. My main objective is to see the effect of disorder in solid ^{4}He on dislocations by growing crystals in aerogel and studying the shear modulus behavior.

Chapter 3

Experimental Details

The basic technique for shear modulus measurements in solid ^{4}He is to excite one piezoelectric transducer (emitter) using a voltage generator [4]. This produces shear displacement in the emitter and as a result, the sample between the transducers is subjected to a strain. This induces a stress on the receiver transducer and creates charge on it. We measure this charge as a current to get the shear modulus of the sample. Therefore, we need something to generate a drive voltage, a preamplifier to amplify the small signal current and a device to measure/record the signal.

3.1 Temperature Measurements

The apparent supersolid behavior of solid helium was observed at temperatures below 200 mK [2-4]. My experiment was to study this unusual behavior, so it was important to measure the temperature carefully. Several things should be considered in choosing appropriate thermometers for low temperature studies. When secondary thermometers are used, they should be properly calibrated using fixed temperature points and primary thermometers; thermometers should be in good thermal contact with the object whose temperature is to be measured so a material with very high thermal conductivity should be chosen to mount the

thermometer, and the internal response time of the thermometer should be conveniently short.

Two thermometers were used in these experiments: a germanium resistance thermometer and a ^{60}Co nuclear orientation thermometer.

A germanium resistance thermometer is the main thermometer used in my experiments above 50 mK, chosen for its stability of calibration (+/- 0.5 mK reproducibility at 4.2 K), sensitivity and quick response (200 ms thermal response time at 4.2 K). Digital temperature controllers (Conductus LTC-21 and Neocera LTC-21) were used with the thermometer to measure and control the temperature.

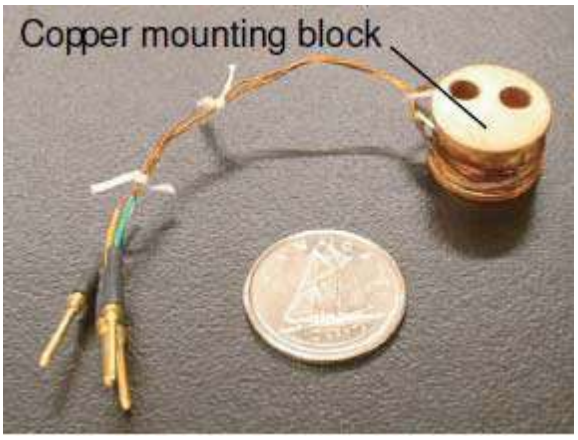

Figure 3.1: The germanium resistance thermometer with its four leads, in a cylindrical copper mounting block [38].

Germanium thermometers are not reliable below about 50 mK, so another thermometer is needed. A ^{60}Co nuclear orientation thermometer was used at lower temperatures. This is a primary thermometer based on the magnetic ordering of nuclear spins, detected by emission of γ rays. It doesn't require any electrical

connections and the high penetrating capability of the high energy γ rays allows for their detection outside of the cryostat. A *NaI* scintillator and a new γ spectrometer were used to measure the count rates. It is useful at temperatures from 50 mK to the fridge's lowest temperature.

3.2 Pressure Measurements

The dependence of supersolid behavior of solid helium on the sample pressure [39] and the different freezing and melting points of solid He in porous materials make accurate pressure measurements important. Measuring pressure in a solid is more difficult than in a liquid since it cannot be done externally. Therefore, a homemade Straty-Adams [40] capacitive gauge with high sensitivity, stability and little temperature dependence below 4.2 K was used to measure the pressure *in situ.* The idea of the gauge is that two capacitor plates come closer to each other in response to an increase of pressure, thereby changing the capacitance. The pressure is determined from the capacitance measured by an automatic digital bridge operating at a frequency of 1 kHz (Andeen-Hagerling 2550A). The capacitance is converted into pressure using calibration data for liquid helium at 4.2 K (capacitance versus pressure in the room temperature gas handling system, measured with a Mensor gauge).

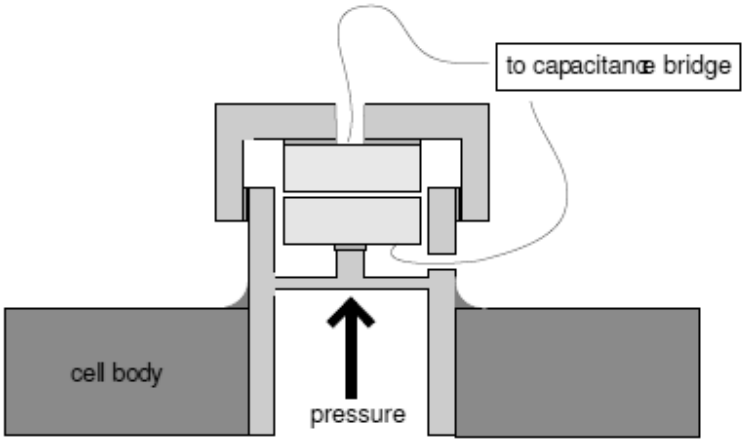

Figure 3.2: Schematic of a Straty-Adams pressure gauge [38]

3.3 Cell Construction

The shear modulus experiment with vycor inside the cell, the measurement with new PZT stacks and the experiment with solid helium in aerogel were all done in the same cell, shown schematically in Fig. 3.3. The samples we studied were grown using the blocked capillary method (discussed more details in Chapter 3.4) so pressures above 1050 psi were required to get a 35 bar solid sample. The cell must allow such high pressures and have a large thermal conductivity at low temperatures. Oxygen-free high-conductivity copper (OFHC) was used to make the cell, which consisted of a large inner volume (18 cm^3) into which our piezoelectric shear transducers were positioned using a brass holder screwed onto the cap of the cell. The transducers were epoxied onto solid brass backing pieces, making sure that the transducers were parallel to each other, and electrically insulated from the brass. Then the backing pieces with transducers were mounted

onto the brass holder. In the aerogel experiment, an aerogel piece of 12 mm diameter and 0.8 mm thickness was held tightly between the transducers without using any glue.

The cell was then mounted onto the bottom of the mixing chamber of the dilution refrigerator using another copper piece (since the cell's screw holes did not match the mixing chamber's holes). ^{4}He gas was admitted the cell through a CuNi capillary thermally anchored at several places on the dilution fridge.

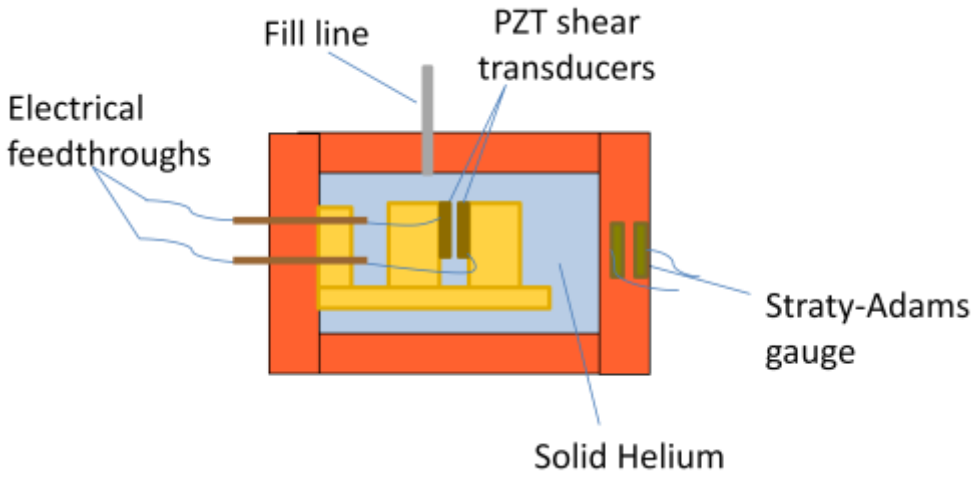

Figure 3.3: Schematic of the cell.

3.4 Crystal growing method

^{4}He does not solidify, even at low temperatures, unless pressures of at least 25 bar are applied. The simplest technique to grow helium crystals is the blocked capillary method (constant volume growth). This method results in polycrystals

with more defects than the other two methods used for high quality crystals: growth at constant pressure and at constant temperature. All the samples used for my studies were grown using the blocked capillary method. In this method, the cell is filled with liquid at high pressure (which depends on the desired pressure of the solid) at liquid helium temperature (4.2 K) and then the cell is cooled. Usually, we start with liquid at about 72 bar and end up with a solid at a pressure of about 35 bar. The fill line to the cell is anchored at the fridge's 1K pot, still, heat exchangers and mixing chamber, which are colder than the cell when the fridge is started by pumping on the 1K pot, so the fill line gets blocked by solid ^{4}He. As the fridge continues to cool, the constant volume of liquid in the cell starts to solidify and the pressure drops. The pressure continues to drop as the temperature is lowered until solidification is complete. The thermodynamic path, i.e. the pressure vs. temperature curve, shows when solidification is complete and this plot also gives the final pressure and the melting point of the sample.

3.5 Shear Modulus Measurements Techniques

Solid helium is grown between the gap of the two transducers and in the surrounding volume. An AC voltage V at frequency f is applied to the driving transducers, producing a proportional shear displacement $\delta x = d_{15}V$ at its front face, where d_{15} is the piezoelectric constant of the piezoelectric transducer. This gives a shear strain $\varepsilon = \delta x / D = d_{15}V/D$ in the solid helium in the gap (D) and a charge is then produced on the second transducer due to the resulting shear stress

$\sigma = \mu\varepsilon = \mu d_{15} V / D$. The charge generated on the face of the stressed electrode is $q = d_{15}\sigma A$ where A is the area of the electrodes. This charge on the second transducer was then measured as a generated current $I = \omega q = 2\pi f q = 2\pi f d_{15}\sigma A = 2\pi f d^2{}_{15}\mu V A / D$, using an ultra low noise current preamplifier. The minimum detectable stress is $\sigma \sim 10^{-5}$ Pa which corresponds to strain $\varepsilon \sim 10^{-12}$. For fixed drive voltage, the shear modulus of the solid helium is thus proportional to I/f [4].

$$\mu = \sigma / \varepsilon = \left(D \big/ 2\pi A d^2{}_{15} V \right) \left(I \big/ f \right) \tag{3.1}$$

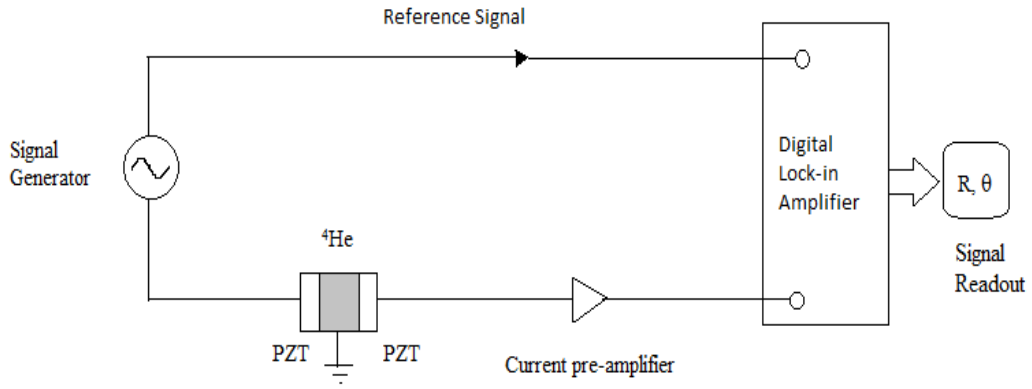

Figure 3.4: Block diagram for the shear modulus measurements.

3.6 Function generator

To excite the emitter piezoelectric transducer, a voltage V was applied at frequency f, using a synthesized function generator (Stanford Research System,

model DSP345). This function generator can produce/generate our desired sinusoidal output with a frequency resolution of $1\,\mu Hz$. Another feature of the signal generator is its switchable amplitude, from 10 mV_{pp} to 10 V_{pp}, which allowed measurements at very low strains.

3.7 Different Preamplifiers

In measuring the shear modulus, we use a simple method - measuring the charge as current instead of voltage. The idea is to use a current preamplifier and detect the signal with a lock-in amplifier.

We use a current amplifier because 1) if we use voltage amplifier we would need very high input impedance (because the PZT has small charges and we want to work at low frequencies) and there are stray voltages much larger than the signal and 2) so that the coaxial cable's capacitance doesn't reduce the signal.

The output current in the shear modulus measurements is very small (in the picoampere range) and the signal-noise ratio is crucial so we use a low-noise current preamplifier together with a lock in amplifier. The current preamplifier injects its own noise but this can be very small. We used three different ultra-low-noise current preamplifiers for measurements in different frequency ranges. These were:

1. **Femto LCA-2-10T:** The preamplifier with the lowest, 0.18 $fA/\sqrt{Hz}$, equivalent noise current, a switchable bandwidth of 0.1, 0.3 and 2 Hz and

switchable gain of $1\times10^{12}V/A$ or $1\times10^{13}V/A$ for the low frequency measurements.

2. **Femto LCA-200-10G:** A similar preamplifier for measurements at higher frequencies, with a 200 Hz bandwidth, a noise current of 1.5 $fA/\sqrt{Hz}$ and a gain of $1\times10^{10}V/A$.
3. **Femto LCA-20K-200M:** Another preamplifier with a 20 kHz bandwidth, 14 $fA/\sqrt{Hz}$ equivalent noise current and a gain of $2\times10^{8}V/A$. This allowed us to sweep frequency up to 10 kHz to look for resonances in the sample to ensure that they do not affect the results.

3.8 Lock-in amplifier

Although the amplified signal has very low noise, the next question is how to measure the signal. To do this, a two phase digital lock-in amplifier (Stanford Research System model SR830 DSP) was used. This gave the amplitude and the phase of the current *I* and allowed the noise to be further reduced by averaging over an adjustable time constant.

3.9 Piezoelectric transducers

Piezoelectric transducers convert energy from one form to another. A piezoelectric element can be used as either a transmitting or a sensing element

since it deforms mechanically when voltage is applied between its faces and it produces a charge when mechanical force is applied to its face.

Two parallel shear transducers with the same thickness and area were used to generate displacements and to detect stresses in the helium-filled gap between their faces. The sizes and dimensions of the transducers are discussed details in the Results chapter.

All the shear transducers used in my studies were made from PZT 5A bought from 'Boston Piezo Optics'. The piezoelectric constant is $d_{15} = 585 \times 10^{-12} m/V$ [41] at room temperature and drops to $d_{15} = 1 \times 10^{-10} m/V$ below 4.2 K. The overlapping area of the transducers $\approx 1.2 \times 10^{-4} m^2$, and the gap between the transducer is 0.8 mm.

3.10 Transducers design

Epoxy layers don't affect transducers' sensitivity but the dielectric constant of PZT (~2000) [41] is enormous compared to that of epoxy (~2) [42] so even thin epoxy layers matter. If the transducers are not properly designed, there is a chance that most of the voltage would be dropped across the epoxy with only a very small drop across the transducers, which is certainly not good for our measurement. A simple calculation below describes this more clearly.

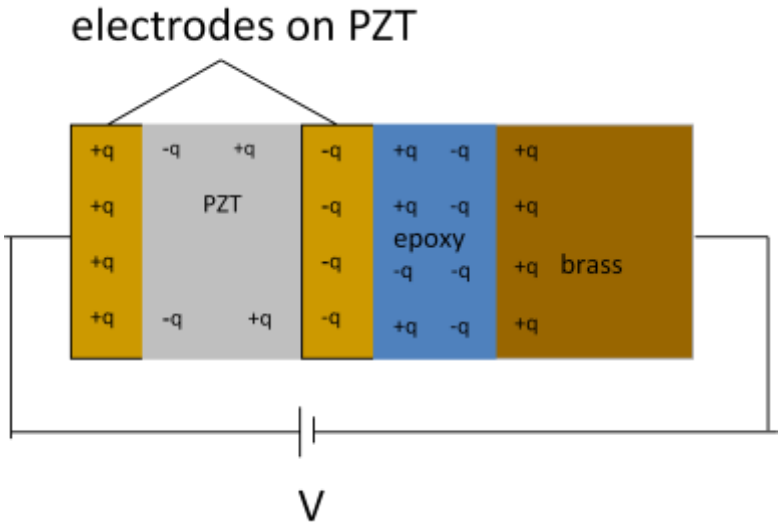

Figure 3.5: The schematic of piezoelectric transducers epoxied with brass piece.

Figure 3.5 shows that a piezoelectric transducer glued to the mounting piece (brass) with blue epoxy (insulator) behaves like two capacitors in series. If the voltage is applied between the front face and the brass mounting piece, the capacitance of the piezo-ceramic is given by,

$$C_p = \frac{K_p \varepsilon_0 A}{t_p} \tag{3.2}$$

and the capacitance of the epoxy by,

$$C_e = \frac{K_e \varepsilon_0 A}{t_e} = \frac{K_e}{K_p} \frac{t_p}{t_e} C_p \tag{3.3}$$

where t_p, t_e K_p, K_e correspond the thicknesses and dielectric constants of PZT and epoxy.

The total capacitance is

$$C_T = \frac{C_e C_p}{C_e + C_p} = \frac{\frac{K_e}{K_p}\frac{t_p}{t_e}C_p^2}{\left(1+\frac{K_e}{K_p}\frac{t_p}{t_e}\right)C_p}$$

$$\Rightarrow C_T = \frac{C_p}{1+\frac{K_p}{K_e}\frac{t_e}{t_p}} = \frac{C_e}{1+\frac{K_e}{K_p}\frac{t_p}{t_e}} \qquad (3.4)$$

Now, let's estimate some typical values for all the parameters,

The ratio of the dielectric constants of epoxy and PZT is roughly

$$\frac{K_e}{K_p} \approx \frac{2}{2000}$$

and a typical thickness ratio is

$$\frac{t_e}{t_p} \approx \frac{0.05mm}{1mm} = 1/20$$

This gives the total capacitance as

$$C_T \approx \frac{C_p}{1+(10^3)(1/20)} \approx \frac{C_p}{50} \approx C_e \qquad (3.5)$$

The total charge and voltage are related to the total capacitance by,

$$q = VC_T$$

So the voltage across the PZT and epoxy are

$$V_p = q/C_p = \frac{C_T}{C_p} V \approx \frac{V}{50} \tag{3.6}$$

and

$$V_e = q/C_e = \frac{C_T}{C_e} V \approx V \tag{3.7}$$

Most of the voltage is across epoxy because $K_p/t_p >> K_e/t_e$.

The transducer displacement is much smaller when the voltage is applied between the front electrodes and the brass backing piece (i.e. across the epoxy) than when it is directly applied across the transducer's front and back electrodes.

There are two ways to overcome this reduced displacement. One is to apply a higher voltage to get desired voltage across the PZT. The other is to make the epoxy layer very thin ($\leq 1\mu m$), but this is very difficult.

The epoxy layer has a similar effect on the receiving transducer, reducing the measured current if the brass backing piece is used as one of the electrodes. This greatly reduces the signal to noise ratio. Therefore, to avoid this problem, both transducers (emitter and receiver) extend past the brass backing pieces and are offset so that wires can be soldered to their back faces to apply a driving voltage and to measure current directly across the transducers. The front faces were kept grounded in order to reduce electronic crosstalk between driving and receiving transducers.

However, one of the experiments was done with PZT stacks instead of single transducers to minimize the electronic crosstalk (details will be explained in Chapter 4.2). The PZT stacks were made using silver epoxy (conductive) instead of blue epoxy (insulator) to avoid the large voltage drop in across the epoxy- the same reason described earlier.

3.11 Phase issue

The total signal measured in the shear modulus experiments is the combination of the solid helium's modulus contribution (which we are interested in) and the electronic crosstalk (the background signal e.g. in liquid). Whether these contributions add or subtract depends on their relative phases. The phase of the shear modulus signal depends on the direction of the transducers' shear axes. Reversing one of the transducers changes this by 180^0, so the transducer orientations are important. However, although their polarization axes are known, the sign of their polarizations usually are not and so the phase of the shear modulus signal can be either 0^0 or 180^0 and must be determined from the signal in solid helium.

The phase difference (θ) between the background crosstalk (measured in the liquid) and the shear modulus contribution is not directly observable. Instead, we measure the phase difference (ϕ) between the crosstalk and the observed total signal (the sum of the crosstalk and the shear modulus contribution).

Case (a): θ=0

The crosstalk and modulus contributions are in phase (θ=0) so their magnitudes add, giving a larger total signal with the same phase (ϕ =0). The solid's modulus contribution is found by subtracting he liquid background from the total signal measured with solid ^{4}He. This case applied to the measurement in James Day's work [4, 38].

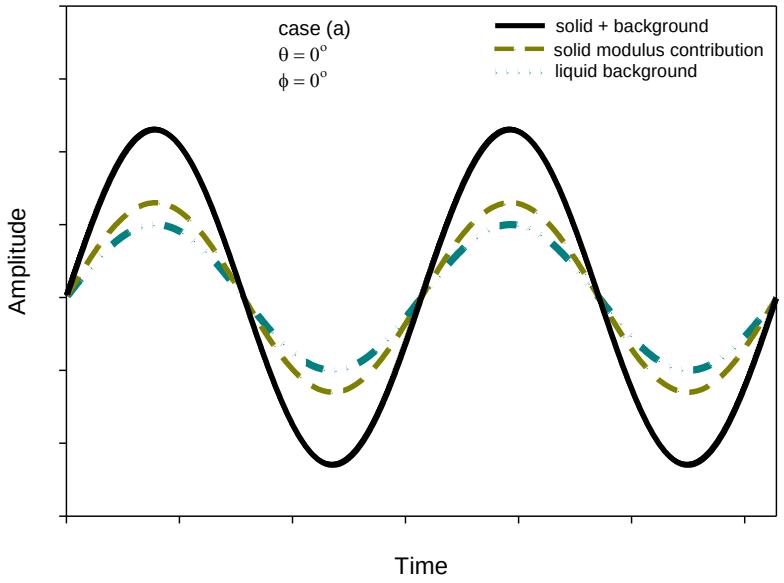

Figure 3.6 (a): Signal with the relative phase difference, θ=0 and ϕ =0.

Case (b): θ=180 and |modulus contribution| < |liquid background|

The modulus contribution subtracts from the liquid background, reducing the magnitude of the total signal, which has the same phase as the liquid signal (ϕ=0). This case applies to the shear modulus measurements with vycor in the cell, described in the next chapter.

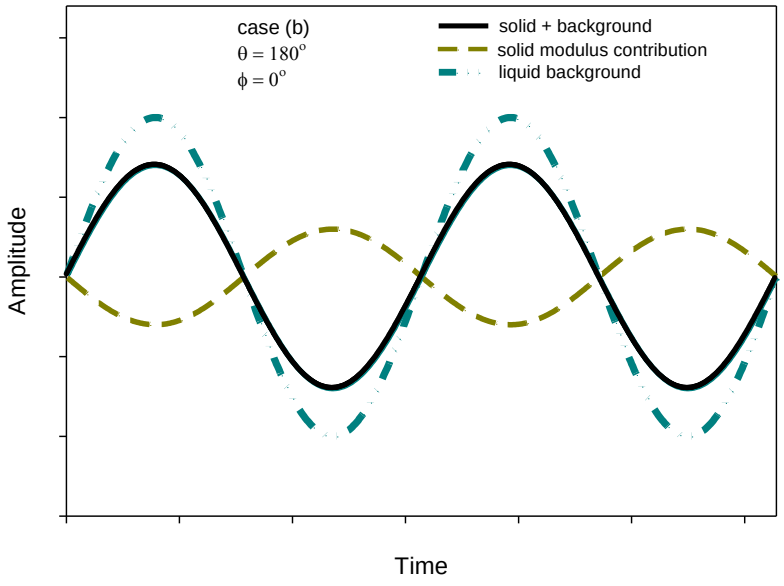

Figure 3.6 (b): Signal with the relative phase difference, θ=180 and ϕ =0.

Case (c): θ = 180 and |modulus contribution| > |liquid background|

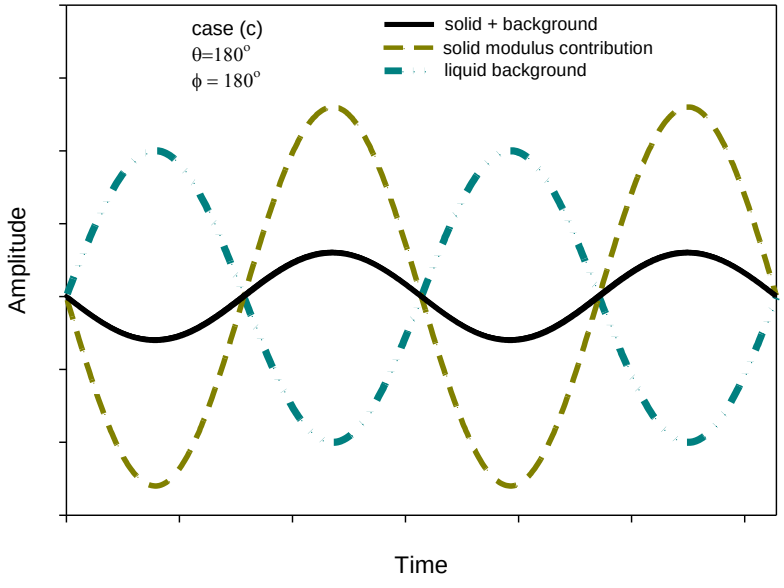

Figure 3.6 (c): Signal with the relative phase difference, θ=180 and ϕ =180.

The modulus contribution again subtracts from the liquid background but, since it is larger, the total signal has the phase of the modulus contribution (ϕ=180). The total signal's magnitude is equal to zero when the two contributions are the same size and is larger than the liquid background if |modulus contribution| > 2 x |liquid background|. This case applies to the measurements with aerogel, described in the next chapter.

All the above three cases then can be drawn as,

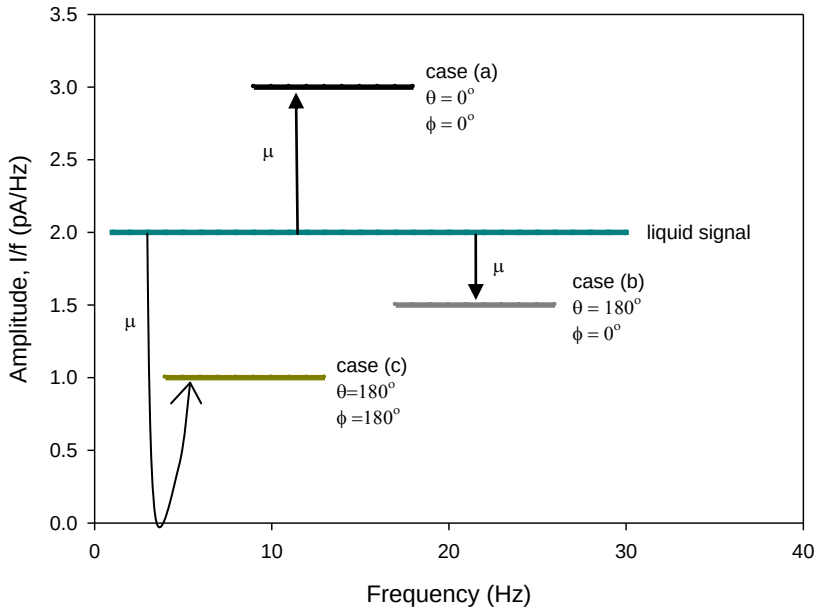

Figure 3.7: Total signal measured in the experiments and relationship to their phase differences.

In the next chapter, in results and discussions, all these three cases will be described in detail with the experimental data.

Chapter 4

Results and Discussions

Supersolid behavior was first observed in torsional oscillator (TO) experiments on solid ^{4}He in porous vycor glass and later in bulk ^{4}He [2]. Later, anomalous shear stiffening was seen in bulk ^{4}He at low temperature [4]. Day and Beamish [4] have explained the shear stiffening as being due to a dislocation network (one dimensional crystallographic defects within a crystal structure, created during crystal growth or deformation). At low temperatures these dislocations are pinned by ^{3}He impurities and the shear modulus increases. The ^{3}He atoms thermally unbind from the dislocations as the temperature is raised, the dislocations are able to move and the shear modulus decreases [4].

We have seen that both TO experiments [43] and shear modulus experiments [4] strongly depend on ^{3}He concentration (X_3). On the other hand, the binding energy for ^{3}He atoms in liquid ^{4}He (1.359 K) is larger than in solid ^{4}He [26]. This means that if there is any liquid left in equilibrium with the hcp solid ^{4}He, the ^{3}He atoms will move to the liquid and make the solid ^{4}He more pure. Details have been discussed in background (Chapter 2.4). We tried to do this by including vycor pieces in the cell. Vycor, a highly porous material, has a porosity of 28% and two thirds of this pore volume is expected to be available for liquid. By growing solid He at low pressure (less than 35 bar, the minimum pressure to freeze liquid in vycor pores), we hoped to get pure solid as the ^{3}He

atoms move to the liquid state in vycor. Using the total volume of vycor in our experimental cell and equation 2.1, I calculated the expected X_3 in the solid (Fig. 2.5). The effect of the vycor on solid ^{4}He will be discussed in the first section of this chapter.

We found that in order to determine the shear modulus of the solid helium itself, the liquid background signal had to be subtracted from the total measured signal. This liquid signal is essentially due to electronic crosstalk which has nothing to do with shear modulus. We designed a new arrangement to reduce the crosstalk and make it easier to extract the signal in the solid. The design was discussed in details in Chapter 3.10. The shear modulus measurements with the newly designed PZT stacks are described in the second section.

In the final section of this chapter, the main experiment, the shear modulus of solid helium in aerogel, is presented. A highly porous material such as aerogel should provide effective pinning sites for dislocations lines in solid ^{4}He grown in its pores. We have measured the shear modulus of solid ^{4}He grown in a 95% porous aerogel (density 110 kg/m^3). The aerogel used in my studies was synthesized from TMOS using a one step, base catalyzed process [28]. These measurements were inspired by previous TO and x-ray diffraction experiments which looked at the effects of disorder on solid ^{4}He in aerogel (95 % porous) [32].

4.1 Shear modulus of solid ^{4}He using vycor in the cell

As described in Chapter 2.4, there is a possibility of making ^{4}He crystals more pure (fewer ^{3}He impurities) by using vycor pieces in the cell. Three vycor pieces

of total volume 0.68835 cm^3 were used for the first experiment. Solid helium was grown in the rest of cell, including the gap of 0.45 mm between the two piezoelectric transducers, using the blocked capillary method.

4.1.2 Sample 300ppb31.7

Figure 4.1 shows the measured thermodynamic path for one sample. Commercial helium gas (300 ppb ^{3}He) was used to grow the crystal. The sample ended up with a pressure of 31.7 bar, which is below than the pressure (~35 bar) at which ^{4}He solidifies in vycor pores. This ensures the vycor pores contain liquid which should bind ^{3}He impurities and purify the crystal.

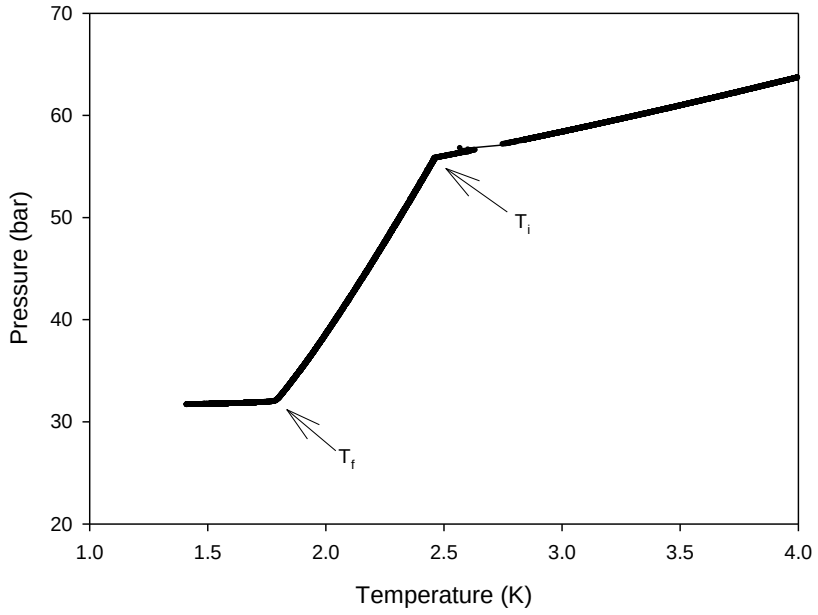

Figure 4.1: The thermodynamic path (pressure vs temperature) for growth of crystal 300ppb31.7. T_i and T_f are the starting and ending temperatures for freezing.

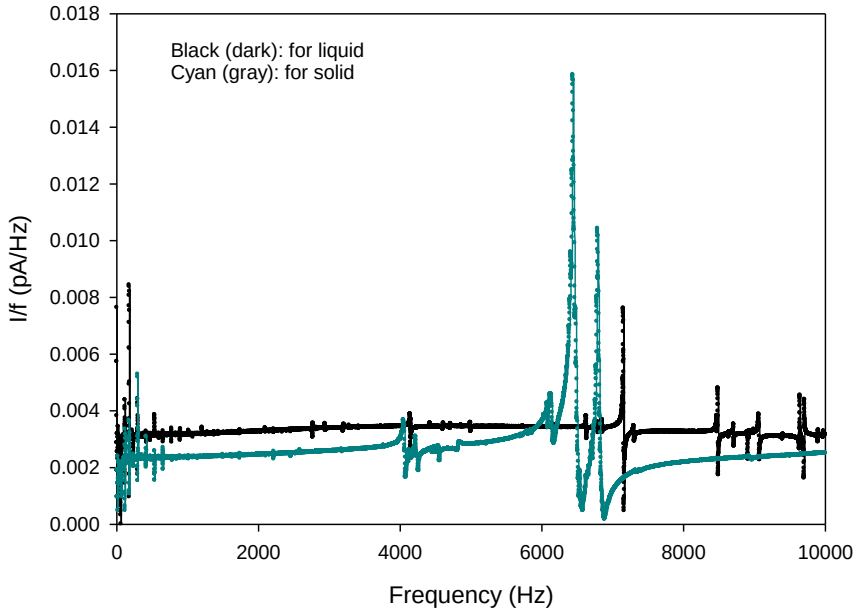

Figure 4.2: The background signal (I/f versus frequency) in liquid (at 4.2 K and 22 bar pressure) and in solid sample 300ppb31.7 (at 43 mK and 31.7 bar), both measured at 52 mV_{pp} driving amplitude.

The liquid background signal (I/f due to electrical crosstalk) and signal with solid helium (the total measured signal including the contribution of shear modulus) are plotted versus frequency in Fig. 4.2. The large peaks in the solid signal (gray) correspond to acoustic resonances of the solid sample. The spikes in the low frequency data (below 2000 Hz) are multiples of the 60 Hz line frequency, which can be avoided. This frequency sweep data was taken with a 20 a kHz bandwidth preamp which has a current noise level of 14 $fA/\sqrt{Hz}$ (see Chapter 3.7 for the comparisons between different preamplifiers).

One of the interesting features of Fig. 4.2 is that the solid signal is smaller than that in the liquid in contrast to the previous shear modulus measurements [4]. As discussed in Chapter 3.11, it is the phase difference between the shear modulus

signal and the electrical crosstalk which makes the solid signal lower than the liquid one. The corresponding phase plot will make this clearer.

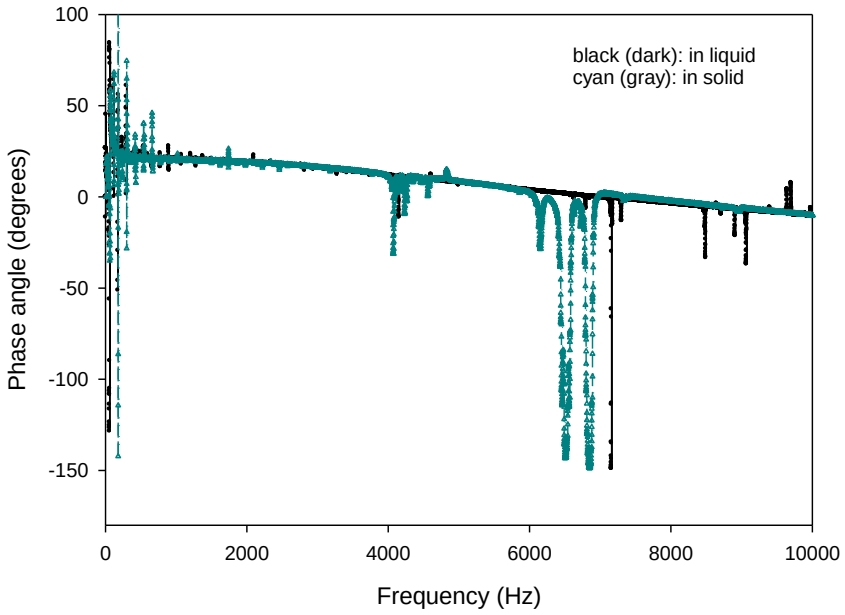

Figure 4.3: Phase angle vs. frequency for the liquid ^{4}He (at 4.2 K and 22 bar pressure) and solid sample 300ppb31.7 (at 43 mK and 31.7 bar), both measured at 52 mV_{pp} driving amplitude.

Figure 4.3 shows that the total solid signal (modulus plus crosstalk contributions) is in phase with the signal in liquid (the crosstalk). Since the solid signal is smaller, the shear modulus contribution is out of phase with that of the crosstalk (see phase issue discussion in Chapter 3.11). In Fig. 4.3 it is difficult to distinguish between the phase of the two signals since they fully overlap except for the features associated within peaks in Fig. 4.2 (downward spikes) which are larger and more numerous in the solid.

The resonance peaks in the frequency sweep plot (Fig. 4.2) make it difficult to take shear modulus measurements above 2000 Hz, so we took measurements at different frequencies lower than 2000 Hz.

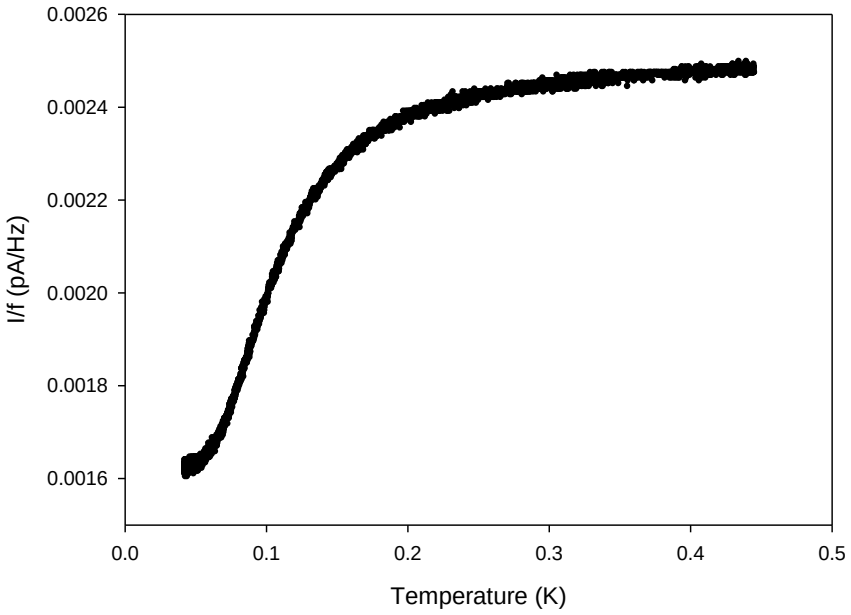

Figure 4.4: Amplitude anomaly as a function of temperature for sample 300ppb31.7 at 1600 Hz and 52 mV_{pp} driving amplitude (raw data).

Figures 4.4 and 4.5 show the temperature dependence of the shear modulus and the corresponding dissipation of the sample 300ppb31.7 measured at 1600 Hz, at a driving voltage of 52 mV_{pp}. The data was taken during cooling.

To explain the plots, it should be remembered that previous shear modulus measurements showed that the solid helium becomes stiffer at low temperature. Those measurements also showed that there is a dissipation peak in the temperature region where the shear modulus changes most rapidly.

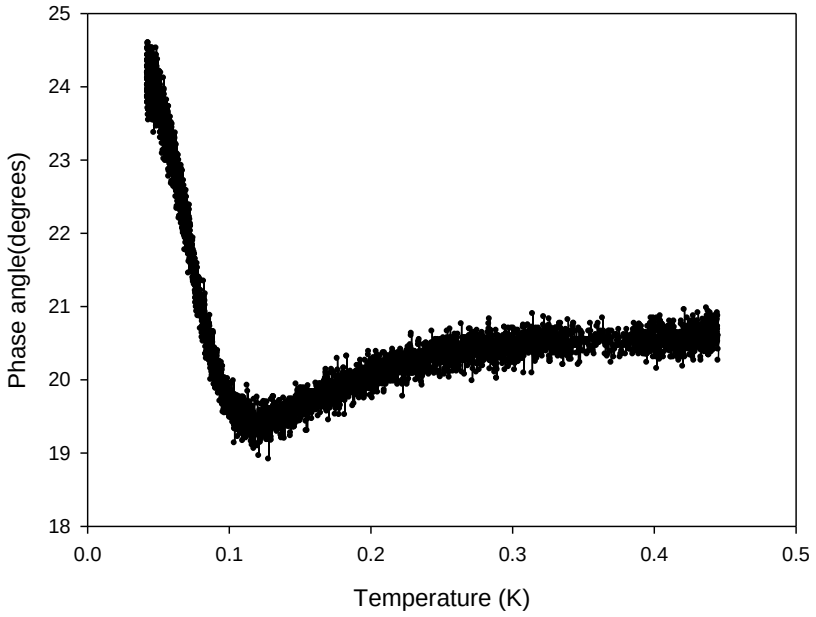

Figure 4.5: Dissipation anomaly as a function of temperature for sample 300ppb31.7 at 1600 Hz and 52 mV_{pp} driving amplitude (raw data).

But, interestingly, from the both shear modulus and dissipation plots (Figs. 4.4 and 4.5), it seems that the solid helium gets softer as the sample is cooled.

These apparently different behaviours are due to the difference between phase of the modulus contributions of solid helium itself and the phase of the crosstalk in the liquid as explained previously.

By subtracting the background signal measured in the liquid, we can correct both the amplitude and the phase, i.e. can determine the contributions due to solid's shear modulus and dissipation. The corrected data is shown in Figs 4.6 and 4.7.

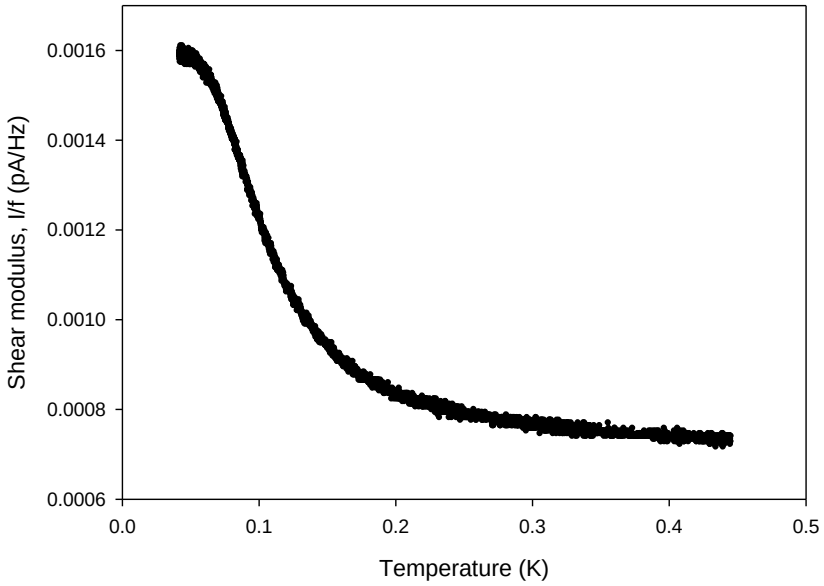

Figure 4.6: Shear modulus anomaly as a function of temperature in the sample 300ppb31.7 measured at 1600 Hz, at a driving voltage of 52 mV_{pp} (corrected).

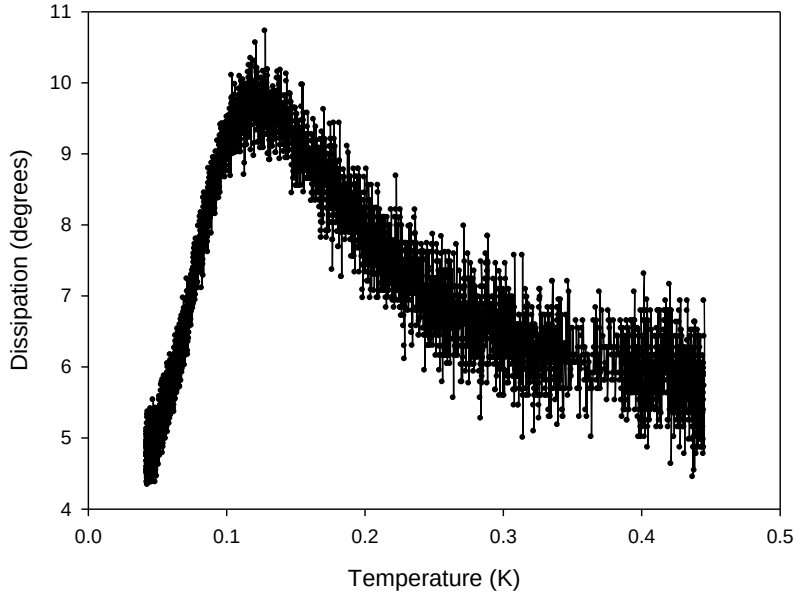

Figure 4.7: Corrected dissipation as a function of temperature in the sample 300ppb31.7 measured at 1600 Hz, at a driving voltage of 52 mV_{pp}.

The corrected plots for both the shear modulus and dissipation show that the solid helium becomes stiffer at low temperature, with an associated dissipation peak. But our hope for the experiment was that the ^{4}He sample would be purified i.e. that the ^{3}He impurities would go to the liquid in the vycor pores. The onset temperature of both the drop in the period of TO experiments [2, 3] and of the stiffening of solid helium in shear modulus measurements [4] shift to lower temperature in samples with fewer ^{3}He impurities. The plots in Fig. 2.5 show the estimated ^{3}He concentration in the solid using our vycor volume. The onset temperature should shift to noticeably lower temperature if the vycor purifies the sample.

However, Figs. 4.6 and 4.7 suggest that using vycor pieces didn't significantly change the onset temperatures, suggesting that they did not purify the sample. As only one set of data is not enough to draw definite conclusions, we took some more measurements in our cell.

Figure 4.8 shows the shear modulus anomaly at a lower frequency, 220 Hz, which also suggests that the onset temperature for stiffening doesn't shift to lower temperature. I took several measurements at different frequencies and at different driving voltage but all of them behaved the same way-the vycor did not reduce the onset temperature.

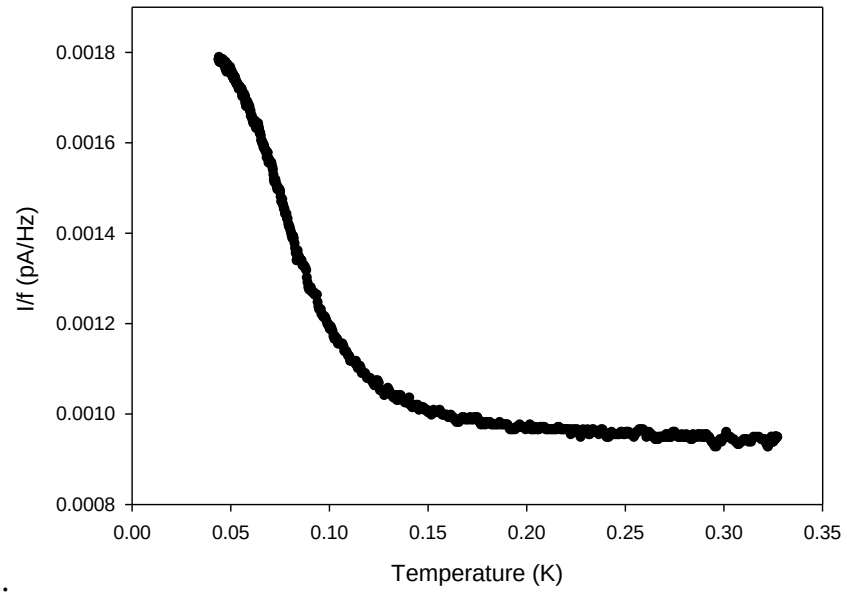

Figure 4.8: Shear modulus anomaly as a function of temperature in the sample 300ppb31.7, measured at 220 Hz, at a driving voltage of 25 mVp (corrected).

4.1.2 Sample 300ppb29

To confirm this behaviour, another crystal was grown at lower pressure using the same constant density method. The thermodynamic path of growing the sample is shown in Fig. 4.9. Figure 4.9 shows that the sample goes through the bcc phase during growth. The inset plot is a blow up of the bcc region. The crystal is at a low enough pressure that the helium in the vycor pores remains liquid.

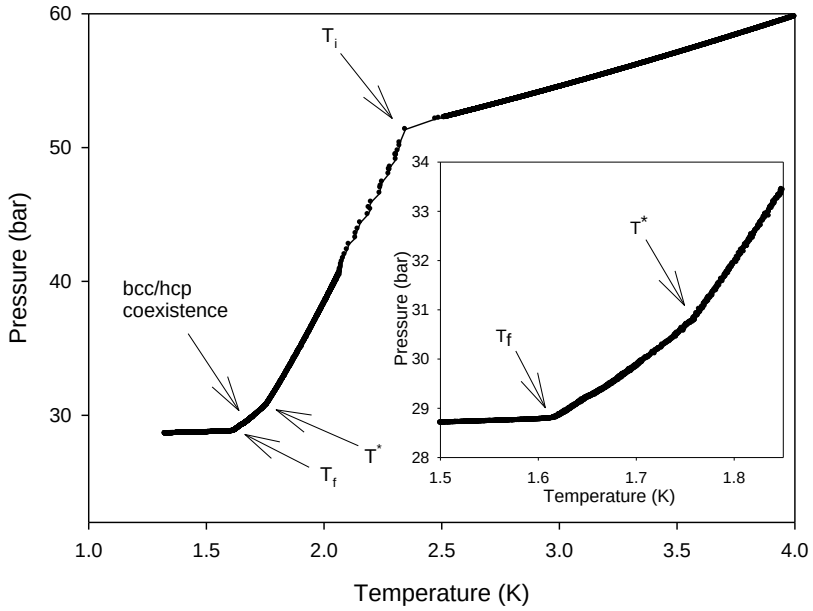

Figure 4.9: Growing a crystal (pressure vs temperature) - the thermodynamic path for the sample 300ppb29. T_i labels for the start of freezing, T^* and T_f indicate the bcc/hcp/liquid triple point and end of bcc/hcp coexistence, respectively.

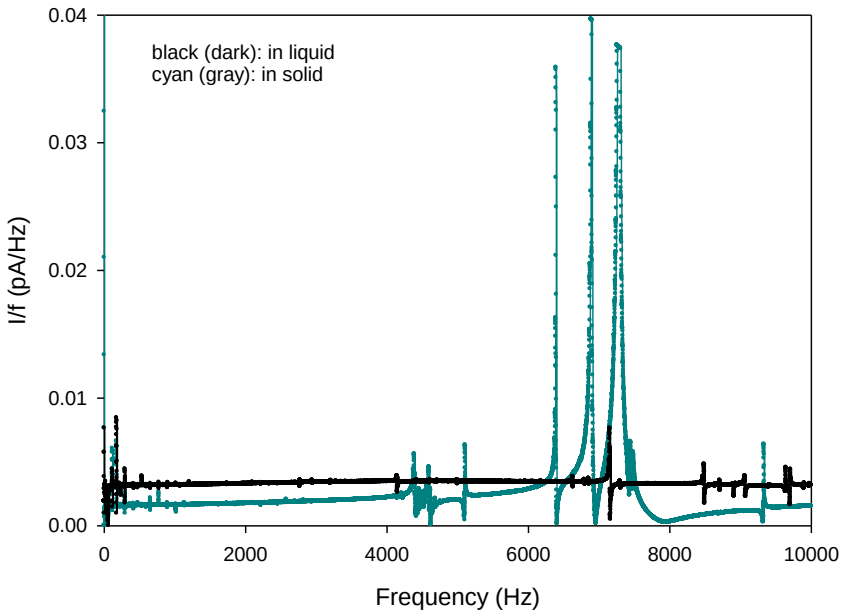

Figure 4.10: The background signal (I/f versus frequency) in liquid (at 4.2 K and 22 bar pressure) and solid sample 300pb29 (at 43 mK and 29 bar), both measured at 52 mV_{pp} driving amplitude.

The frequency sweep plots for this low pressure crystal, in Fig.4.10, are essentially the same as for the previous sample (31.7 bar), i.e. the solid background signal is smaller than that of liquid.

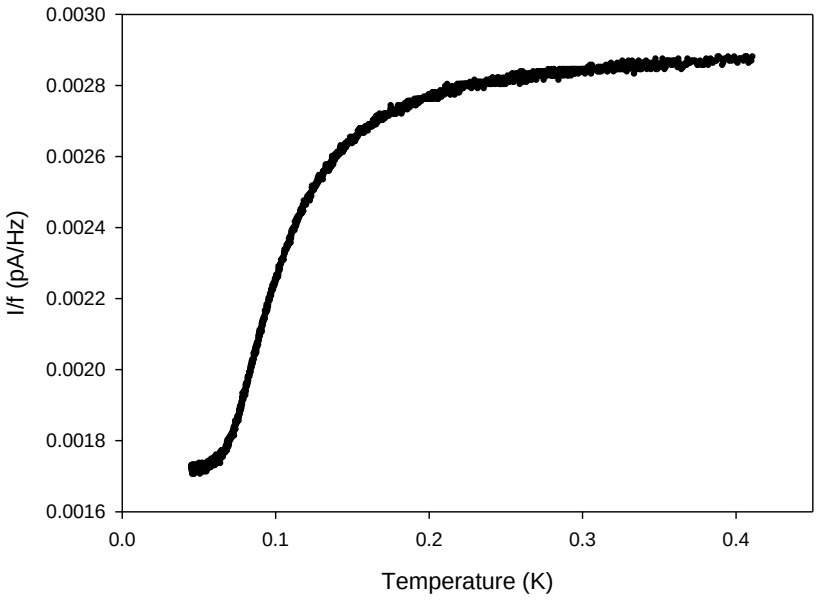

Figure 4.11: Amplitude anomaly as a function of temperature in the sample 300ppb29 measured at 1600 Hz, at a driving voltage of 52 mV_{pp} (raw data).

A couple more measurements at low pressure didn't show any effect of vycor so we are not including the plots, except the shear modulus anomaly with temperature measured at 1600 Hz in Figs. 4.11 and 4.12.

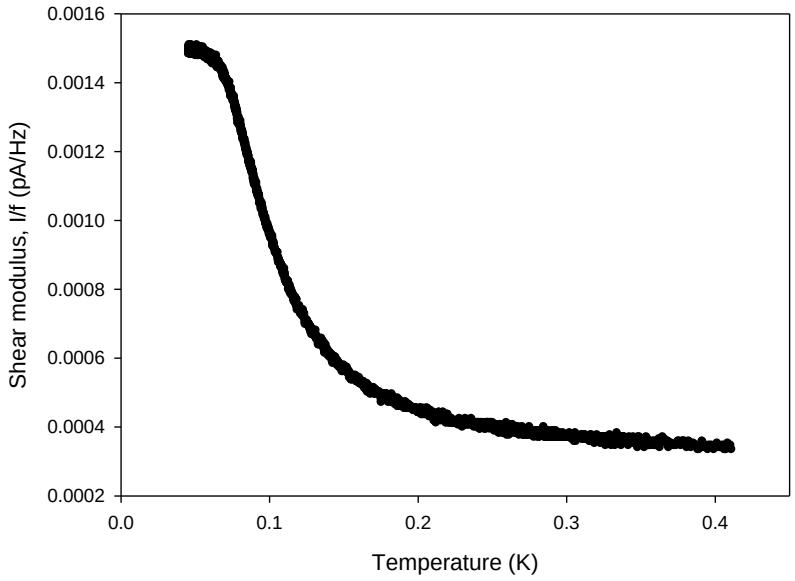

Figure 4.12: Shear modulus anomaly as a function of temperature in the sample 300ppb29 measured at 1600 Hz, at a driving voltage of 52 mV_{pp} (corrected).

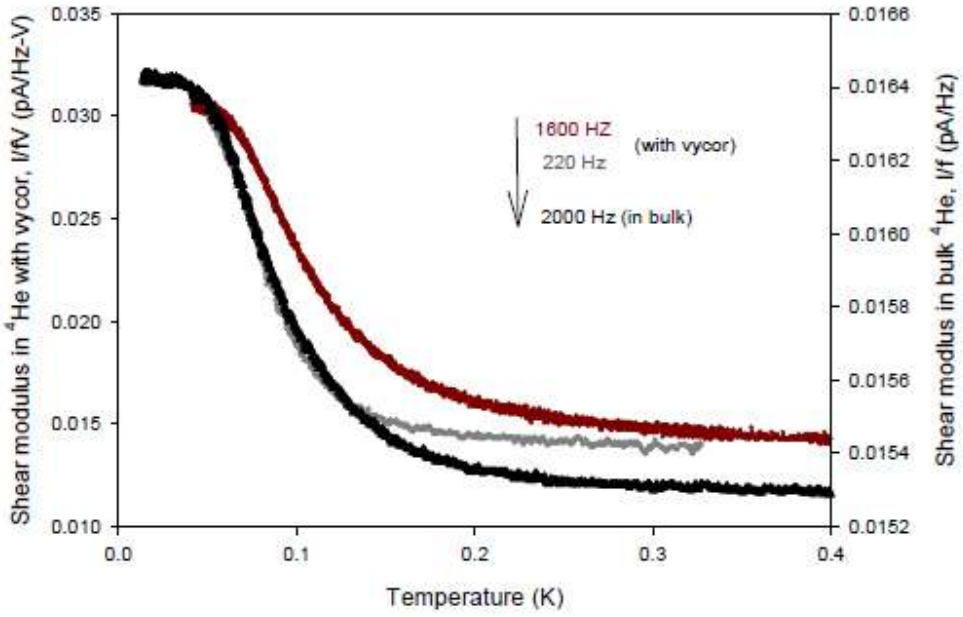

Figure 4.13: Shear modulus anomaly as a function of temperature in the sample 300ppb29 measured at 1600 Hz and 220 Hz (corrected) compared with that in bulk solid ^{4}He in the sample 300ppb33.3 measured at 2000 Hz.

Figure 4.13 shows that the onset temperatures of ~180 mK at 1600 Hz for the shear modulus change in the solid ^{4}He sample with vycor are similar to that in bulk solid ^{4}He, at 2000 Hz with the normal 0.3 ppm ^{3}He concentration [4]. Comparison between 220 Hz data in solid ^{4}He with vycor and 200 Hz data in bulk ^{4}He also show no improvement of the onset temperature of using vycor (not shown here).

Now, the question is why the vycor didn't do anything? Well, that's not really mysterious.

In a recent paper, Rojas et al. [24] shows that high quality ultra pure ^{4}He single crystals can be grown at 25 mK in contact with a liquid. During this growth, essentially all ^{3}He impurities remain stuck in the liquid, leaving the solid very pure. They measured the stiffness from the acoustic resonance frequency and found no stiffening. However, after the sample was warmed up to 300 mK and cooled again, they found that the resonance frequency increased at low temperature, which means the crystal stiffened. They interpreted this as being due to some ^{3}He impurities entering the solid from the liquid at 120 mK and pinning the dislocation network (at 120 mK the equilibrium concentration ratio of ^{3}He in solid and in liquid is 10^{-3}). When the sample is again cooled down, the ^{3}He atoms remain bound to the dislocation network and produce the stiffening. Basically, ^{3}He impurities do not migrate from solid to liquid very quickly i.e. to achieve equilibrium concentrations takes many hours and vibrations may be needed to "shake" ^{3}He impurities off dislocations.

In our case the sample was grown using the constant density method, where the solid forms at high temperatures where the ^{3}He concentration in the solid is not significantly reduced. This means that the ^{3}He atoms do not stay in the liquid left at the vycor pores. At low temperatures they should leave the solid for the liquid but the work of Rojas et al. [24] shows that this is a very slow process. As a result, we saw no effects of the vycor. Unfortunately, the work of Rojas et al. was published after we did these experiments, so we did not realize this until the measurements had been done.

4.2 Shear modulus measurement using a stack of PZTs

In the next experiment, we tried to improve the shear modulus measuring technique. Instead of using single transducers as emitter and receiver, two PZT stacks were designed to try to reduce the background crosstalk and to increase the shear modulus signal so that background corrections are minimized. Details of the design have been described earlier (in Chapter 3.10)

The PZT stacks were made with two transducers which were glued to make the stack by silver (conductive) epoxy with a thin brass sheet between them to apply the driving voltage and to detect the receiver charge (current). A top plate of brass was also glued on the top of the PZT stacks. Silver epoxy was also used to mount the whole thing on the rigid brass backing piece. The new idea of using a brass plate on the top was intended to reduce the crosstalk; it was tested on the bench and worked nicely. We have used conductive epoxy because if an

insulating epoxy (dielectric constant ~2) is used, most of the voltage drop occurs across the epoxy and only a very small voltage is applied across transducer (the dielectric constant of the piezoceramic material is~2000), reducing the transducers' sensitivity (see Chapter 3.10 for details).

A crystal was grown in the cell, including the gap of 0.45 mm between the two PZT stacks, using the blocked capillary method, ending at a pressure of 30.5 bar (Fig. 4.14). We hoped that the modulus contribution from the solid would now be larger than the liquid signal (crosstalk).

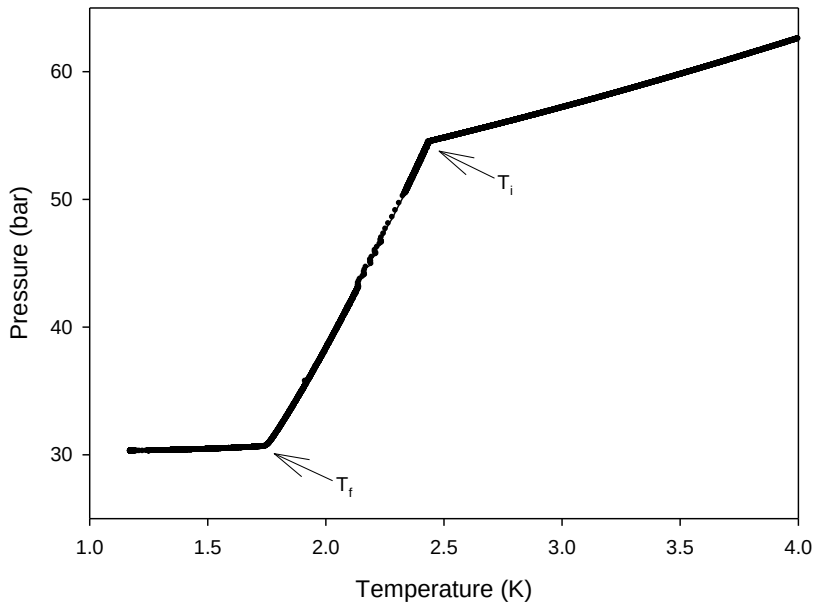

Figure 4.14: Growing a crystal (pressure vs. temperature) - the thermodynamic path for the sample 300ppb30.5. T_i and T_f are the starting and ending points of freezing the crystal, respectively.

Figure 4.15 shows frequency sweeps in the liquid and solid and Fig. 4.16 shows the temperature dependence of the signal amplitude at 635 Hz.

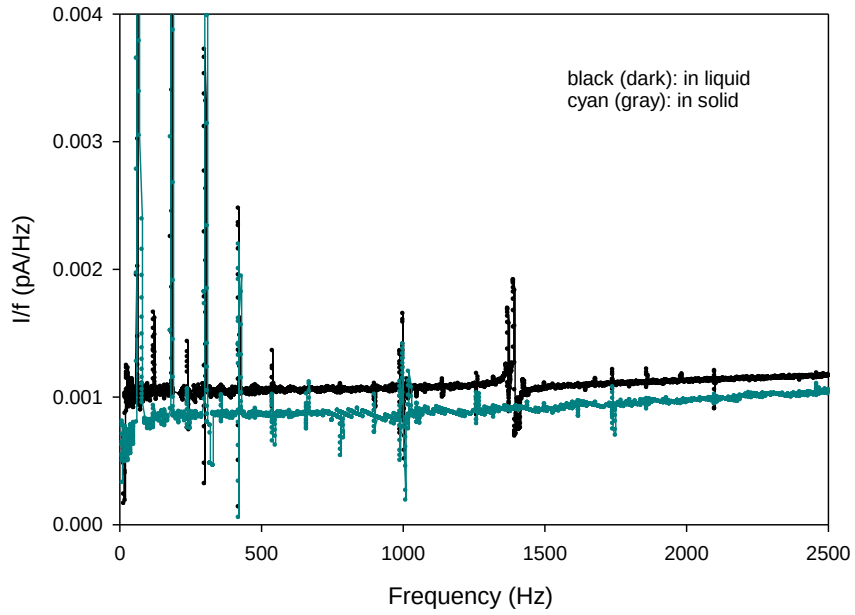

Figure 4.15: The background signal (I/f versus frequency) in both liquid (at 4.2 K and 21 bar) and solid sample 300ppb30.5 (at 1.2 K and 30.5 bar), measured at 100 mV_{pp} driving amplitude.

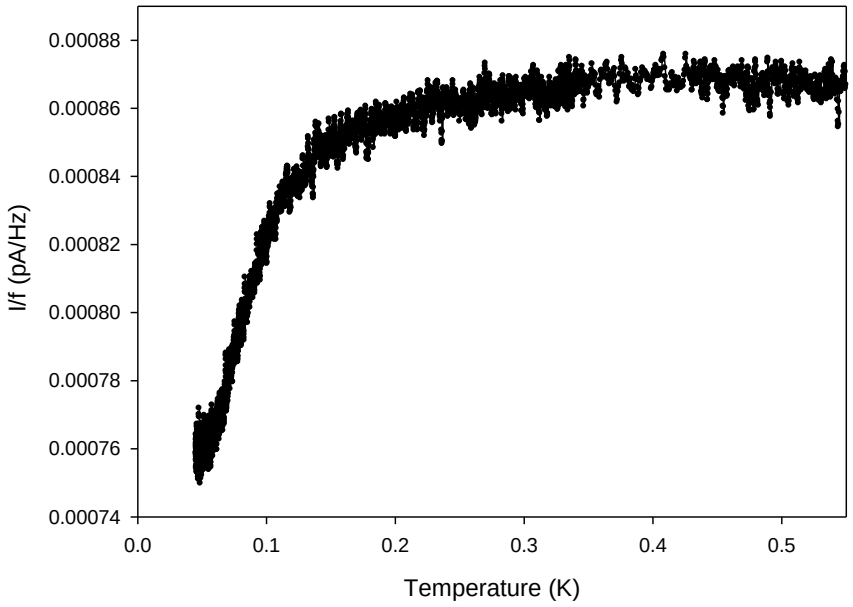

Figure 4.16: Amplitude anomaly as a function of temperature in the sample 300ppb30.5 measured at 635 Hz, at a driving voltage of 100 mV_{pp}.

The behaviour is the same as in the previous measurement (the cell with vycor). It appears that the solid helium becomes softer instead of stiffer. The explanation is the same. The modulus contribution is still out of phase with and smaller than the liquid background. The corrected data (Fig. 4.17) shows that there is a shear modulus change of 37% at low temperature.

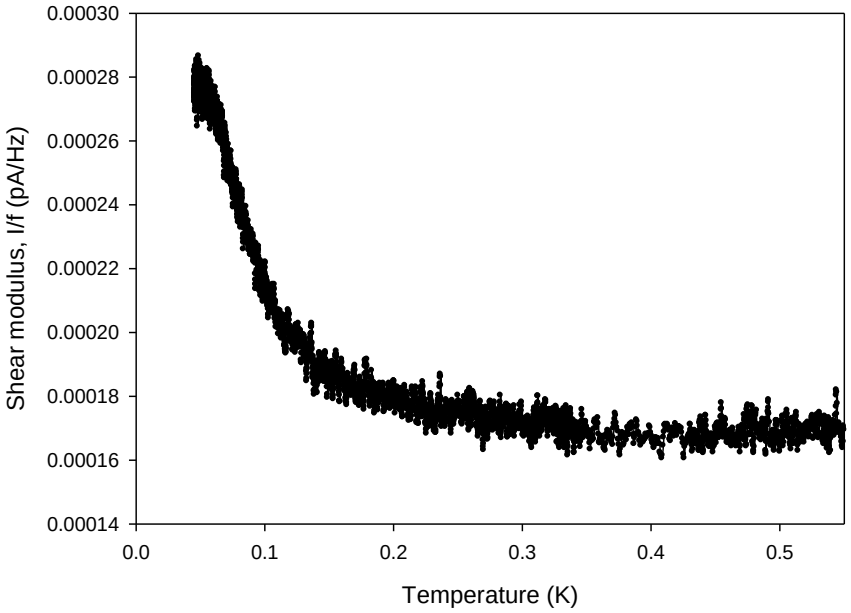

Figure 4.17: Shear modulus anomaly as a function of temperature in the sample 300ppb30.5 measured at 635 Hz, at a driving voltage of 100 mV_{pp} (corrected).

This, and other data not presented here, show that the new stacks of PZT with metal plates did not really improve the sensitivity.

This insensitivity was not due to a problem in the design; rather it happened because one of the two stack transducers was assembled with the wrong polarity for one PZT plate. Instead of adding, the signals from the two plates basically cancelled each other. Two small transducer pieces cut from a larger

piece were epoxied to make the stack but it is hard to keep track of the two transducers' polarization directions and even tougher when they are covered with the glue. The smaller sensitivity of one of the stacks was first detected by reversing the receiver and emitter during the shear modulus measurement at low temperature. The signal measured in the receiver transducer depends non-linearly on the amplitude applied to the driving transducer (with other parameters constant). The nonlinearity will set in at higher drive for a less efficient driving transducer. Later, the inefficiency of one of the transducers was confirmed with an oscilloscope by applying shear forces to the stacks and comparing their responses.

Two new stacks have since been made carefully using the same design. They have been tested on the bench with the oscilloscope but not yet at low temperature. They both seem to be working properly, creating large signals with small distortion.

4.3 Shear modulus of solid ^{4}He in aerogel

Previous TO and x-ray diffraction experiments looked for the effects of disorder on solid ^{4}He in aerogel [32]. Unexpectedly, these showed that the helium behaved like a high quality crystal with a small supersolid fraction (0.04%) despite having many defects and grain boundaries.

The nanometer scale glass strands of aerogels should provide strong pinning of dislocations in solid helium and so should have large effects on its

elastic behavior. We therefore made measurements of the shear modulus of solid ^{4}He grown at constant density in the pores of an aerogel with porosity of 95% (similar to that used in early experiments [32]). A disc of 12.5 mm diameter and 0.8 mm in thickness was positioned in the gap between two rigidly mounted piezoelectric transducers.

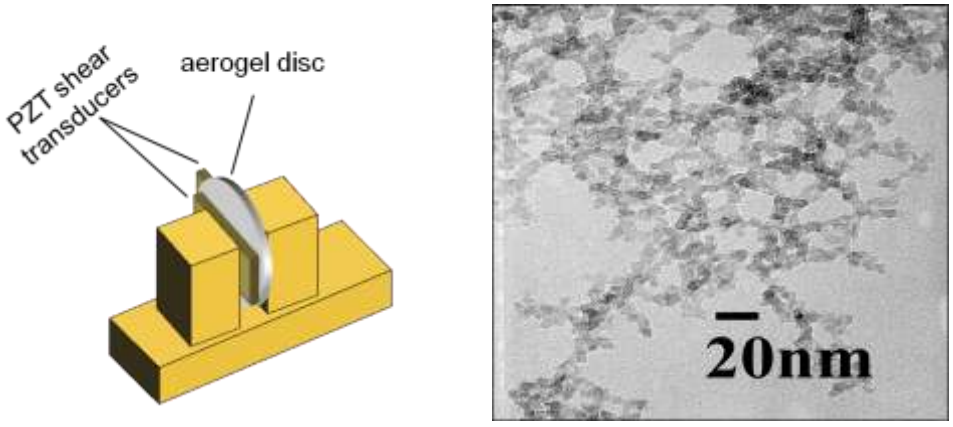

(a) (b)

Figure 4.18: (a) Schematic of the transducers (mounted on the brass blocks) holding the aerogel piece between the gap, (b) TEM of the aerogel [28].

The estimated shear modulus of aerogel is much smaller (~ $\mu_{aerogel} \approx 3\times10^5 Pa$) than that of the solid helium (~ $\mu_{He} \approx 2\times10^7 Pa$) and so that we essentially measure the modulus of the helium, with only a small correction due to the aerogel's shear modulus.

The frequency sweeps in Fig. 4.19 at different temperatures were taken to make sure that the setup was working properly.

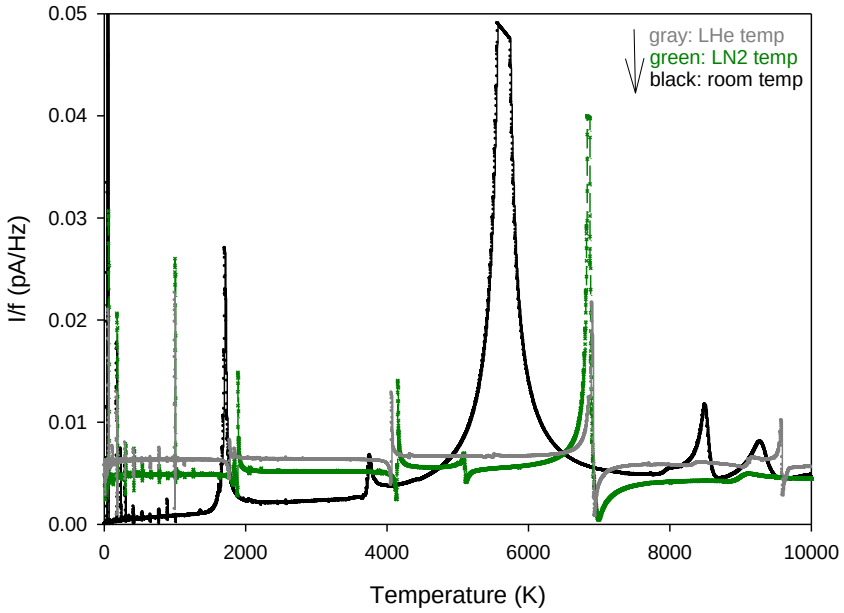

Figure 4.19: The background signal (amplitude versus frequency) at room temperature (300 K) [empty cell], liquid nitrogen temperature (77 K) [gas filled cell at 13 bar] and liquid helium temperature (4.2 K) [filled cell at 23 bar], all measured at 100mV$_{pp}$ driving amplitude.

4.3.1 Sample 300ppb29.7

Figure 4.20 shows the thermodynamic path of the growth of the crystal which produced a 29.7 bar sample. The pressure is high enough to ensure that all the ^{4}He in the aerogel pores is frozen (see the phase diagram of solid helium in aerogel in Fig. 2.11). The jumps around 1.7 K are due to refilling the 1K pot which caused a sudden drop in temperature. It took more than 35 hours to grow the sample but the 1K pot has to be refilled every 36 hours.

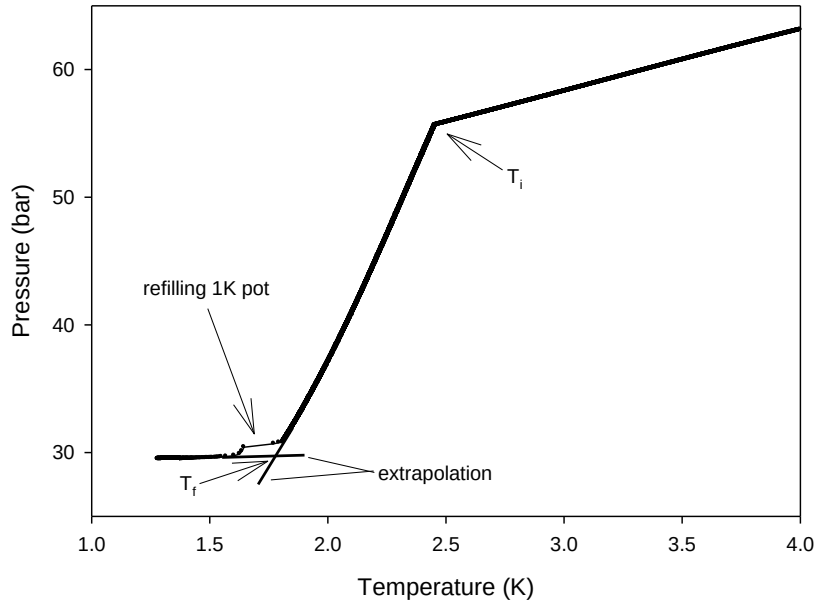

Figure 4.20: Growing crystal (pressure versus temperature) - the thermodynamic path for the sample 300ppb29.7. T_f is the melting point (1.78 K and was confirmed when the crystal was melted later).

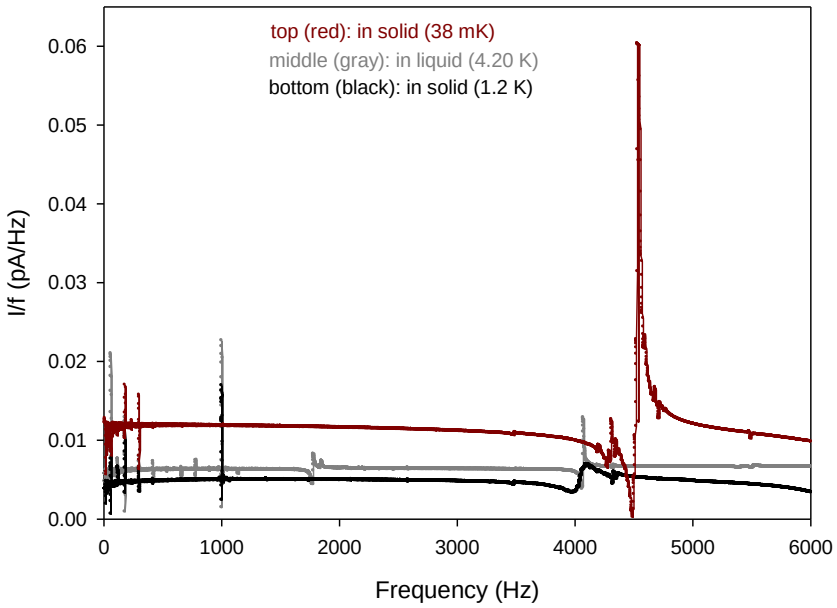

Figure 4.21: The background signal (amplitude versus frequency) in liquid (at 4.2 K and 23 bar pressure) and solid sample 300ppb29.7 (at 1.2 K and 38 mK at 29.7 bar), all measured at 100 mV_{pp} driving amplitude.

In Fig. 4.21, the liquid background (amplitude measured in liquid) and the total solid signal (measured at 1.2 K and 38 mK) have been plotted vs. frequency. Later, in Fig. 4.22, the corresponding phase plot vs. frequency shows that the total solid signal is out of phase with the signal in liquid. This means that the phase due to the solid helium modulus contribution is out of phase with but larger than the crosstalk (see details in Chapter 3.11, case c).

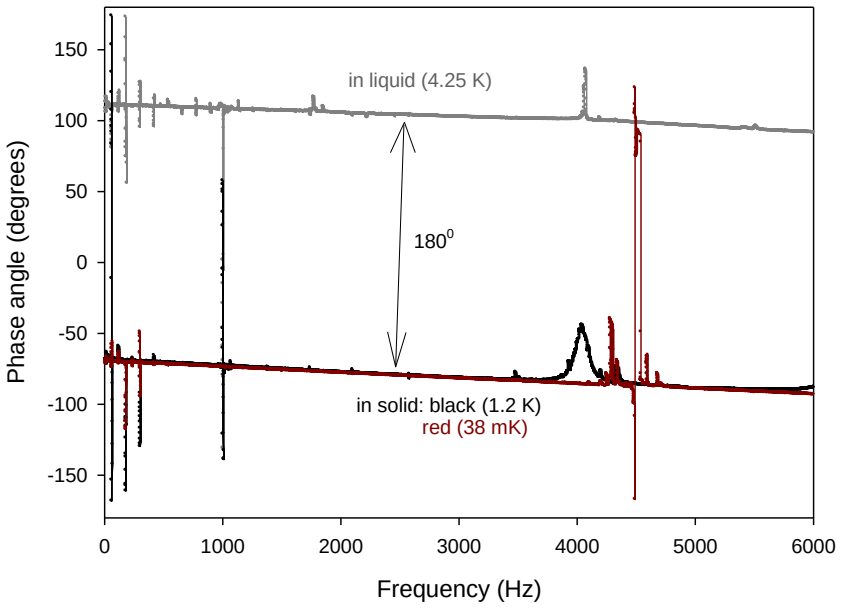

Figure 4.22: Phase angle corresponding to Fig. 4.21, as a function of frequency for the background signal in liquid (at 4.2 K and 23 bar pressure) and solid sample 300ppb29.7 (at 1.2 K and 38 mK), all measured at 100 mV_{pp} driving amplitude.

The frequency sweep in Fig. 4.21 also shows that the shear modulus value at very low temperature (38 mK) is larger than the value at high temperature (1.2 K). The spikes in the low frequency data (below 1000 Hz) are multiples of the 60 Hz line frequency, as it was seen in previous data (e.g. Fig. 4.2) and the spike at

1000 Hz is due to the turned on of the capacitance bridge, which can be avoided. The corresponding phase plots at 38 mK and 1.2 K are essentially the same except for the peaks at high frequency. These are narrower at low temperature, indicating that the damping of these acoustic resonances is smaller.

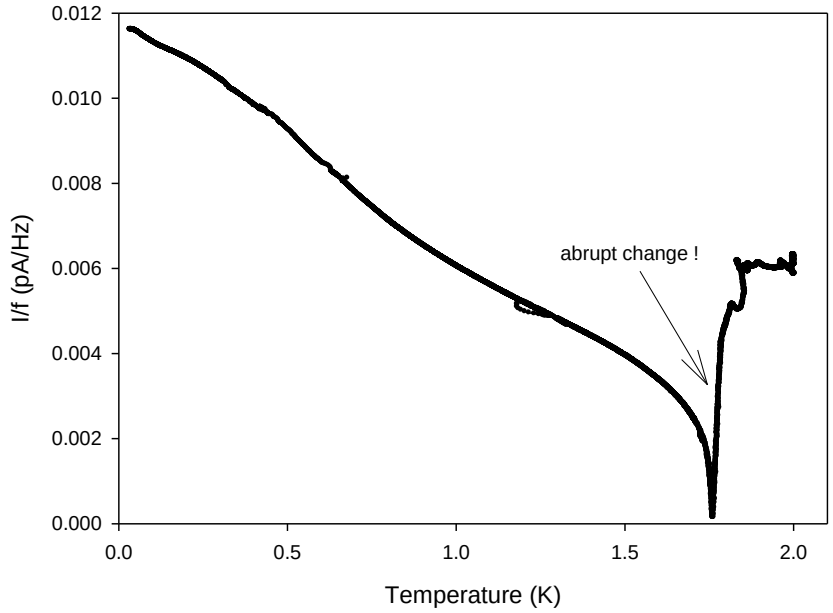

Figure 4.23: The raw data for the total amplitude, measured at 2000 Hz and 100 mV_{pp} driving amplitude in the sample 300ppb29.7.

To measure the total shear modulus change due to the solid ^{4}He in aerogel, the cell heater was used to raise the temperature from 34 mK up to 2K, above the melting point (1.75 K) of the crystal, with the raw data shown in Figs. 4.23 and 4.24.

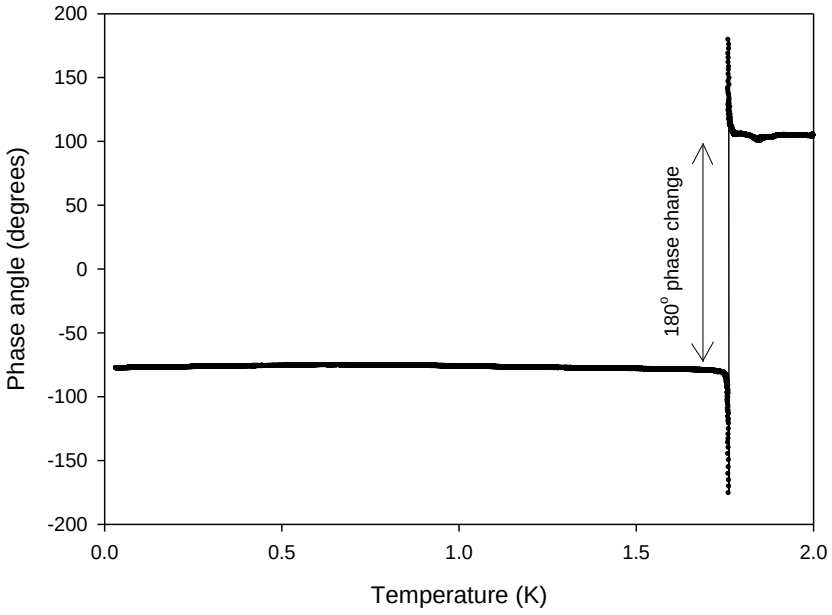

Figure 4.24: Raw data for the phase change corresponding to Fig. 4.24 at 2000 Hz and 100 mV_{pp} driving amplitude in the sample 300ppb29.7.

The sharp dip in shear modulus near 1.75 K (Fig. 4.23) can be clearly understood from the corresponding phase plot (Fig. 4.24) which shows a 180 degree phase change at 1.75 K. This occurs at the temperature where the shear modulus contribution of the solid helium exactly cancels the crosstalk (which is 180^o out of phase with it).

The raw data must be corrected to find the shear modulus change in the solid helium in the aerogel.

Figure 4.25 shows that the shear modulus of solid ^{4}He in aerogel (black curve) decreases by about 50% on warming from low temperature to near melting.

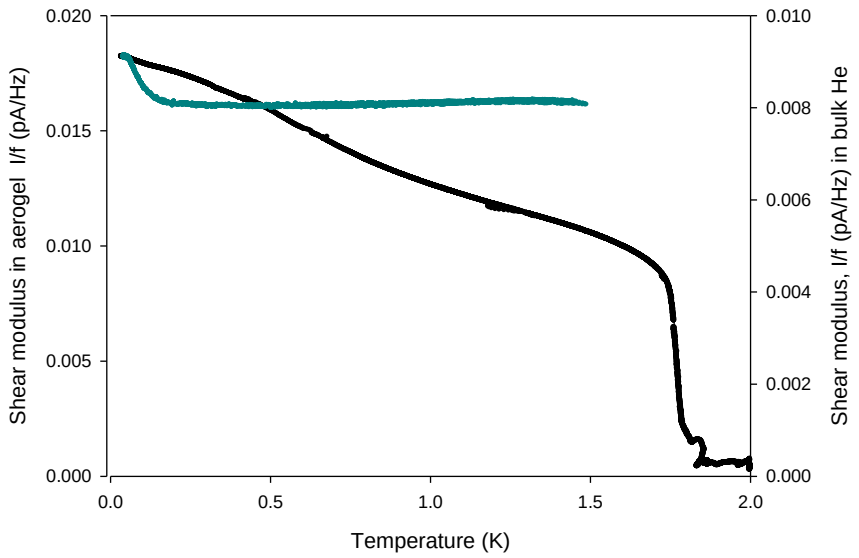

Figure 4.25: The total (corrected) shear modulus change of solid helium in aerogel (black), measured at 2000 Hz and 100 mV_{pp} driving amplitude in the sample 300ppb29.7, compared with the typical shear modulus change of bulk ^{4}He [4].

In Fig. 4.25, the contrast of the broad modulus decrease in aerogel to the fairly sharp one in bulk helium is due to fact that in bulk ^{4}He (gray curve) the smaller change (typically about 10%) occurs at much lower temperatures, since the dislocations are pinned by ^{3}He impurities at low temperatures and unbind at temperatures above 100 mK [44], making the shear modulus change flat at higher temperature. On the other hand, in aerogel the dislocations may be pinned by the aerogels' strands and need higher temperature to unbind, making the modulus change broad. The magnitude of shear modulus in the liquid above 1.75 K (the melting temperature) should vanish but appears to be slightly greater than zero. This is not too surprising as the liquid background signal (electronic crosstalk)

was measured at 4.2 K, whereas this data was taken at much lower temperature, so the background corrections may be slightly inaccurate.

To understand the elastic response of solid helium in aerogel, we took measurements at different frequencies, at different amplitudes, during warming as well as cooling, and after annealing.

All the rest of the modulus and phase plots in this chapter have been corrected for crosstalk using the liquid background signal.

4.3.2 Frequency dependence

The background frequency sweeps for solid helium (Fig. 4.21) show that there is a resonance above 4000 Hz and that the data are bit noisy at low frequency. Shear modulus measurements were not taken above 2 kHz to avoid possible resonance effects. We did take measurements at very low frequencies, even at 2 Hz, using the lowest noise preamplifier, although it required slow temperature sweeps (e.g. 18 hours at 2 Hz measurement) because long averaging times were needed to achieve the necessary signal-to-noise ratio.

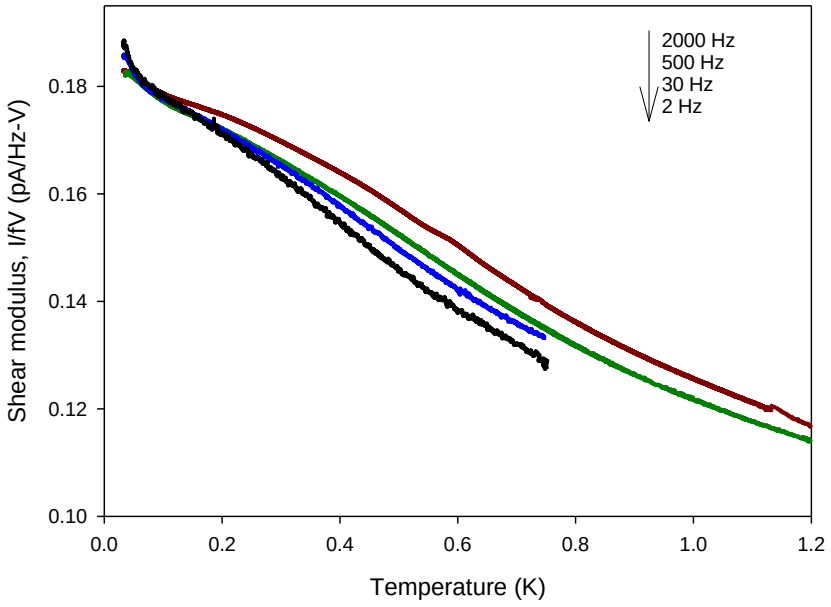

Figure 4.26: Shear modulus change of ^{4}He in aerogel as a function of temperature at different frequencies, measured at 100 mV_{pp} driving amplitude in the sample 300ppb29.7. Different frequency data was taken with different current preamplifiers, so the current (I) was found using different gains (see explanation below for details).

Figure 4.26 shows the shear modulus anomaly at different frequencies (2 Hz, 30 Hz, 500 Hz and 2000 Hz) in the sample 300ppb29.7. All the data have been taken at 0.1 V_{pp} driving voltage, which corresponds a strain of 4.4 x 10^{-9}. All the plots in Fig. 4.26 are corrected for crosstalk but are not shifted vertically. Different current preamplifiers were used to measure the current at different frequencies and these had different gains, so the currents were computed using the appropriate gain. In particular, the 2 Hz data was taken with the lowest noise preamp but during measurement the preamp was set at 0.3 Hz bandwidth rather than 2 Hz. As a result the appropriate current was smaller than expected when the

signal was divided by the nominal gain (10^{12} V/A). To get the corrected value the signal was divided by 0.16 to make up the loss due to 0.3 Hz bandwidth in the preamp. This gain correction is pretty close to the expected gain (division by 0.15) for 2 Hz with a 0.3 Hz cutoff (3 dB point) of a first order filter.

The gain for a 1st order filter is,

$$G = G_o (w_o/w) = 10^{12} \text{ x } (0.3/2) = 0.15 \text{ x } 10^{12}.$$

Therefore, the gain difference due to using 0.3 Hz bandwidth instead of 2 Hz is $(0.15 \text{x} 10^{12})/(1 \text{x} 10^{12}) = 0.15$, which is pretty close to the gain correction (dividing by 0.16) we used.

The behavior of the shear modulus with temperature is consistent at all frequencies above 0.2 K. The low temperature (below 0.2 K) behavior resembles the bulk ^{4}He behavior; the transition is sharper at low frequency.

Stress and applied strain are in phase in purely elastic deformations but in general the stress lags the strain by a phase angle. This phase is related to the dissipation by $1/Q = \tan\phi \approx \phi$ (when ϕ is very small). The response has real and imaginary parts (the amplitude and phase of the current) which are the shear modulus and dissipation, although other phase shifts make it hard to measure the absolute dissipation.

The dissipations (phase angles) corresponding to the moduli (amplitudes) of Fig. 4.26 are shown in Fig. 4.27.

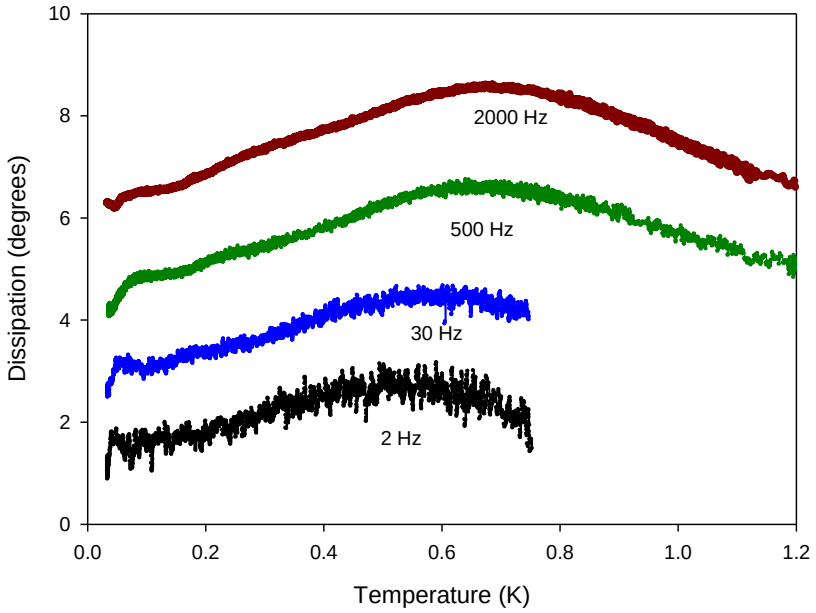

Figure 4.27: Dissipation corresponding to Fig. 4.26. The temperatures for the phase peaks and peaks height for corrected data (showed) are the same as the raw data.

From Figs. 4.26 and 4.27, we see that, as the frequency decreases, the dissipation peaks and modulus changes shift to lower temperature, as expected as for a thermally activated relaxation process. It is hard to pick a temperature to characterize the modulus changes but the dissipation plots are clearer.

Modulus seems roughly independent of frequency (all the shear modulus plots at different frequencies lie together below 100 mK (Fig. 4.26)) and the decrease in modulus is broad in temperature. The dissipation peaks occur roughly at the midpoint of the 50% modulus decrease (Figs. 4.26 and 4.27).

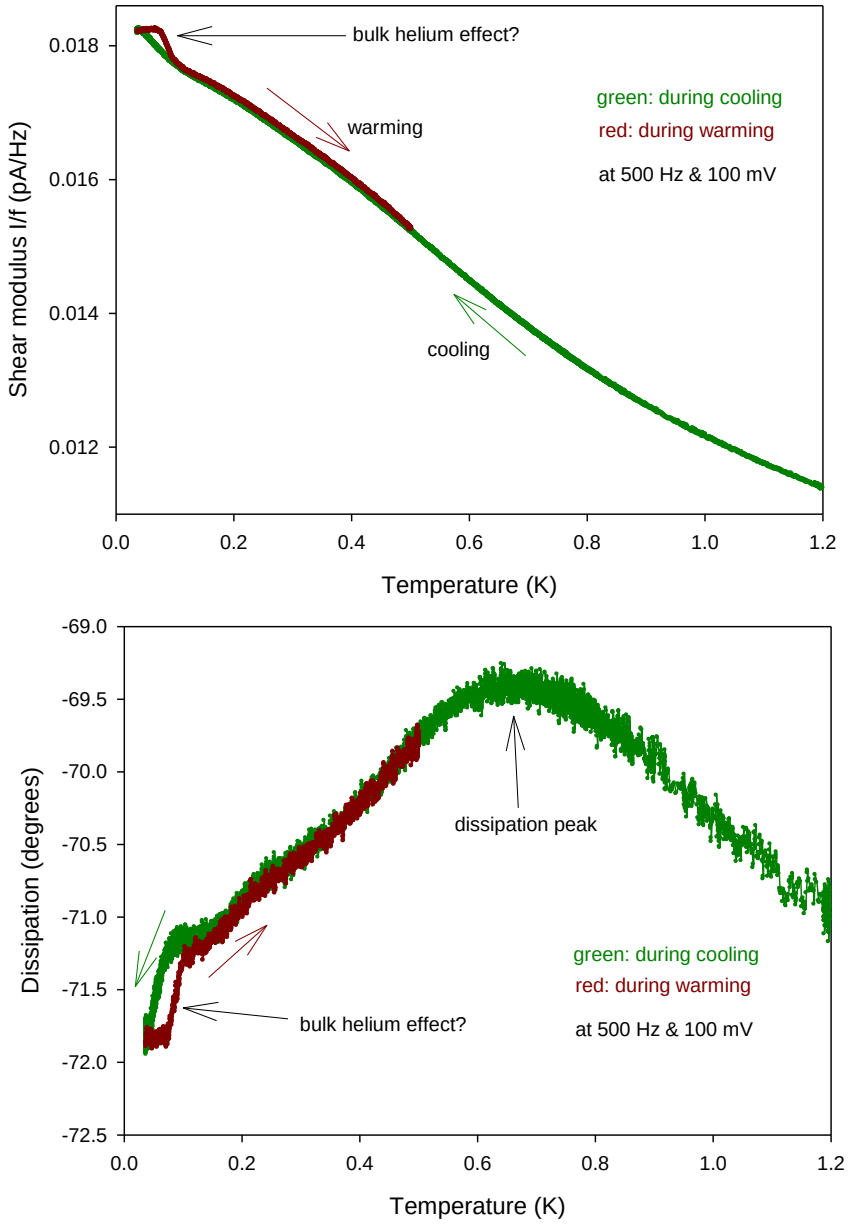

Figure 4.28: Shear modulus (top) and corresponding dissipation (bottom) anomaly as a function of temperature during cooling and warming, measured at 500 Hz & 100 mV_{pp} driving amplitude in the sample 300ppb29.7.

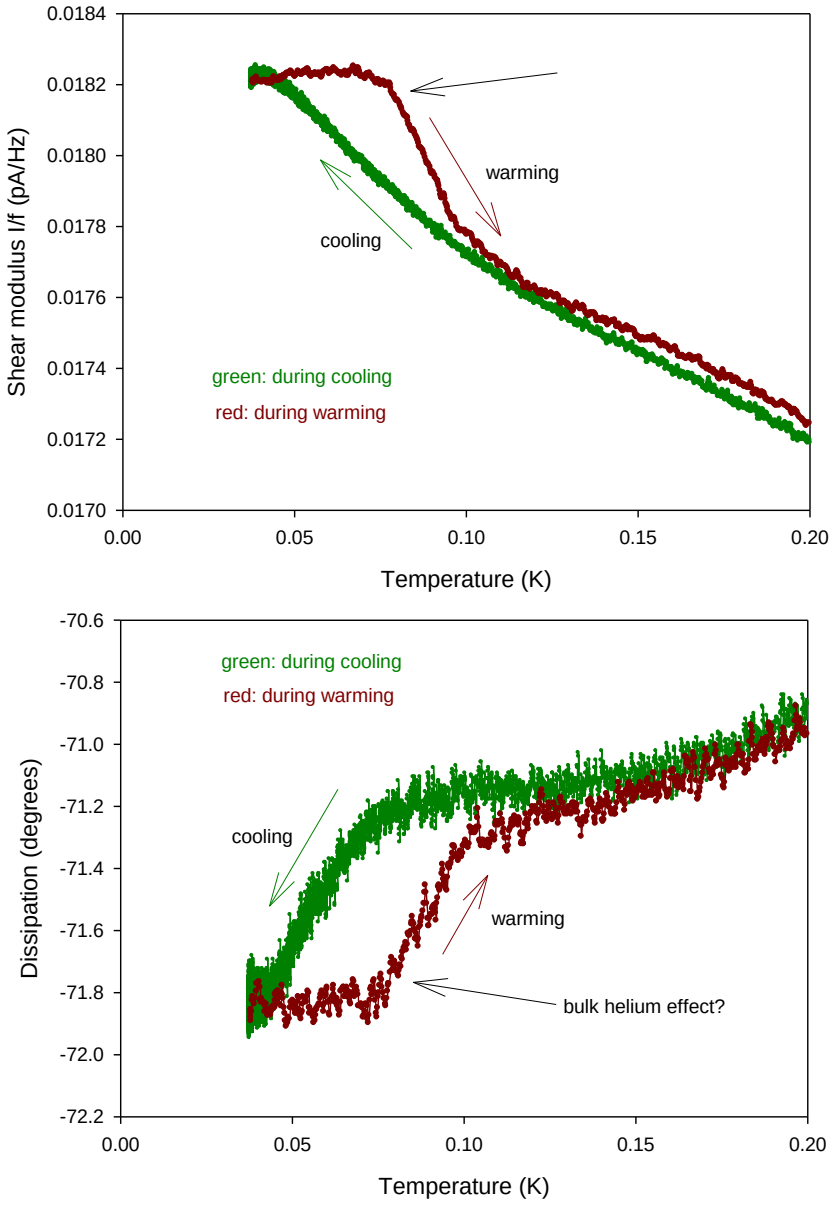

Figure 4.29: Low temperature blow up of shear modulus (top) and corresponding dissipation (bottom) anomaly from Fig 4.28.

In addition to the broad modulus decrease and dissipation peaks around 0.7 K, we saw small changes in both shear modulus and phase at temperatures below 150 mK. These showed amplitude dependence at low strains, as well as hysteresis between data taken during cooling and warming. Figure 4.28 shows an

example; this data was taken during the first time cooling and subsequent warming of the sample. Figure 4.29 shows the low temperature behavior on an expanded scale.

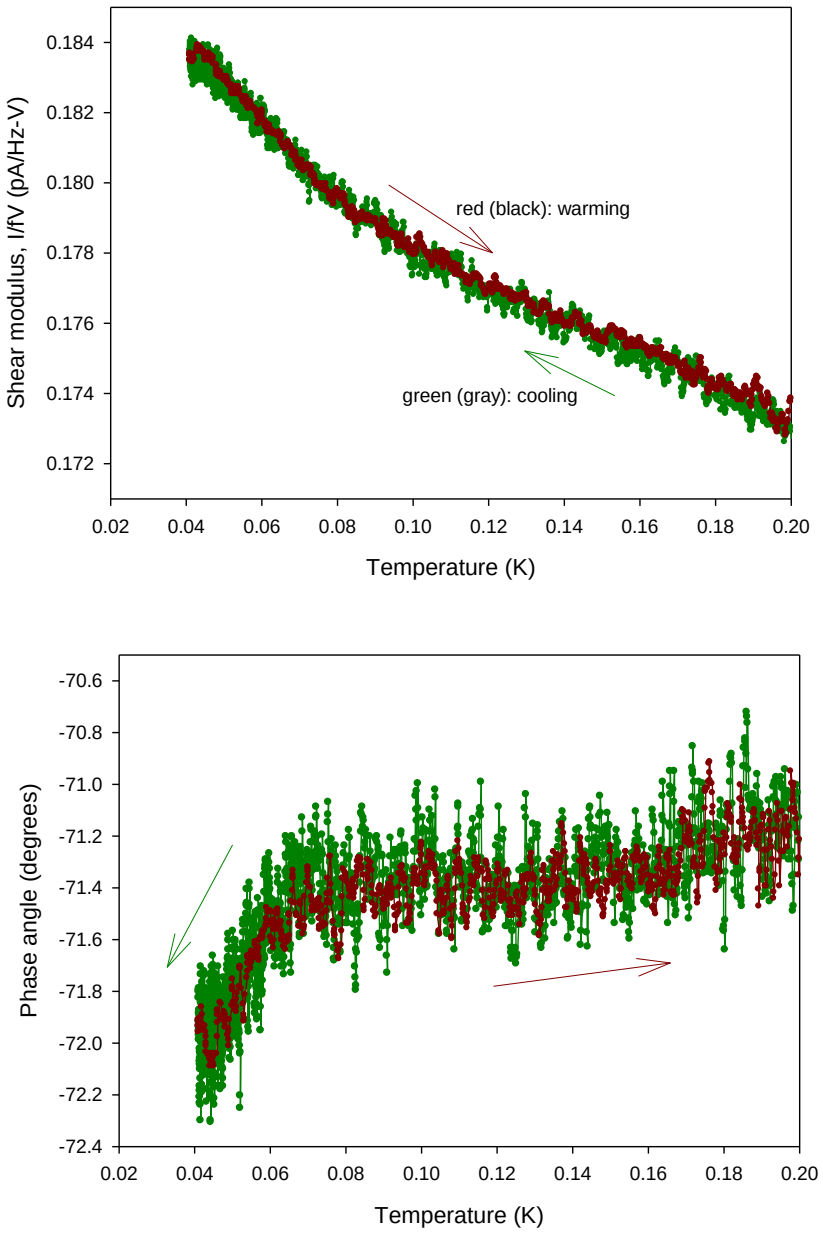

Figure 4.30: Low temperature behaviour of shear modulus (top) and dissipation (bottom) anomaly as a function of temperature during cooling and warming, measured at 500 Hz & 25 mV_{pp} driving amplitude in the sample 300ppb29.7.

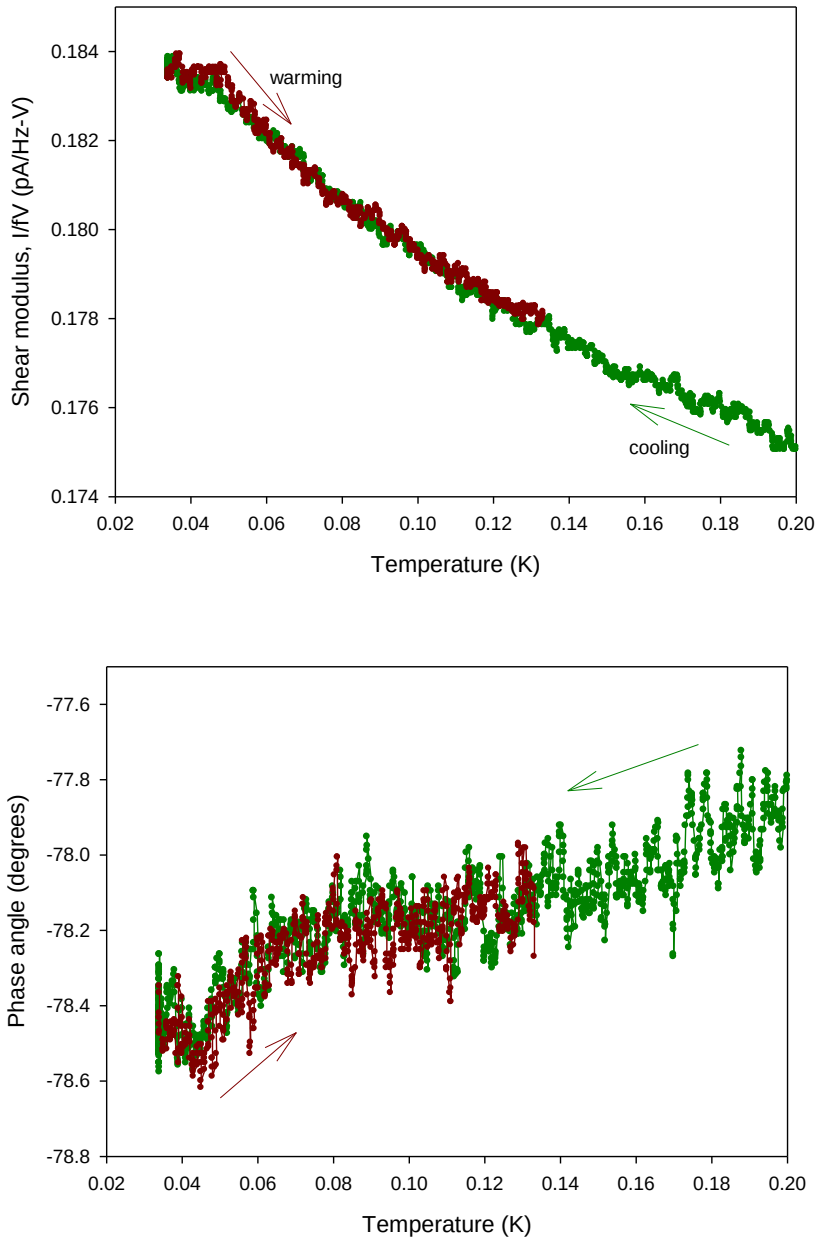

Figure 4.31: Low temperature behaviour of shear modulus (top) and dissipation (bottom) anomaly as a function of temperature during cooling and warming, measured at 2000 Hz and 10 mV_{pp} driving amplitude in the sample 300ppb29.7.

In bulk helium, the amplitude dependence of the shear modulus and dissipation produces hysteresis between cooling and warming. To check whether

the hysteresis loops in Fig. 4.29 are similar, we took measurements at lower driving amplitudes. Figure 4.30 shows that the loops at 500 Hz essentially disappear at lower driving amplitude (25 mV_{pp}). Figure 4.31 shows similar data at 2000 Hz at even lower amplitude (10 mV_{pp}). This data was taken quite slowly at cooling and warming rates of 1mK per ~80 sec. The data from the first time cooling and warming (Fig. 4.29) was taken at higher cooling and warming rates 1mK per ~50 sec.

4.3.3 Activation energy

Figures 4.27 and 4.28 show clear dissipation peaks at high temperatures (above 0.5 K). In bulk ^{4}He, the modulus changes and dissipation peaks occurred at much lower temperatures (below 200 mK) [4, 45]. For relaxation processes, dissipation peaks occur at the temperatures where the modulus changes most rapidly.

Figure 4.27 shows that for solid ^{4}He in aerogel, the dissipation peaks shift to lower temperature with descending frequency, which suggests a thermally activated process.

For a thermally activated process, the relaxation time τ is related to the temperature by $\tau(E) = \tau_0 e^{E/T}$, where E is the activation energy. At the temperature where $\omega\tau = 1$, (where $\omega = 2\pi f$ is the angular measurement frequency) the dissipation is maximum and 50% of the total modulus change has occurred.

Plotting $\ln f$ versus $1/T$ will provide a slope which is essentially the activation energy E.

In order to determine the activation energy, it is crucial to know the temperatures of the broad dissipation peaks. Cubic polynomials were used to fit the dissipation data to get precise peak temperatures. Taking the 1st derivative of the cubic equation equal to zero, the roots of the derivative were found and using the given cubic coefficients, the local maximum points were calculated for each frequency. Temperatures of these peak maxima were then used with their corresponding frequencies to calculate the thermal activation energy.

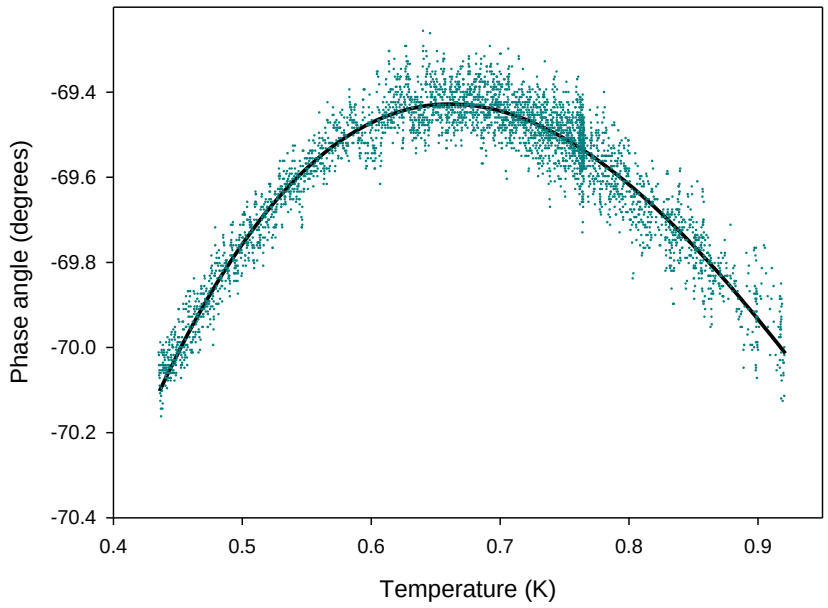

Figure 4.32 (a): Cubic fit of the dissipation at 500 Hz and 100 mV_{pp} driving amplitude in the sample 300ppb29.7. The gray dots are the data and the thick line is the fitted curve. The fitted maximum is at T= 0.6612 K.

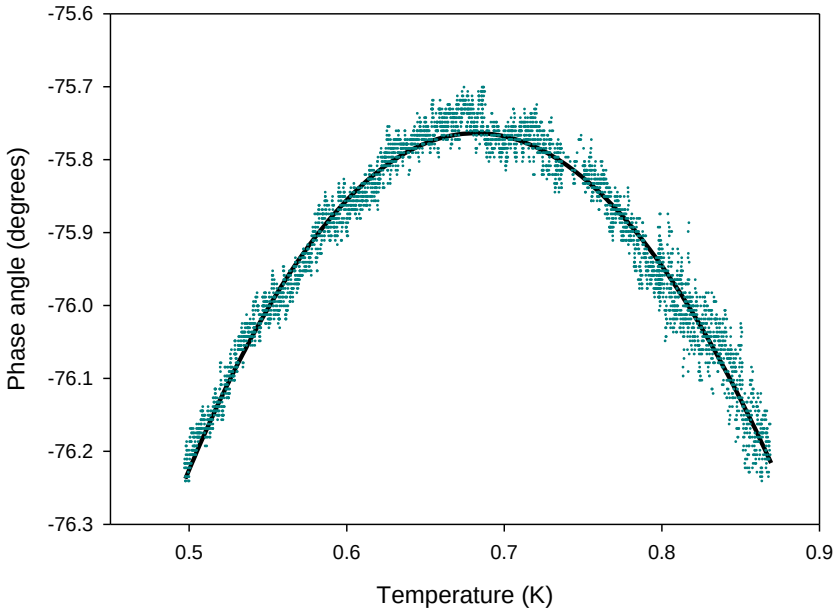

Figure 4.32 (b): Cubic fit of the dissipation at 2000 Hz and 100 mV_{pp} driving amplitude in the sample 300ppb29.7. The gray dots are the data and the thick line is the fitted curve. The fitted maximum is at T= 0.6820 K.

In Fig. 4.27, we have seen the dissipation corresponding to Fig. 4.26 at different frequencies. The total temperature ranges are different for the various frequencies. Therefore, in Figs. 4.32 (a) and 4.32 (b), temperature ranges near to the peak were used for the cubic fits. Peaks were found for each frequency shown in Figs. 4.26 and 4.27 using cubic polynomial fits. Figures 4.32 (a) and 4.32 (b) show the cubic fits of the dissipation peaks at 500 Hz and 2000 Hz. A couple of other equations (e.g. four parameter Gaussian equations) were used to fit the dissipation data but cubic fits were better.

Although cubic fits provides better estimations of the dissipation peaks, in Figs. 4.32 (a) and (b) and in the other plots (not shown here), I estimate that the peaks

could be located at around ~ 10-30 mK either way from the peak provided by cubic fits. For example, peak positions calculated with Gaussian fits (not shown here) show difference of +/- 10-25 mK from the temperatures where the dissipation peaks were found with the cubic fits.

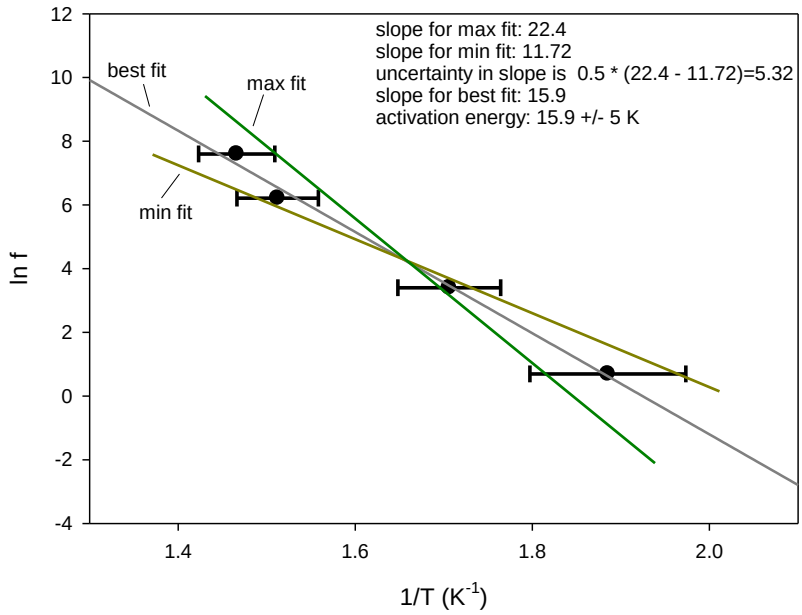

Figure 4.33: Thermal activation plot (ln f vs. 1/T with respective errors) for the crystal 300 ppb29.7. The lines are fit and their slopes corresponding to activation energies of (15.9 +/- 5) K.

The inverse of the peak temperatures found from the cubic fits with the estimated errors are plotted versus the natural logarithm (ln f) of the corresponding frequencies in Fig. 4.33. The slope of the best linear fit line with the uncertainty is the activation energy, (15.9 +/- 5) K. The uncertainty is due to the errors associated with the temperatures.

The frequency dependence of the shear modulus and dissipation are consistent with a thermally activated process with an effective energy $\Delta \sim$ (15.9 +/- 5) K. This is much larger than the effective activation energy of 0.7 K seen in previous shear modulus measurements in bulk solid ^{4}He which was interpreted as a binding energy for ^{3}He impurities which pin dislocations [45].

Vacancies are another kind of crystal defect which are created in helium crystals at finite temperatures but with much larger activation energy. For ^{4}He crystals with molar volume ~20 cm^3, several experimental NMR [46], X-ray [47] and neutron scattering [48] experiments give typical values of 10-11 K for the activation energy of vacancies. This agrees with theoretical work which suggests vacancies activation energies in the range of 10-15 K [49].

The energy of ~ (15.9 +/- 5) K inferred from our measurement may reflect the activation energy of vacancies.

The temperature and frequency dependence of the complex shear modulus can be described using a Debye relaxation. For a simple Debye process, with a single relaxation time, the shear modulus μ and the dissipation 1/Q are related to the real and imaginary parts of the response [45].

$$\frac{\mu}{\mu_0} = 1 - \frac{\delta\mu}{\mu_0}\frac{1}{1+(\omega\tau)^2} \tag{4.1}$$

$$\frac{1}{Q} = \frac{\delta\mu}{\mu_0}\frac{\omega\tau}{1+(\omega\tau)^2} \tag{4.2}$$

where τ is the relaxation time of the Debye process, $\mu_0 - \delta\mu$ is the relaxed modulus and μ_0 is the unrelaxed modulus. At a particular frequency *f*, the crossover occurs at the temperature when $\omega\tau = 1$ (where $\omega = 2\pi f$). At this temperature, 50% of the shear modulus has occurred and the dissipation is maximum. Using the value of ω we can find τ at the crossover temperature.

Figure 4.34 shows the shear modulus and dissipation at 500 Hz and 2000 Hz for a Debye relaxation process (equations 4.1 & 4.2) using the activation energy (15.9 K) from Fig. 4.34. In the calculation it was assumed that the "strength" of the relaxation gave a total modulus change of 50% and the characteristic relaxation time was $\tau = 10^{-14}$ sec in order to get the temperature of the crossover in the right place.

The crossover from the unrelaxed to relaxed modulus will occur over a wider temperature range, with a smaller, broader dissipation peak if the relaxation process has a range of activation energies rather than a single value.

The dissipation peak and modulus decrease in crystal 300ppb29.7 (Figs. 4.26 and 4.27) and much broader than those in Fig. 4.34, which indicates that there must be a broad distribution of relaxation times in the crystal.

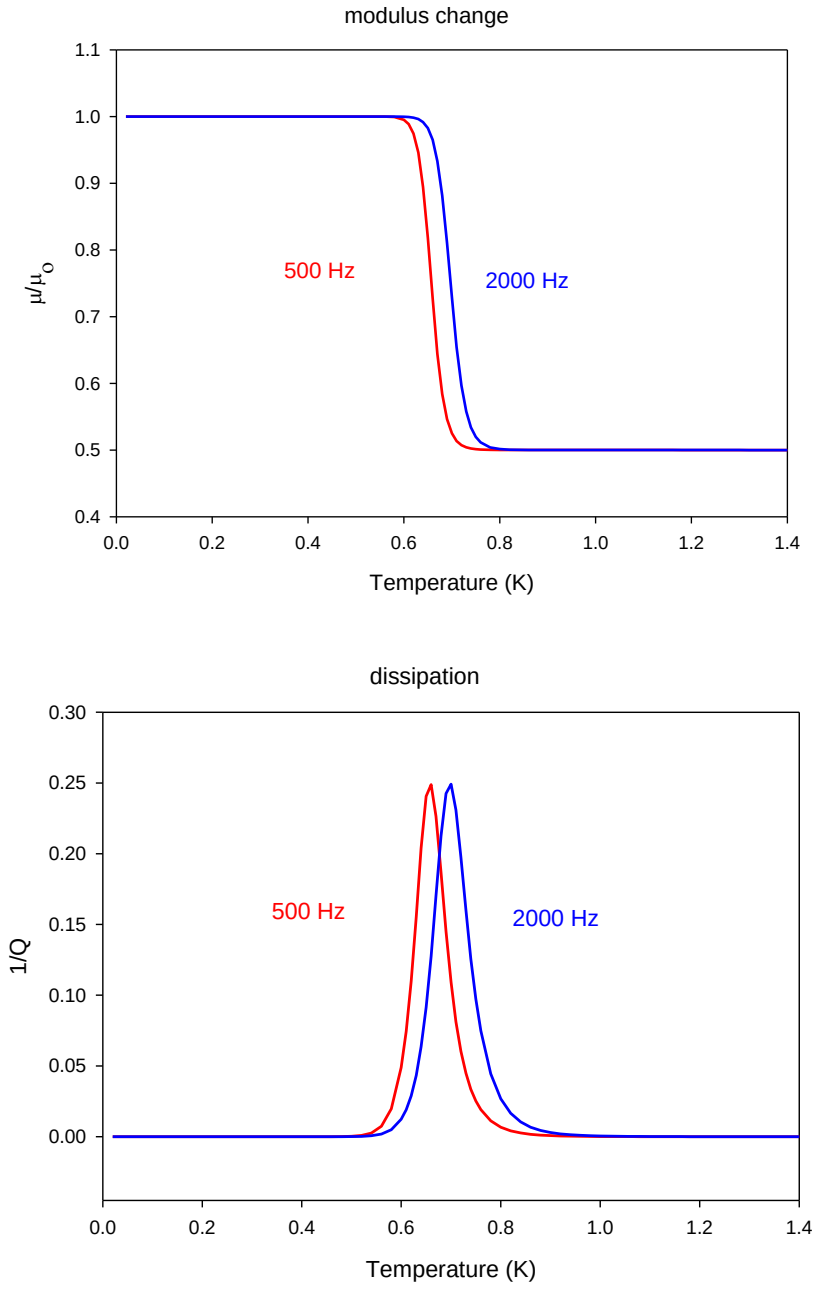

Figure 4.34: Debye single activation fit of thermally activated relaxation to both shear modulus and dissipation at 500 Hz and 2000 Hz for the sample 300ppb29.7.

4.3.4 Amplitude dependence

In bulk solid ^{4}He, it was seen that the shear modulus anomaly is independent of drive amplitude up to strains of 2.2 x 10^{-8} and then starts to decrease at higher

amplitudes [4], which says that ^{3}He impurities unpin from dislocations at strains larger than 2.2 x 10^{-8}. In Figs. 4.28-4.30, we have seen amplitude dependence in the hysteresis loops in both the shear modulus and dissipation anomalies as functions of temperature while cooling and warming.

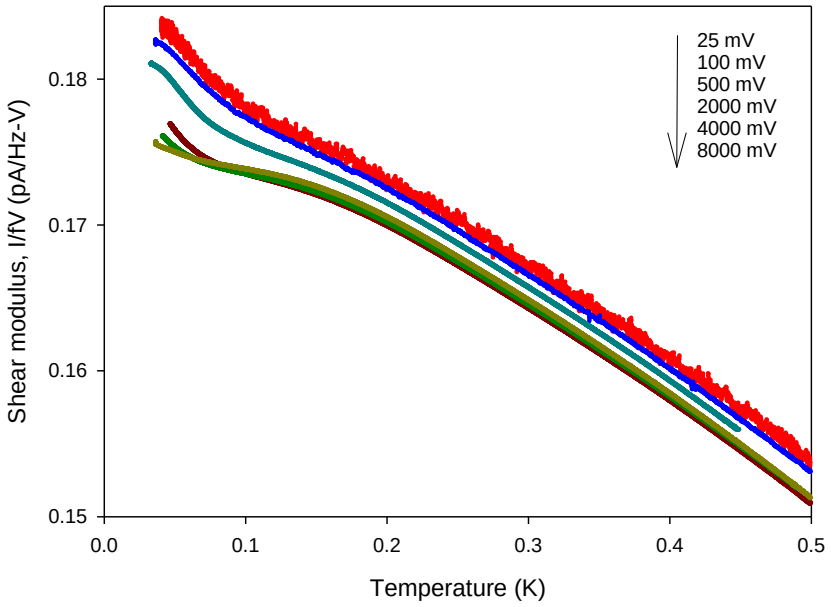

Figure 4.35: The shear modulus as a function of driving amplitude at 500 Hz in sample 300ppb29.7. The legend gives the drive voltages.

Figure 4.35 shows the amplitude dependence of the shear modulus of solid ^{4}He in aerogel at 500 Hz for sample 300ppb29.7. The curves correspond to different driving voltages on the transducer, i.e. to different strains. These data were taken during cooling. In the high temperature region (above 0.2 K), the shear modulus is essentially amplitude independent whereas the low temperature part shows amplitude dependence above a critical strain.

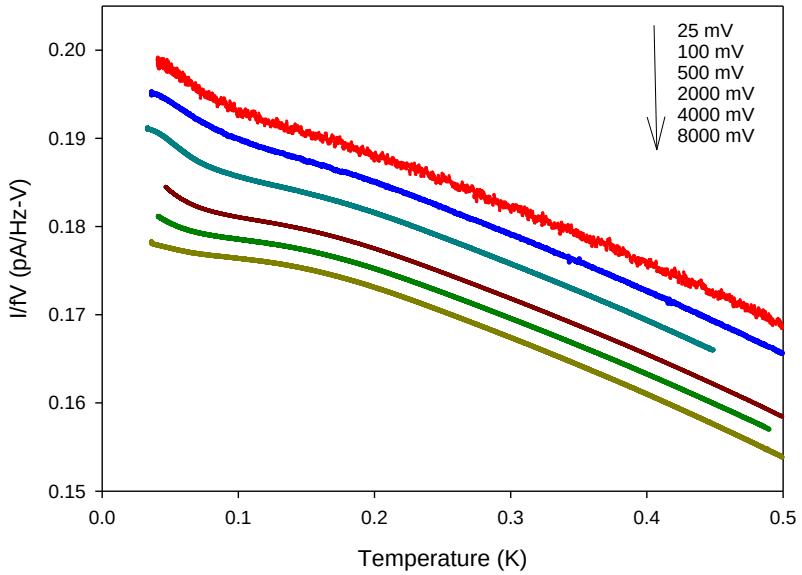

Figure 4.36: Shifted plot of the amplitude dependent data of Fig. 4.35.

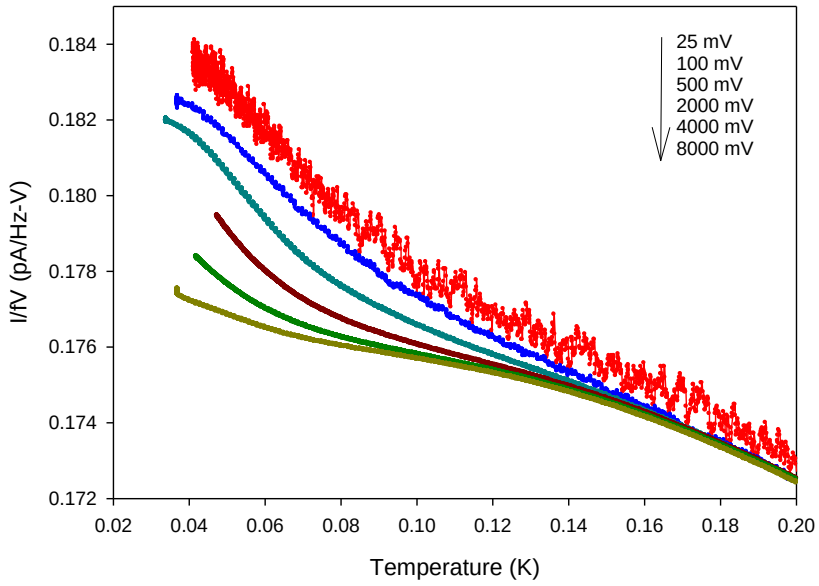

Figure 4.37: The modulus is dependent of amplitude above strain of 4.4 x 10^{-9} which correspond the driving amplitude of 100 mV_{pp} or stress of 0.066 Pa. Curves have been shifted vertically to agree at high temperature.

In Figs. 4.36 and 4.37, the shear modulus curves have been shifted vertically for clarity. In Fig. 4.37, the low temperature region has been blown up to show that the amplitude dependence occurs only at low temperature (below 150 mK).

The magnitude of the low temperature stiffening decreases and its onset temperature shifts to lower temperature as the strain increases. This amplitude dependence is very similar to that seen in bulk ^{4}He.

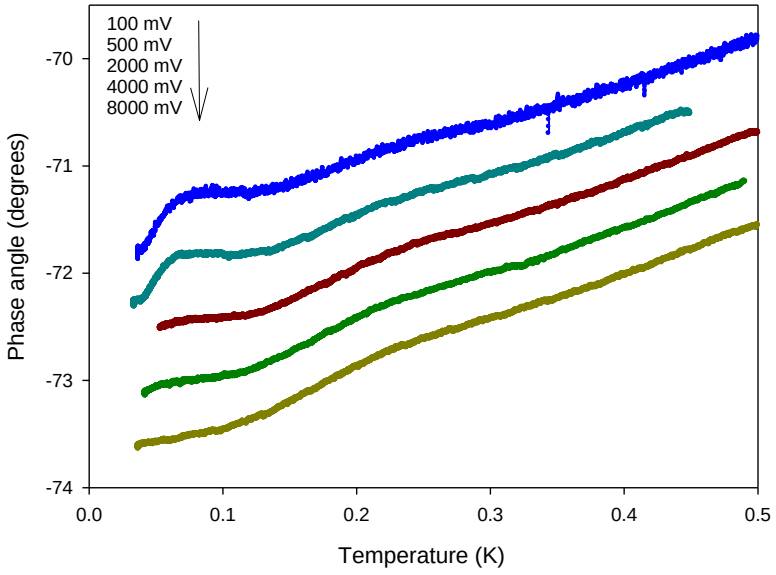

Figure 4.38: Amplitude dependence of the phase angle corresponding to the modulus data of Fig. 3.35. The phase at 25 mV_{pp} is very noisy and is not plotted. Curves have been shifted vertically for clarity.

In addition to the shear modulus anomaly's dependence on strain amplitude, in Fig. 4.38 we have plotted the corresponding dissipation at different strain amplitudes. The curves have been shifted vertically for clarity. At high temperature the phase is essentially independent of amplitude, like the modulus.

The small peaks at low temperature shift to lower temperature and become smaller at high amplitudes.

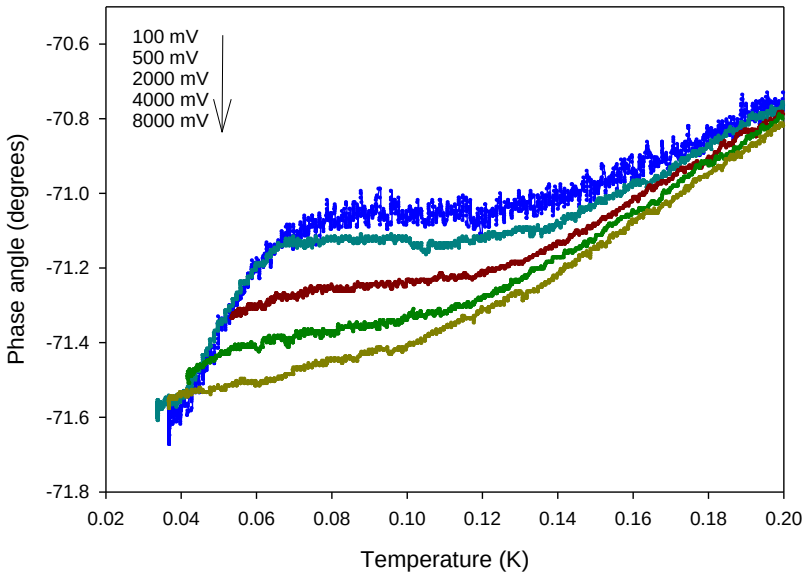

Figure 4.39: Low temperature region of phase angle versus temperature as a function of driving amplitude at 500 Hz in the sample 300ppb29.7. The plots are shifted vertically to agree at high temperature.

The high temperature (above 0.2 K) behavior of both the shear modulus and dissipation show their independence of strain amplitude. The low temperature behavior, on the other hand, is similar to that of bulk ^{4}He. This leaves the question – are the small stiffening and dissipation peaks below 150 mK something happening in aerogel or are they the effects of bulk helium in the gaps between the transducers and the aerogel piece or at the edges of the aerogel sample?

4.3.5 Amplitude hysteresis

It has been shown in TO experiments with bulk solid ^{4}He that the behavior is hysteretic at low temperature. The TO frequency i.e. the NCRI, rises as the amplitude reduced at low temperature but does not decrease when the amplitude is then increased – it remains constant even at large amplitude. This hysteretic amplitude dependence of the NCRI disappears at temperatures above 70 mK [50, 51].

In previous shear modulus measurement on bulk ^{4}He, similar hysteretic behavior was observed. We have made similar measurements to look for the hysteretic behavior in our shear modulus measurements for solid ^{4}He grown in aerogel.

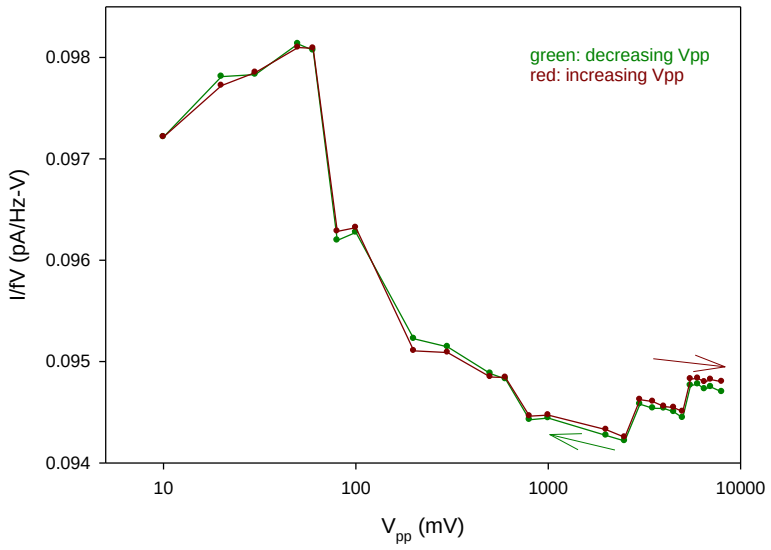

Figure 4.40: Shear modulus at 420 mK in sample 300ppb29.7. No hysteresis is seen when the amplitude is decreased then increased.

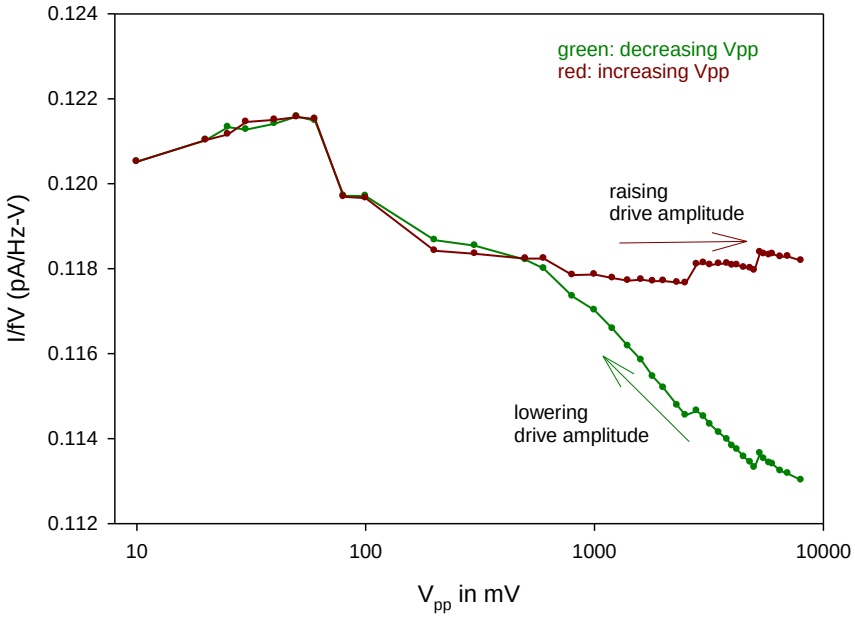

Figure 4.41: The hysteresis (raw data) between the shear modulus while decreasing and then increasing the drive amplitude at low temperature (37 mK) in sample 300ppb29.7.

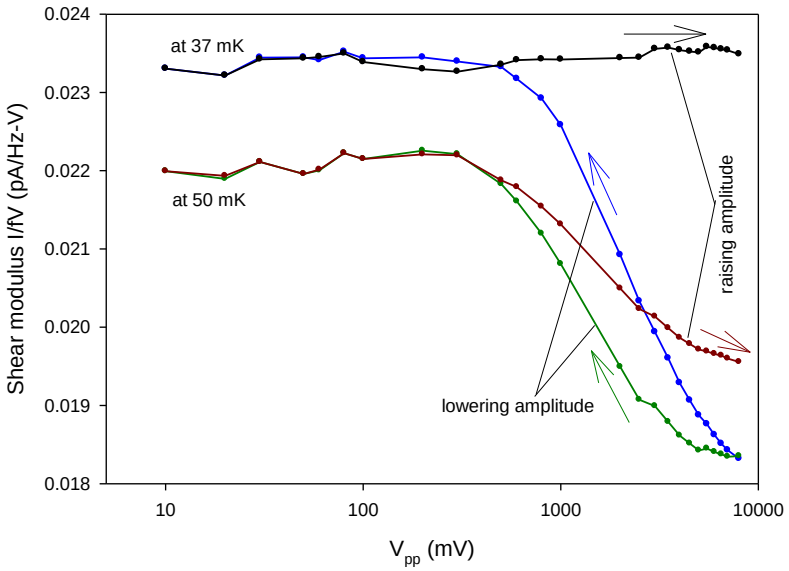

Figure 4.42: Hysteresis between the shear modulus while decreasing and increasing the drive amplitude at temperature 37 mK and 50 mK. The shear modulus has been corrected using the 420 mK data of Fig. 4.42 as described in the text.

Figure 4.40 shows the data at 420mK, taken by decreasing the driving amplitude from a high value of 8 V_{pp} to the lowest amplitude of 10 mV_{pp} and then increasing the amplitude up to the starting voltage. There is no hysteresis at this temperature, in contrast to the behavior at 37 mK (Figs. 4.40 and 4.42). For the low temperature hysteresis measurement, the sample was cooled from high temperature (420 mK) to low temperature (37 mK) while driving at high amplitude (8 V_{pp}). At 37 mK, the driving voltage was then decreased to 10 mV (the open circles) in steps, waiting for couple of minutes at each amplitude for stable data. After reaching the lowest value, the amplitude was then again raised in the same way up to 8 V_{pp}. Hysteresis data was also taken at 50 mK, in the same way of taking data at 37 mK.

Figure 4.42 shows the hysteresis in the shear modulus at 37 mK and 50 mK after subtracting the the background (hysteresis data taken at 420 mK). Below driving amplitude of 500 mV_{pp}, corresponding to a strain of 2.2 x 10^{-8}, there is no hysteresis. At the lowest temperature, 37 mK, even a driving voltage of 8 V_{pp} is not enough to reduce the shear modulus when increasing voltage. At slightly higher temperature, 50 mK, the hysteresis plot changes, with a decrease in modulus at large amplitudes.

Similar hysteresis is seen in bulk ^{4}He and has been interpreted in terms of ^{3}He pinning and unbinding under high stresses [52]. When sample is driven at high voltage, i.e. at high strains, ^{3}He impurities can't bind to the moving dislocations but when the sample is cooled and lower strains are applied, the dislocations get pinned by impurities, thus increasing the modulus. When the

amplitude is raised again at low temperature, the modulus remains constant to higher voltage because larger stress is then required to unpin the impurities from dislocations.

This hysteresis found in my shear modulus experiment with solid ^{4}He grown in aerogel closely resembles that of bulk helium.

4.3.6 Annealing effect

One of the interesting aspects of TO experiments is the dependence of NCRIf on sample history; the NCRIf can be changed and sometimes almost eliminated by annealing, which indicates the importance of defects [21]. Computations also suggest that there is no supersolid behavior in perfect crystals. We have also learned that annealing affects the high temperature shear modulus in bulk ^{4}He but leaves low temperature part unaffected [53].

We kept the sample at 1.5 K, near to its melting temperature (1.75 K), for 15 hours in order to study the effects of annealing. Figures 4.43 and 4.44 show the shear modulus anomaly and corresponding dissipation as function of temperature while cooling, before and after annealing. Annealing does not have a large effect on the behavior above 0.2 K.

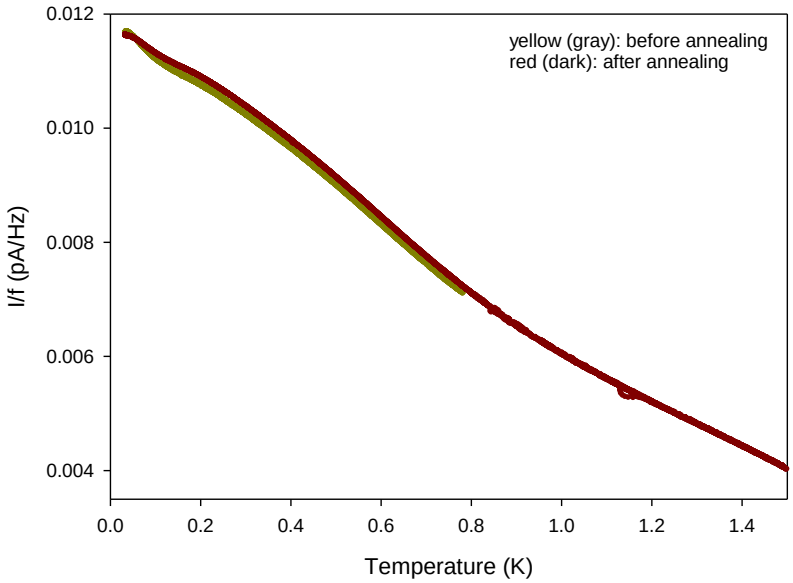

Figure 4.43: Effect of annealing on shear modulus of sample 300 ppb29.7, measured at 2000 Hz and 0.1 V_{pp} driving amplitude. Both sets of data were taken during cooling.

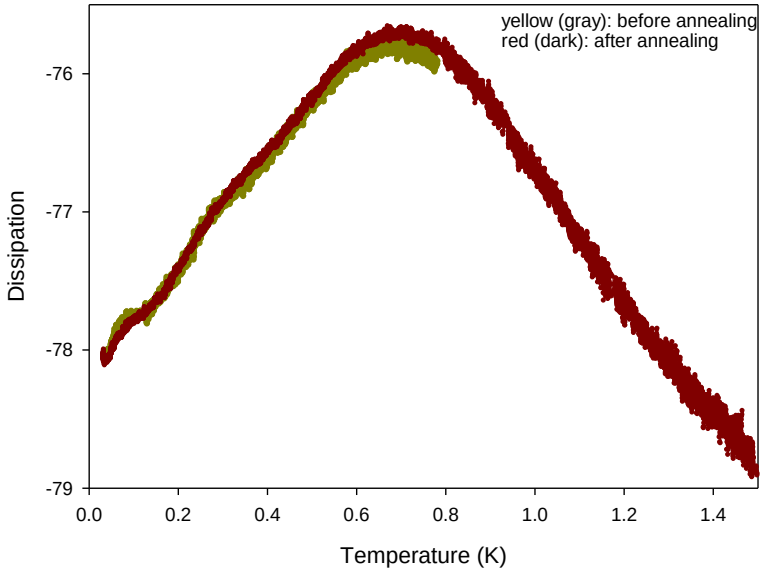

Figure 4.44: Effect of annealing on dissipation corresponding to Fig. 4.43 in sample 300 ppb29.7, measured at 2000 Hz and 0.1 V_{pp} driving amplitude. Both sets of data were taken during cooling.

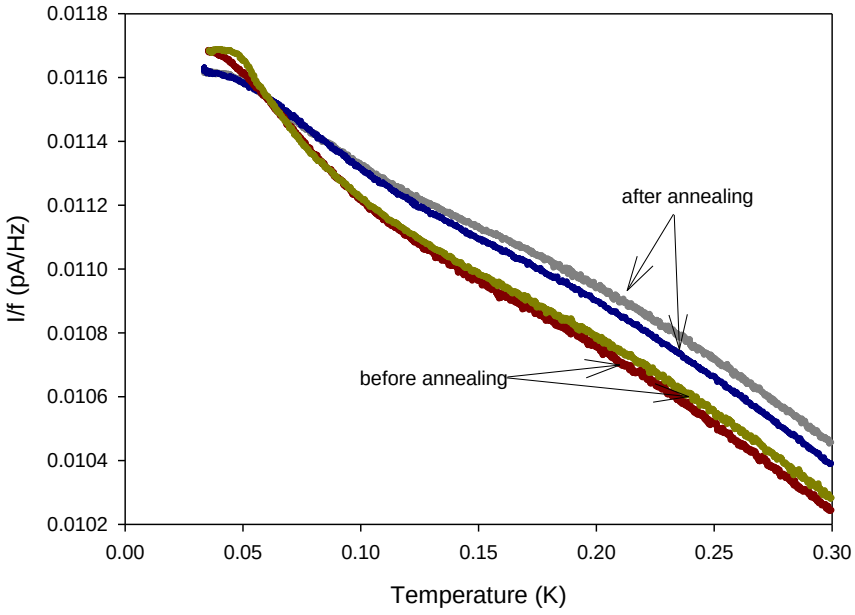

Figure 4.45: Low temperature region of the effect of annealing on shear modulus of the sample 300ppb29.7 at 2000 Hz 0.1 V_{pp}, the two sets of data are for cooling and warming the sample before and after annealing.

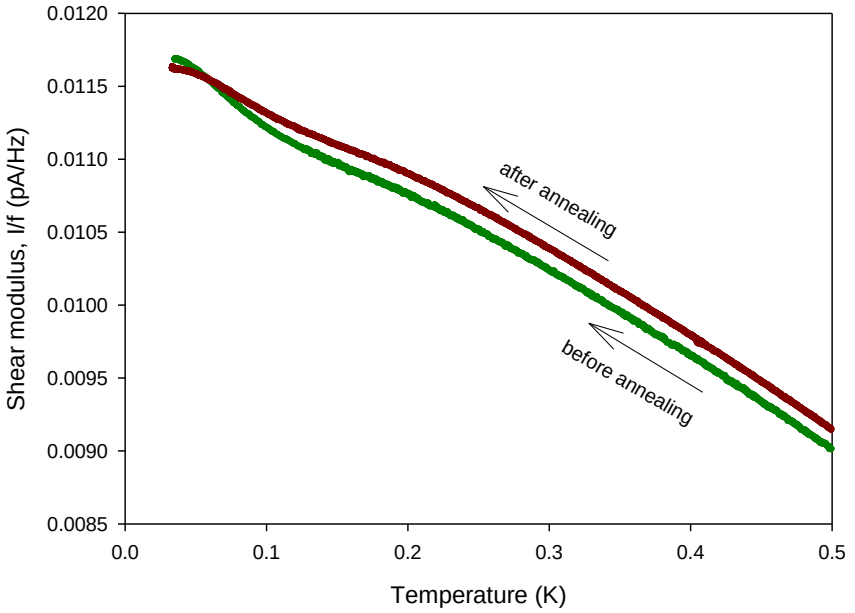

Figure 4.46: Effect of annealing on the shear modulus of the sample 300ppb29.7 at 2000 Hz 0.1 V_{pp}, Data was taken while cooling.

Figure 4.45 shows a blow up of the low temperature behaviour of the shear modulus at 2000 Hz; one set is the cooling and warming data before annealing and the other is after annealing. The effect of annealing is shown in Fig. 4.46 comparing the shear modulus data at 2000 Hz taken during cooling, before and after annealing.

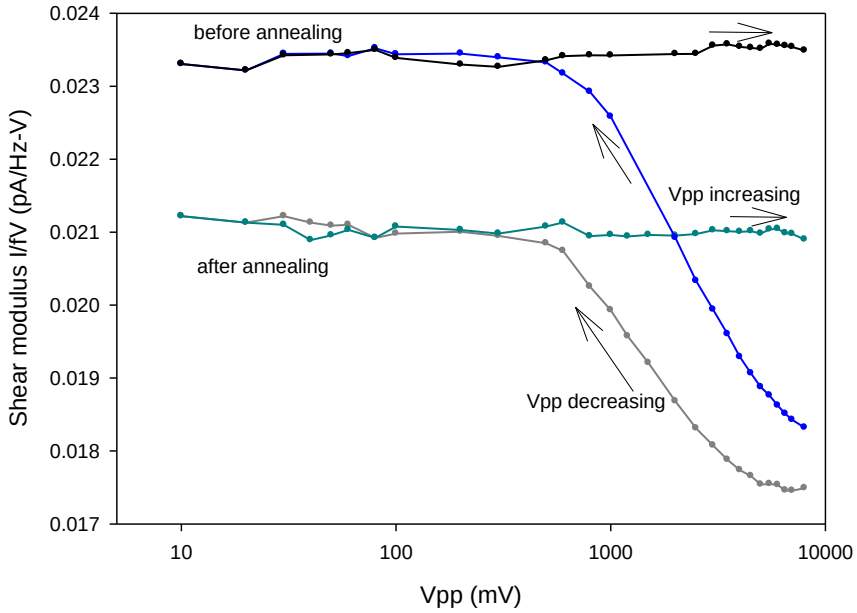

Figure 4.47: Annealing effect on the amplitude hysteresis at 37 mK in the sample 300ppb29.7.

In Fig. 4.42, we have seen the hysteresis at 37 mK between the shear modulus measured while decreasing and increasing the driving amplitude. The effect of annealing on hysteresis is shown in Fig. 4.47 at the same temperature. The hysteresis is similar but annealing reduced its magnitude by 8%. The hysteresis after annealing in Fig. 4.47 was also corrected using the background (shear modulus with amplitudes at 420 mK, not shown here).

Figures 4.43-4.46 show that annealing has little effect on either the modulus or dissipation at high temperature (above 150 mK). Annealing does change the behaviour at low temperatures, much as in bulk solid helium behaviour.

4.3.7 Sample 300ppb35.9

To confirm the behaviour of solid helium confined in aerogel, another sample was grown at higher pressure using the same blocked capillary method. The thermodynamic path of this sample is shown in Fig. 4.48. This higher pressure (35.9 bar) sample ensures that all the ^{4}He in the aerogel pores is solid.

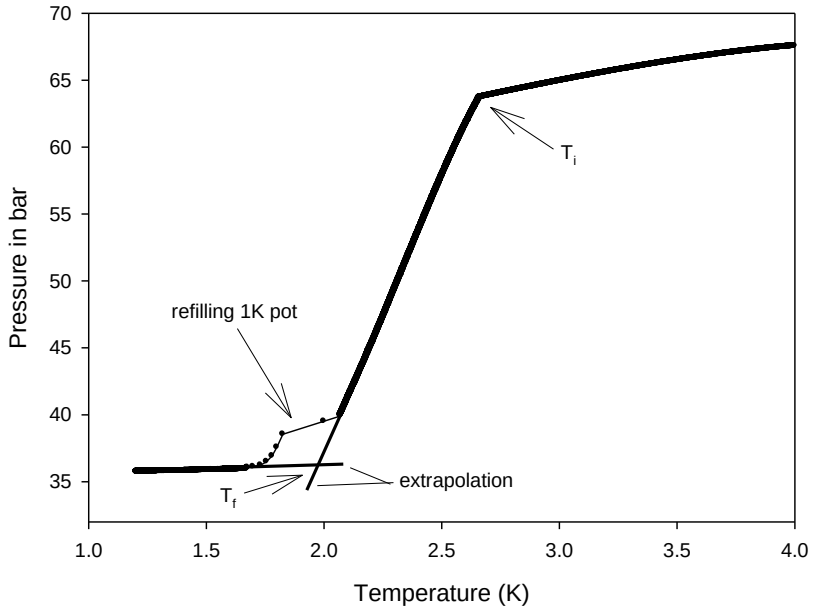

Figure 4.48: Growing the crystal (pressure versus temperature) - the thermodynamic path for the sample 300ppb35.9. T_f is the melting point.

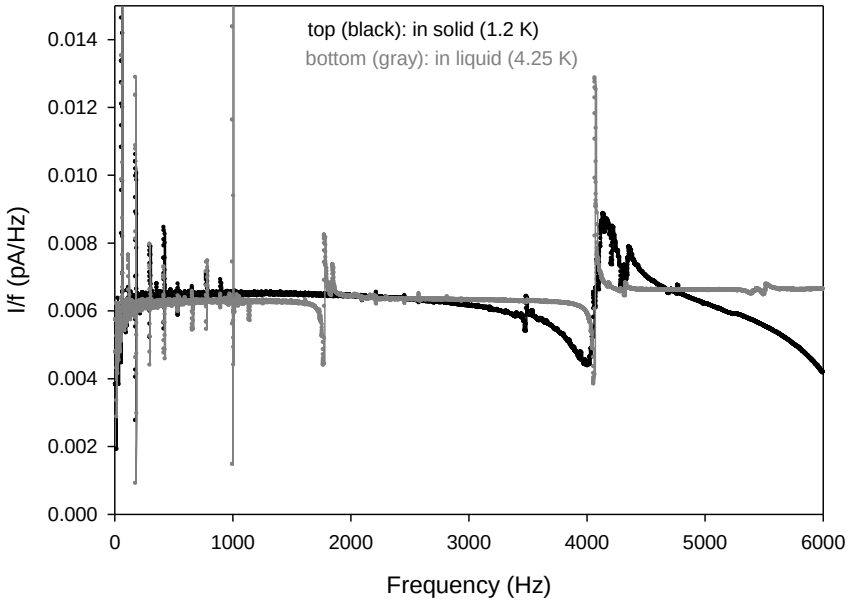

Figure 4.49: The background signal (amplitude versus frequency) in liquid (at 4.2 K and 23 bar pressure) and solid sample 300ppb35.9 (at 1.2 K and 35.9 bar), all measured at 100mV$_{pp}$ driving amplitude.

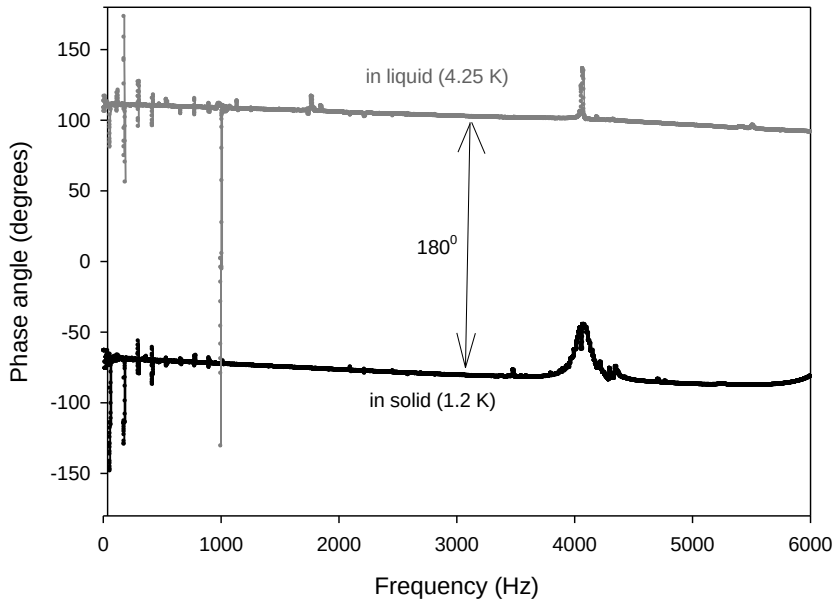

Figure 4.50: Phase angle corresponding to Fig. 4.50, as a function of frequency for the background signal in liquid (at 4.2 K and 23 bar pressure) and solid sample 300ppb35.9 (at 1.2 K and 38 mK), all measured at 100 mV$_{pp}$ driving amplitude.

The frequency sweep data shown in Fig 4.49 shows the comparison between the amplitude measured in liquid at 4.2 K and the total solid signal measured at 1.2 K. Although this figure seems to show that both the signals are almost the same in magnitude, they are not. The corresponding phase plot in Fig. 4.50 shows that there is 180^0 phase difference between the total measured signal in solid and the liquid background. This behaviour represents case (c) of the phase issue (chapter 3.11). This higher pressure sample (35.9 bar) has a larger signal than the previous sample (see Fig. 4.21) at 1.2 K.

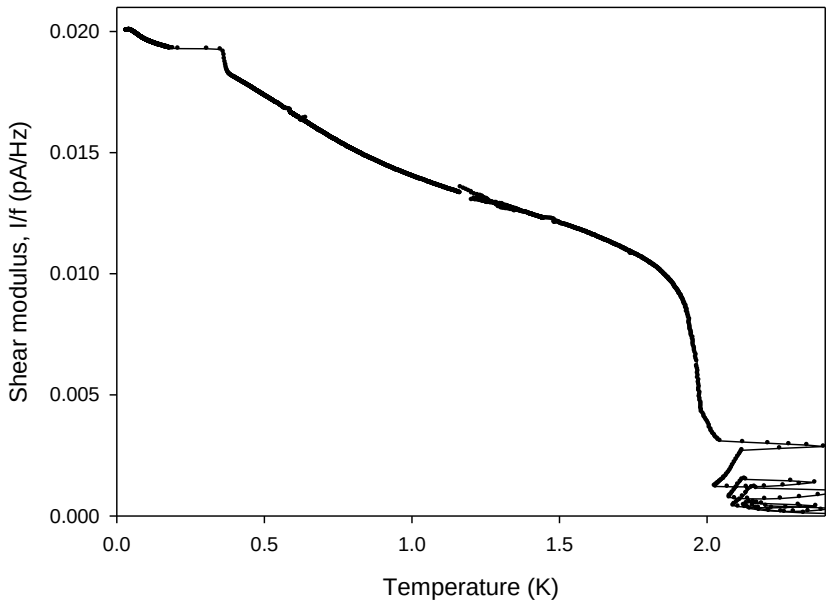

Figure 4.51: The total (corrected) shear modulus change in the sample 300ppb35.9, measured at 500 Hz and 100 mV_{pp} driving amplitude.

The shear modulus change in sample 300ppb35.9 (corrected from raw data) is shown in Fig. 4.51. As in the first sample, the shear modulus of solid ^{4}He in aerogel decreases by about 50% upon warming from low temperature to near melting.

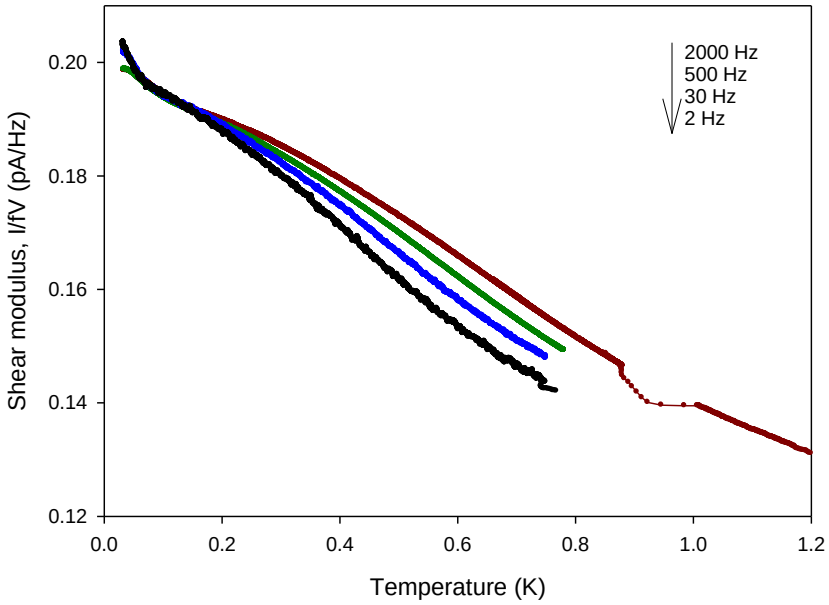

Figure 4.52: Shear modulus change of ^{4}He in aerogel as a function of temperature at different frequencies, measured at 100 mV_{pp} driving amplitude in the sample 300ppb35.9.

The shear modulus anomaly is shown in Fig. 4.52 at different frequencies (2 Hz, 30 Hz, 500 Hz and 2000Hz) in the sample 300ppb35.9. All the data are corrected for crosstalk but are not shifted vertically. Data at 2 Hz was corrected in the same way as for the previous crystal; the measured signal was divided by 0.16 to make up the loss due to the 0.3 Hz bandwidth of the preamp. Figure 4.52 shows that the temperature and frequency dependence of the shear modulus is similar to

that of the previous crystal, including the bulk ^{4}He like behavior at low temperatures.

The corresponding dissipation in Fig. 4.53 shows that the dissipation peaks shift to lower temperature as the frequency decreases, consistent with the shear modulus behavior, again indicating a thermally activated relaxation process.

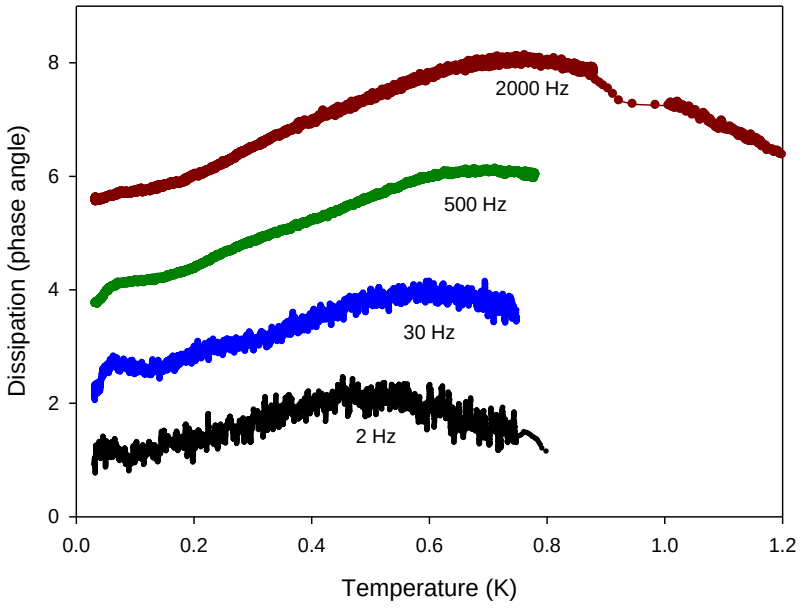

Figure 4.53: Dissipation corresponding to Fig. 4.52. The temperatures for the dissipation peaks and their heights are the same for the raw data as for the corrected data (shown).

The thermal activation energy for this thermally activated process can be found from Fig. 4.54. In order to find the activation energy, cubic polynomials were again used to fit the dissipation data to get precise peak temperatures. Figure 4.54 shows a plot of the inverse of those temperatures versus the logarithm of the corresponding frequencies. The activation energy, (9.59+/-1.7) K, is found from

the slope of a polynomial straight line fit. The uncertainty comes due to the estimated errors associated with dissipation peaks' locations.

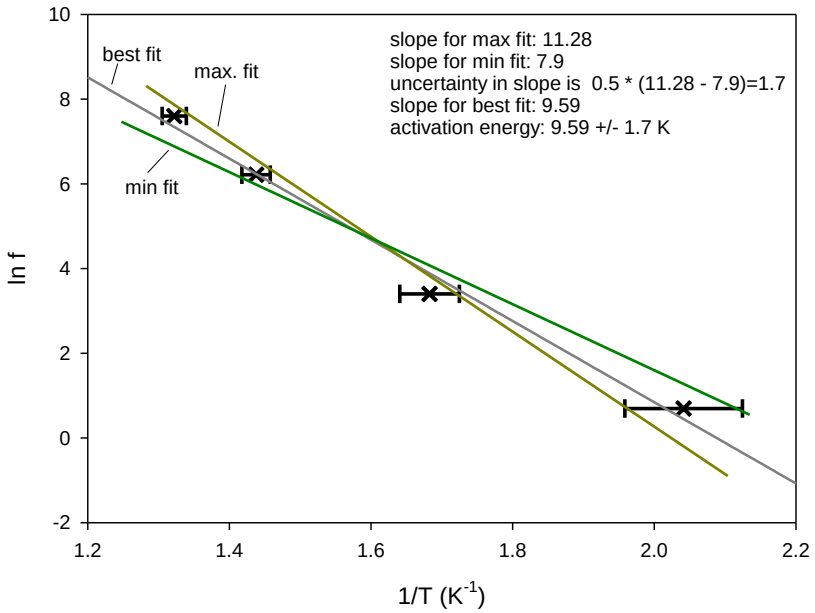

Figure 4.54: Thermal activation plot (ln f vs. 1/T with respective errors) for the crystal 300 ppb35.9. The lines are fit and their slopes corresponding to activation energies of (15.9 +/- 5) K.

This value of (9.59+/-1.7) K is smaller than the activation energy of (15.9+/-5) K found in the previous sample. The smaller uncertainty in activation energy in this sample is due to the sharper dissipation peaks in sample 300 ppb35.9.

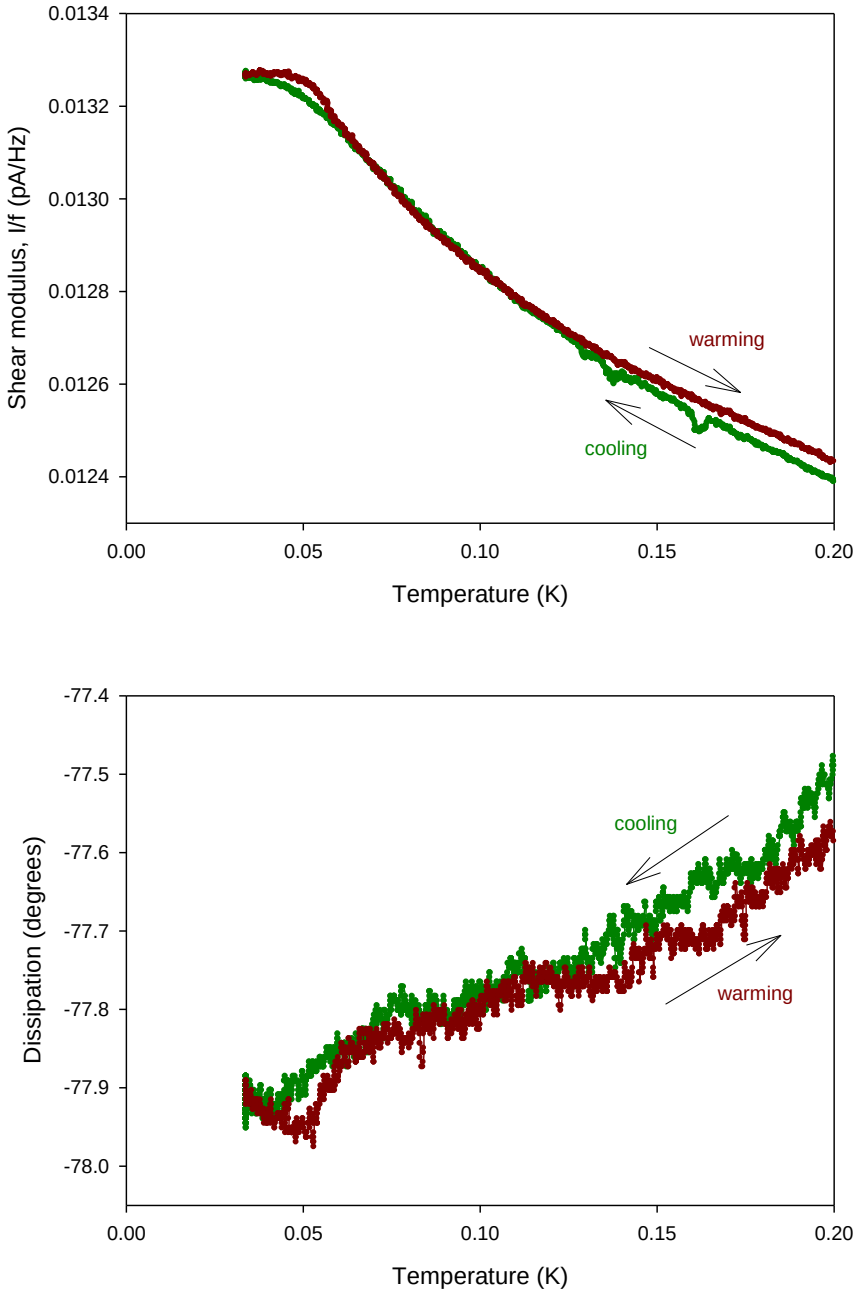

Figure 4.55: Low temperature blow up of shear modulus (top) and corresponding dissipation (bottom) anomaly as a function of temperature during cooling and warming, measured at 2000 Hz & 100 mV_{pp} driving amplitude in the sample 300ppb35.9.

The low temperature behaviour of the shear modulus and corresponding dissipation is shown in Fig. 4.55 in expanded scale. This first time cooling and warming data also shows hysteresis at temperatures below 150 mK, like the previous sample, which probably indicates some amplitude dependence even at the low strains used.

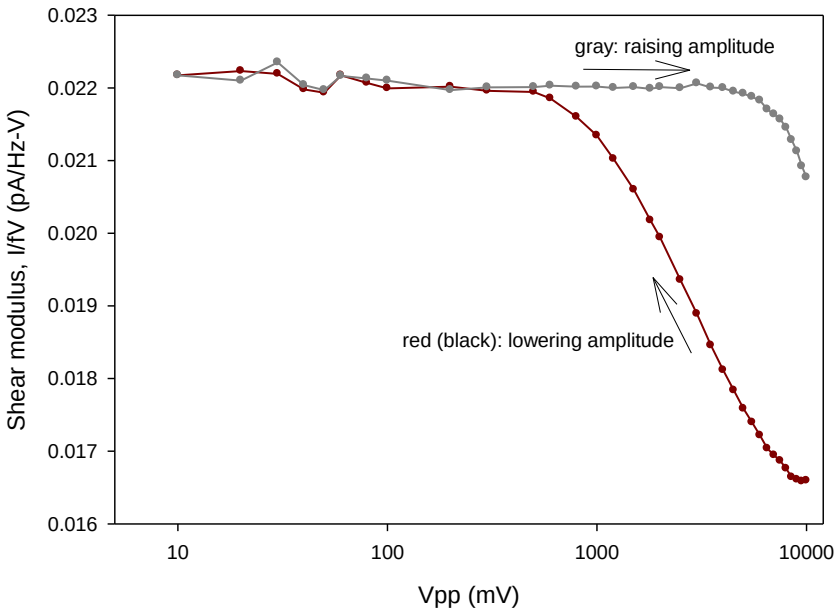

Figure 4.56: Hysteresis between the shear modulus while decreasing and increasing the drive amplitude at temperature 37 mK. The shear modulus has been corrected using the 420 mK data (not shown here).

In order to compare the behavior of this higher pressure sample with that of the previous lower pressure sample, the amplitude dependence was also measured. Figure 4.56 shows the hysteresis between the shear modulus and driving amplitude while decreasing (from 10 V_{pp} to 10 mV_{pp}) and increasing

(from 10 mV_{pp} to 10 V_{pp}) the amplitude at 37 mK. This data was corrected using the data measured at 420 mK where there was no hysteresis.

The results for this sample confirm that solid ^{4}He in aerogel shows consistent behavior in two samples at different pressures.

Chapter 5

Conclusions

The results of shear modulus measurements in aerogel show that the total shear modulus change is large, occurs at higher temperature and is broad, compared to the transition in bulk helium. The dissipation associated with the modulus change also occurs at high temperature. In addition to these broad changes, there is also a small effect at low temperature (below 150 mK where bulk ^{4}He effects occur).

In this chapter, I discuss the behavior of solid helium in aerogel in the two regions: high temperature and low temperature.

5.1 High temperature behavior (above 200 mK)

The total shear modulus decrease is large ($\frac{\Delta\mu}{\mu} \approx 50\%$) and most of it occurs over a broad temperature range, between 200 mK and melting at 1.75 K. Softening in aerogel occurs at much higher temperature than in bulk helium. This may be due to strong pinning of dislocations network by the glass strands of the aerogel. The dissipation shows a broad peak near the midpoint of the shear modulus change (in the range of 0.6 K - 0.8 K).

Above 200 mK, both the shear modulus and dissipation are independent of the strain amplitude (at the strains that can be achieved in our experiments), have no hysteresis, and neither is affected by annealing, all quite different behavior from that of bulk ^{4}He.

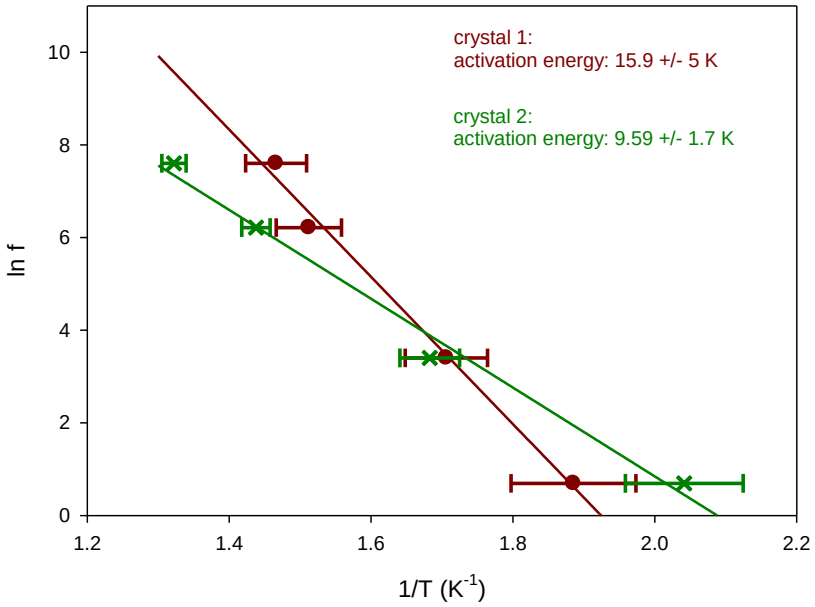

Figure 5.1: *ln f* vs. the inverse of temperature of maximum dissipation with respective errors. The lines are fit and their slopes corresponding to activation energies of (15.9 +/- 5) K and (9.6 +/- 1.7) K for the sample 300ppb29.7 and 300ppb35.9, respectively.

The dissipation peaks (and modulus changes) shift to higher temperature at higher frequencies which suggests a thermal activation process. Plotting *ln f vs. 1/T*, Fig. 5.1, for the dissipation peaks in our measurement, gives activation energies of (15.9 +/- 5) K and (9.6 +/- 1.7) K for the two different samples. Although those two values are quite different, the uncertainty associated with them suggests that the difference may not be significant. The dissipation peaks and modulus changes are much broader than a Debye relaxation with a single activation energy would predict so these must be averages of an activation energy distribution (Fig. 4.34). The activation energy for unpinning ^{3}He from dislocations networks in bulk ^{4}He is less than 1 K [45], so cannot be responsible for the

relaxation. Vacancies in solid ^{4}He, however, have comparable activation energies (~ 8-18 K) at this density [46-49] and so may be involved. At high temperatures, vacancies diffusion occurs rapidly and can cause relaxation of the effective modulus.

Thermally activated vacancies could reduce the shear modulus of solid ^{4}He in at least two ways. First, for helium confined in small pores, vacancies can diffuse in strain gradients and relax stresses. This mechanism was used to explain the temperature and frequency dependence of the shear modulus of solid ^{4}He in porous vycor glass [54]. In that early experiment [54], an activation energy of 14.2 K was obtained from the frequency dependence of the position of the dissipation of transverse ultrasonic waves (Fig. 5.2).

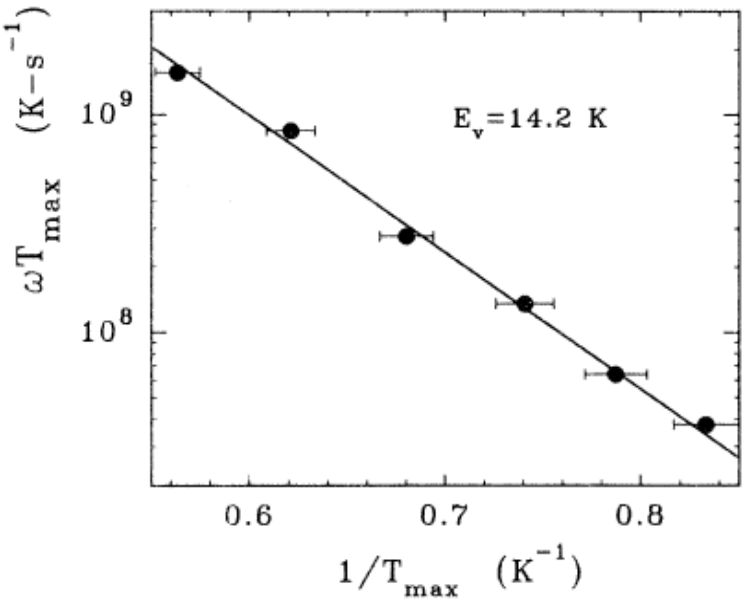

Figure 5.2: Frequency vs. the inverse of temperature of maximum attenuation in solid ^{4}He in porous vycor glass, which gives activation energy of 14.2 K [54].

They described the thermally activation process of relaxation of ultrasonic stress by means of diffusion of vacancies. Moreover, in comparison with bulk solid ^{4}He, they concluded that the confinement of helium in the pores of vycor did not significantly change the diffusion of vacancies. This suggests that confinement in aerogel would not have much effect in vacancies in our experiment.

Another possibility is that shear stresses relax via dislocation motion, as in bulk ^{4}He. However, dislocations could be so strongly pinned by aerogel strands that they cannot glide and so can only move via 'climb', which requires vacancies.

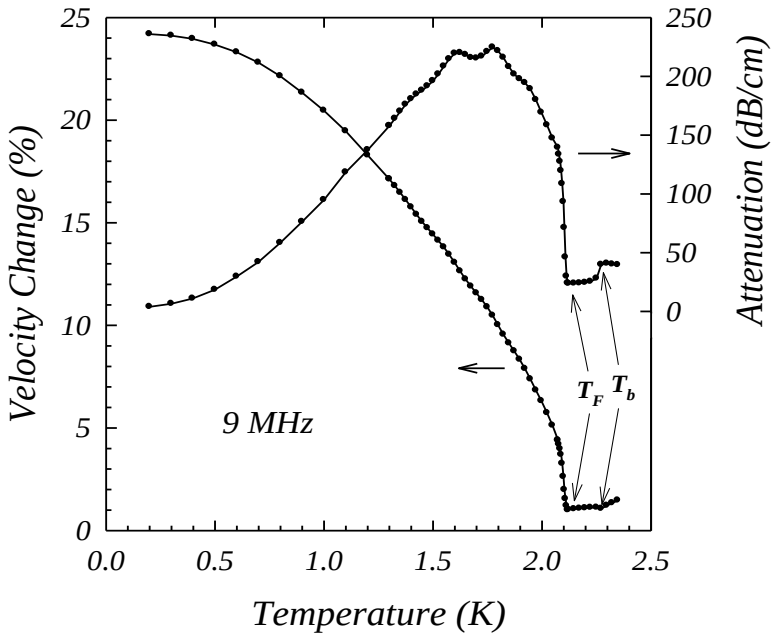

Figure 5.3: Velocity and attenuation during freezing of ^{4}He in silica aerogel for 9 MHz longitudinal waves at helium pressure of 477 bar [25].

However, the ultrasonic experiment on solid helium in aerogel, in Fig. 5.3, showed the broad change in velocity (which essentially reflects the shear modulus change in the helium) and they also found an attenuation peak (essentially the dissipation) at higher temperature (2 K). The wiggles in the attenuation near the peak and the very high attenuation prevented them from measuring the attenuation at other frequencies to find the activation energy. However, the fact that the dissipation peak in these measurements at 9 MHz is at higher temperature than in our measurements below 1 kHz is consistent with the idea of a thermally excited relaxation.

5.2 Low temperature behavior (shown below 150 mK only)

Both the shear modulus and the dissipation behavior at low temperature (below ~200 mK) resembles that of bulk helium, except the effects are smaller than in bulk.

The small hysteresis loops at low temperatures during the first cooling and warming (Fig 4.28) essentially disappeared at lower strain amplitude, which is similar to bulk ^{4}He behavior.

The stiffening and dissipation peaks below 200 mK are similar to those in bulk ^{4}He, except that they are much smaller [4].

The hysteresis in the shear modulus upon increasing and decreasing the drive amplitude at low temperatures (37 mK and 50 mK) and the absence of

hysteresis at high temperature (420 mK) were also seen in bulk solid ^{4}He, where they have been interpreted in terms of ^{3}He pinning and unbinding under high stresses. Annealing does affect the low temperature modulus and dissipation, as in bulk ^{4}He.

A rough estimate of the effects of the effects of bulk ^{4}He on the modulus measurements, using the overlapping area of the two transducers, and their spacing, suggests that edge effects could contribute ~ 5-10 % to the measured modulus. In addition to the edge effects, small gaps between the aerogel and transducers (mostly due to the roughness of the aerogel's surface) may also give a bulk ^{4}He contribution.

The bulk- like behavior observed at low temperature (below ~200 mK) may be due to bulk helium in the gaps and surrounding the aerogel and transducers.

On the other hand, N. Mulders et al. [32] found a very small NCRIf (0.04 %) in their TO experiment of solid ^{4}He in aerogel and suggested that this small NCRIf was occurring in the solid ^{4}He inside the aerogel.

It is clear that high temperature behavior of the shear modulus which is quite different from bulk ^{4}He occurs in the ^{4}He in aerogel. The low temperature behavior could be the effects of bulk ^{4}He in the gaps between the transducers and the aerogel piece or at the edges of the aerogel sample but some of it might still be associated with ^{4}He confined in the aerogel.

References

[1] A.F. Andreev and I.M. Lifshitz, Sov. Phys. JETP 29, 1107 [1969].

[2] E. Kim and M.H.W Chan, Nature **427**, 225 (2004).

[3] E. Kim and M. H. W. Chan, Science **305**, 1941 (2004).

[4] J. Day and J. Beamish, Nature **450**, 853 (2007).

[5] P. W. Anderson, W. F. Brinkman, and D. A. Huse, Science **310**, 1164 (2005).

[6] M. Boninsegni, A. B. Kuklov, L. Pollet, N. V. Prokof'ev, B. V. Svistunov and M. Troyer, Phys. Rev. Lett. **99**, 035301 (2007).

[7] L. Pollet, M. Boninsegni, A. B. Kuklov, N. V. Prokof'ev, B. V. Svistunov and M. Troyer, Phys. Rev. Lett. **98**, 135301 (2007).

[8] M. Boninsegni, N. Prokof'ev and B. Svistunov, Phys. Rev. Lett. **96**, 105301 (2006).

[9] C. Enns and S. Hunklinger, Low Temperature Physics, Springer, 2005.

[10] http://guava.physics.uiuc.edu/~nigel/courses/569/essays_f2004/files/barath.pdf.

[11] F. London, Nature **141**, 643 (1938).

[12] L. Tisza, Nature **141**, 913 (1938).

[13] L. Landau, Phys. Rev. **60**, 356 (1941).

[14] E. L. Andronikashvili, Zh. Eksp. Teor. Fiz. **16**, 780 (1946).

[15] O. Penrose and L. Onsager, Phys. Rev. **104**, 576 (1956).

[16] G. V. Chester, Phys. Rev. **A 2**, 256 (1970).

[17] A. J. Leggett, Phys. Rev. Lett. **25**, 1543 (1970).

[18] D. S. Greywall, Phys. Rev. B **16**, 1291 (1977).

[19] D. J. Bishop, M. A. Paalanen, and J. D. Reppy, Phys. Rev. B **24**, 2844 (1981).

[20] G. A. Lengua and J. M. Goodkind, J. Low Temp. Phys. **79**, 251 (1990).

[21] A. S. C. Rittner and J. D. Reppy, Phys. Rev. Lett. **98**, 175302 (2007).

[22] Yu. Mukharsky, A. Penzev, and E. Varoquaux, Phys. Rev. B **80**, 140504 (R) (2009).

[23] D. Y. Kim, H. Choi, W. Choi, S. Kwon, E. Kim and H. C. Kim, *preprint*.

[24] X. Rojas, A. Haziot, V. Bapst, S. Balibar, and H. J. Maris, Phys. Rev. Lett. **105**, 145302 (2010).

[25] E. R. Molz and J. R. Beamish, J. Low. Temp. Phys. **101**, 1055-1077(1995).

[26] C. Pantalei, X. Rojas, D. O. Edwards, H. J. Maris, and S Balibar, J. Low. Temp. Phys. **159**, 452-461 (2010).

[27] http://eetd.lbl.gov/ecs/aerogels/sa-making.html.

[28] T. Herman, PhD thesis, University of Alberta, 2005.

[29] D. R. Daughton, J. MacDonald, and N. Mulders, Physica B, **329-333**, 1233 (2003).

[30] H. S. Ma, A. P. Roberts, J.H. Prevost, R. Jullien, and G.W. Scherer, J. Non-Cryst. Solids **277**, 127 (2000).

[31] T. Herman, J. Day, and J. Beamish, Phys. Rev. B **73**, 094127 (2006).

[32] N. Mulders, J. T. West, M.H.W. Chan, C.N. Kodituwakku, C.A. Burns, and L.B. Lurio, Phys. Rev. Lett. **101**, 165303 (2008).

[33] I. V. Kalinin, E. Kats, M. koza, V. V. Lauter, H. Lauter, and A. V. puchkov, JETP Lett. **87** (11), 645 (2008).

[34] I. V. Kalinin, E. I. Kats, M. koza, V. V. Lauter, H. Lauter, and A. V. puchkov, JETP Lett. **111** (2), 215 (2010).

[35] X. Lin, A.C. Clark, and M.H.W. Chan, Nature **449**, 1025 (2007).

[36] J. Day and J. Beamish, Phys. Rev. Lett. **96**, 105304 (2006).

[37] D. S. Greywall, Phys. Rev. B **16(3),** 1292 (1977).

[38] James Day, PhD thesis, University of Alberta, 2007.

[39] E. Kim and M.H.W. Chan, Phys. Rev. Lett. **97,** 115302 (2006).

[40] G. C. Straty and E. D. Adams, Rev. Sci. Inst. 40, 1393 (1969).

[41] http://www.bostonpiezooptics.com/?D=25

[42] Ernest W. Flick, Adhesives, sealants, and coatings for the electronics industry, Noyes Publications, 1992.

[43] E Kim, JS Xia, JT West, X Lin, AC Clark, and MHW Chan, Phys. Rev. Lett. **100**, 065301 (2008).

[44] J. Day, O Syschchenko, and J. Beamish, Phys. Rev. B **79**, 214524 (2009).

[45] O. Syshchenko, J. Day and J. Beamish, Phys. Rev. Lett. **104**, 195301 (2010).

[46] T. Mizusaki, Y. Hirayoshi, S. Maekawa and A. Hirai, Phys. Lett. A **50**, 165 (1974).

[47] B. A. Fraass, P. R. Granfors and R. O. Simmons, Phys. Rev. B **39**, 124 (1989).

[48] E. Blackburn, J. Goodkind, S.K. Sinha, C. Broholm, J. Copley, and R. Erwin, J. Phys. **71**, 673 (2008).

[49] M. Boninsegni, A. B. Kuklov, L. Pollet, N.V. Prokof'ev, B.V. Svistunov and M. Troyer, Phys. Rev. Lett. **97,** 080401 (2006).

[50] A. S. C. Rittner and J. D. Reppy, Phys. Rev. Lett. **101**, 155301 (2008).

[51] A. C. Clark and M. H.W. Chan, Phys. Rev. B **77**, 184513 (2008).

[52] J. Day, O Syschchenko, and J. Beamish Phys. Rev. Lett. **104**, 075302 (2010).

[53] O. Syshchenko, J. Day and J. Beamish, J. Low Temp. Phys. **34**, 340-343 (2008).

[54] J. R. Beamish, N. Mulders, A. Hikata, and C. Elbaum, Phys. Rev. B **44**, 9314 (1991).